AD-A248 006

PAGE 1

**1. AGENCY USE ONLY** *(Leave blank)*

**2. REPORT DATE**
9 January 1992

**3. REPORT TYPE AND DATES COVERED**
Final Technical: 1 Oct 88-30 Sept 91

**4. TITLE AND SUBTITLE**
Solid Rocket Combustion Phenomena

**5. FUNDING NUMBERS**
AFOSR-89-0023

**6. AUTHOR(S)**
D.R. Kassoy, M. Wang, Q. Zhao

**7. PERFORMING ORGANIZATION NAME(S) AND ADDRESS(ES)**
University of Colorado
Campus Box 26
Boulder, CO 80309

**8. PERFORMING ORGANIZATION REPORT NUMBER**
CCR Report #92-01

**9. SPONSORING/MONITORING AGENCY NAME(S) AND ADDRESS(ES)**
AFOSR

**10. SPONSORING/MONITORING AGENCY REPORT NUMBER**
AFOSR-TR- 92 0208



**11. SUPPLEMENTARY NOTES**

**12a. DISTRIBUTION / AVAILABILITY STATEMENT**

This document has been approved for public release and sale; its distribution is unlimited.

**12b. DISTRIBUTION CODE**

**13. ABSTRACT** *(Maximum 200 words)*

This Final Technical Report describes completed research accomplishments and ongoing activities that are focused on the evolution of boundary driven acoustic disturbances in a low Mach number shear flow like that found in the chamber of a solid rocket engine. The completed work (manuscripts in Appendices A and B) focuses on the relatively complex wave systems that appear in a two-dimensional planar shear flow following the refraction of very simple, initially planar axial disturbances. Work in progress emphasizes; (1) the characteristics of acoustic disturbances driven by sidewall mass addition in semi-confined channels and tubes, (2) the role of "strongly injected" Stokes boundary layers in providing a transition from the acoustic flow to the no-slip condition on the wall, and (3) mathematical methods required to deal with nonlinear processes within an acoustically disturbed flow. The review of our work emphasizes the importance of studying the evolution of boundary driven acoustic disturbances, primarily to gain an understanding of how small burning rate transients (modelled by unsteady wall injection) lead to large engine chamber responses observed in unstable solid rockets.

**14. SUBJECT TERMS**

**15. NUMBER OF PAGES**
39

**16. PRICE CODE**

**17. SECURITY CLASSIFICATION OF REPORT**
U

**18. SECURITY CLASSIFICATION OF THIS PAGE**
U

**19. SECURITY CLASSIFICATION OF ABSTRACT**
U

**20. LIMITATION OF ABSTRACT**

# SOLID ROCKET COMBUSTION PHENOMENA

Final Technical Report

prepared for

Dr. Mitat Birkan

Air Force Office of Scientific Research
(Grant No. AFOSR–89–0023)

David R. Kassoy, Meng Wang, and Qing Zhao

January 9, 1992

CCR Report No. 92-01

Center for Combustion Research
Department of Mechanical Engineering
University of Colorado at Boulder
Boulder, CO 80309-0427

# Contents

# Abstract

This Final Technical Report describes completed research accomplishments and ongoing activities that are focused on the evolution of boundary driven acoustic disturbances in a low Mach number shear flow like that found in the chamber of a solid rocket engine. The completed work (manuscripts in Appendices A and B) focuses on the relatively complex wave systems that appear in a two-dimensional planar shear flow following the refraction of very simple, initially planar axial disturbances. Work in progress emphasizes; (1) the characteristics of acoustic disturbances driven by side-wall mass addition in semi-confined channels and tubes, (2) the role of "strongly injected" Stokes boundary layers in providing a transition from the acoustic flow to the no-slip condition on the wall, and (3) mathematical methods required to deal with nonlinear processes within an acoustically disturbed flow. The review of our work emphasizes the importance of studying the evolution of *boundary driven* acoustic disturbances, primarily to gain an understanding of how small burning rate transients (modelled by unsteady wall injection) lead to large engine chamber responses observed in unstable solid rockets.

# Chapter 1

# Introduction

Burning rate transients of a combusting solid propellant produce gaseous products that are "injected" into the rocket engine chamber as an unsteady flow. This type of transient mass injection is known (Kassoy 1979) to be a source of mechanical and thermodynamic disturbances that can be described in terms of acoustic phenomena. Our research program is focused on relating the evolution of acoustic phenomena in semi-confined low Mach number shear flows to specific types of boundary driving, particularly that associated with mass addition normal to the surface of injection. The ultimate objective of our studies is to demonstrate that the long-time (nonlinear) evolution of initially small acoustic disturbances is intimately coupled to the specified boundary forcing.

Traditional studies of acoustic phenomena in models of solid rocket engines (e.g., Culick 1990) are based on linear and weakly nonlinear stability theory. The results of this work have been shown to describe many of the events observed in stable and unstable engines. From the perspective of a modeler, the formulation decouples the evolution of acoustic amplitudes from the driving mechanisms associated with burning rate transients. It is also notable that the normal mode expansions used to develop the mathematical model are valid formally only for a totally closed chamber, so that the effect of the nozzle on chamber losses is not properly accounted for.

Our work emphasizes an initial-boundary value approach for modeling. An initially steady, low Mach number flow field is disturbed by specific boundary disturbances. Solutions describe the totality of wave systems generated by the disturbance and their evolution. These complete solutions are in contrast to those based on the quasi-steady assumption. In particular, we can describe resonant solutions with amplitude growth that are not part of the solution set arising from the quasi-steady assumption. It is notable that our analyses predict the appearance of relatively complex wave systems for a given, more elementary boundary disturbance.

The manuscripts in Appendices A and B describe refraction effects on the acoustic time scale in a planar channel. On this time scale only linear phenomena are important in determining the wave pattern evolution, a conclusion verified by the use of rational approximation methods for small Mach number shear flows. The results demonstrate that prescribed axial disturbances are altered by refraction to create higher order axial, oblique and even purely transverse modes. Hence refraction provides a pathway for converting energy in one wave mode into others, depending on geometrical and boundary forcing properties. For example, an axial boundary disturbance in a semi-infinite shear flow (traveling waves) can, for resonance conditions, produce a purely transverse wave of growing amplitude. This type of result provides a source of understanding about the appearance of unexpected wave modes in a semi-confined system. Such an insight could not be obtained from more traditional analyses based on the quasi-steady approximation or on formulations where only one-dimensional (axial) processes are assumed to exist.

Work in progress is described in modest detail in Chapters 2–4. Acoustic modes in a rectangle with one open end, generated by sizable wall injection transients, are described in Chapter 2. In Chapter 3 we consider a steady injection-induced low

Mach number flow in an open-ended tube and predict acoustic configurations arising from endwall forcing and from sidewall injection transients. The former case includes a discussion of the viscous accommodation layer that provides a smooth, but oscillatory transition between the acoustic flow and the no-slip condition at the wall. An analog problem is described in Chapter 4, where we investigate the impact of the acoustic properties of one boundary of a slab when the other boundary exhibits small amplitude harmonic motion. The eigenfunction properties are shown to be dependent on the explicit conditions chosen and that is shown to have a profound effect on the evolution of the entire flow in the semi-contained gas.

Engineering design of reliable solid rocket engines can benefit from an awareness of the character of all wave systems present in the chamber. The primarily analytical approach presented in this report provides a sound basis for prediction of wave system behavior on the acoustic time scale of the engine chamber. Additionally, the results provide a starting point for the consideration of longer time period nonlinear solutions that describe the appearance of the relatively large amplitude response of low Mach number chamber flows to smaller prescribed boundary disturbances. It is important to recognize that typical computational solutions to model rocket engine problems (e.g., Baum 1989) do not provide detailed information about acoustic wave structure, but rather, give only point-wise time dependent responses. It would be valuable to develop data analysis techniques that can be used to predict acoustic wave structure from nodal point data.

# Chapter 2

# Acoustic Wave Modes Generated by Transient Sidewall Mass Addition

## 2.1 Problem Statement

Sidewall mass addition is used to mimic the gasification of a burning solid propellant in a model of a rocket engine chamber. Velocity injection along the sidewalls of an open ended rectangle induces a low Mach number internal shear flow. A positive transient component of the injected mass, superimposed on a steady distribution of the same magnitude, is the source of initially transverse acoustic wave disturbances in a basically steady, inviscid rotational background flow. These disturbances are associated with an axial pressure gradient which acts as a source of axial acoustic waves. Reflection processes alone in the semi-confined open ended rectangle create distinct axial, oblique and transverse wave patterns. Explicit harmonic mass transient frequencies are associated with rapid amplification of specific wave mode amplitudes, due either to beat phenomena or actual resonance. The primary objectives of this study are to show that complex, identifiable wave patterns are created by relatively simple boundary disturbances, and that boundary driven disturbances can be the source of large acoustic instabilities.

## 2.2 Mathematical Model

Rational perturbation methods are used to derive the limiting form of the mathematical model that describes acoustic phenomena in a low Mach number ($M \ll 1$), large Reynolds number ($R_e \gg 1$) flow:

$$p = \rho T, \tag{2.1}$$

$$\rho_t + M\left[(\rho u)_x + (\rho v)_y\right] = 0, \tag{2.2}$$

$$\rho\left[u_t + M(uu_x + vu_y)\right] = -\frac{1}{\gamma M} p_x, \tag{2.3}$$

$$\rho\left[v_t + M(uv_x + vv_y)\right] = -\frac{\delta^2}{\gamma M} p_y, \tag{2.4}$$

$$\rho C_v\left[T_t + M(uT_x + vT_y)\right] = -(\gamma - 1)Mp(u_x + v_y), \tag{2.5}$$

where transport effects are neglected because $M/R_e \ll 1$. The axial velocity $u$ is nondimensionalized with respect to a mean induced speed $U'_m = v'_{w0}\delta$ where $\delta = L'/D'$ is the rectangle aspect ratio and $v'_{w0}$, the characteristic velocity of the injected fluid, is used to nondimensionalize the transverse velocity component $v$. The parameters $M$ and $R_e$ are defined with respect to $U'_m$. The axial and transverse dimensions $(x, y)$ are referred to $(L', D')$ and the time is nondimensionalized by the axial acoustic time $t'_A = L'/c'_0$ where $c'_0$ is the characteristic sound speed.

Mass addition on the sidewalls is described by

$$y = (0, 1): \qquad v = (+, -)\left[v_0(x) + V_w(x, t)\right] \tag{2.6}$$

where the steady and transient components are of the *same* magnitude, and are both responsible for positive mass addition only.

The induced steady internal flow arising from $v_0(x)$ alone is described by $(p, \rho, T) =$

$1 + M^2(P, R, \theta)$, $(u, v)$, the lowest order inviscid, rotational equation system,

$$u_{0x} + v_{0y} = 0, \tag{2.7}$$

$$u_0 u_{0x} + v_0 u_{0y} = -\frac{1}{\gamma} P_{0x}, \tag{2.8}$$

$$u_0 v_{0x} + v_0 v_{0y} = -\frac{\delta^2}{\gamma} P_{0y}, \tag{2.9}$$

$$\theta_0 = \frac{\gamma - 1}{\gamma} P_0, \qquad R_0 = P_0 - \theta_0 \tag{2.10}$$

and (2.6), with a $V_w = 0$. Eqs. (2.10) show that isentropic conditions prevail. The wall acts as a source of vorticity, so that the no-slip condition $u_0(x, y = 0, 1) = 0$ can be satisfied. Analytical solutions can be obtained easily for $\delta \gg 1$. However, the flow and pressure fields have no direct effect on the first order acoustic waves, and are not considered further.

## 2.3 Acoustic Disturbances

The steady flow described by (2.7)-(2.10) is disturbed by turning on the injection transient $V_w(x, t)$ in (2.6) at $t = 0$. The mechanical effect on the boundary creates a velocity field $(\hat{U}, \hat{V})$ and thermodynamic disturbances defined by $(p, \rho, T) = 1 + M(\hat{P}, \hat{R}, \hat{\theta})$. One may reduce the equations for the acoustic fields to the initial-boundary value problem,

$$\hat{P}_{0tt} = \hat{P}_{0xx} + \delta^2 \hat{P}_{0yy}, \tag{2.11}$$

$$t = 0; \qquad \hat{P}_0 = \hat{P}_{0t} = 0, \tag{2.12}$$

$$x = 0; \qquad \hat{P}_{0x} = 0, \qquad x = 1; \qquad \hat{P}_0 = 0, \tag{2.13}$$

$$y = 0, 1; \qquad \hat{P}_{0y} = -\frac{\gamma}{\delta}(+, -)\hat{V}_{wt}(x, t). \tag{2.14}$$

The downstream condition in (2.13) is chosen for simplicity. A more physically viable condition might be $\hat{P}_{0x}(1, t) = \alpha \hat{P}_{0t}(1, t)$ where $\alpha$ may be thought of as an admittance function. The complete velocity field formula given by

$$(u, v) \sim (u_0(x, y), v_0(x, y)) - \frac{1}{\gamma} \int_0^t \left( \widehat{P}_{0x}, \frac{\delta^2}{\gamma} \widehat{P}_{0y} \right) d\hat{t} \tag{2.15}$$

shows how the wall transient enhances the steady flow field described by (2.7)–(2.10). Additionally $\widehat{\theta}_0 = (\gamma - 1)\widehat{R}_0 = ((\gamma - 1)/\gamma)\widehat{P}_0$.

Solutions to (2.11)–(2.14) are written for the case when

$$\widehat{V}_w(x, t) = \frac{\delta^2 K}{\gamma\omega} [1 - \cos(\omega t)] \cos\left(\frac{\pi x}{2}\right) \tag{2.16}$$

which describes an axially distributed non-negative injection velocity with a harmonic time variation.

### 2.3.1 Nonamplified Solutions

For $\omega \neq \Omega_{m0} \equiv \left[(\pi/2)^2 + (2m\pi\delta)^2\right]^{1/2}, m = 0, 1, 2, \cdots,$

$$\begin{aligned} \frac{\widehat{P}_0}{\delta^2 K} = \cos\left(\frac{\pi}{2} x\right) \Bigg\{ & \left[ \frac{2}{\left(\frac{\pi}{2}\right)^2 - \omega^2} + 4 \sum_{m=1}^{\infty} \frac{\cos(2m\pi y)}{\Omega_{m0}^2 - \omega^2} \right] \sin(\omega t) \\ & - \frac{4\omega \sin\left(\frac{\pi}{2} t\right)}{\left(\frac{\pi}{2}\right)^2 - \omega^2} - 4 \sum_{m=1}^{\infty} \frac{\omega \cos(2m\pi y) \sin(\Omega_{m0} t)}{\Omega_{m0}\left(\Omega_{m0}^2 - \omega^2\right)} \Bigg\}. \end{aligned} \tag{2.17}$$

The first complete term within the parentheses represents the quasi-steady response of the gas to the injection transient. The second term can be written as a pair of counter-propagating purely axial traveling waves. Finally, each of the components of the series can be rewritten as a pair of oblique traveling waves. Clearly one will find beats when $\omega \rightarrow \Omega_{m0}$ and rapid amplitude amplification when $\omega = \Omega_{m0}$, arising from interaction between one of the quasi-steady modes and one of the eigenvalue solutions. These possibilities are not captured in a traditional quasi-steady analysis. This elemetary solution displays the rich complexity of wave types initiated by a relatively simple boundary disturbance. Even more complexity will appear if the spatial distribution of the injection transient contains more axial eigenfunctions than used in (2.16).

### 2.3.2 Amplified Solutions

When $\omega = \Omega_{m0}$, $m = 0, 1, 2, \cdots$, (2.17) fails formally and one must seek a solution in which discrete modes are amplified. For example, when $\omega = \pi/2$,

$$\frac{\widehat{P}_0}{\delta^2 K} = -\frac{2}{\pi} t \cos\left(\frac{\pi}{2}t\right) \cos\left(\frac{\pi}{2}x\right) + \cdots \tag{2.18}$$

so that the amplitude of the purely axial mode (pairs of axial traveling waves) grows linearly with time. The remaining terms in the solution, represented by the dots, describe bounded quasi-steady and oblique modes.

When the forcing frequency is larger, $\omega = \Omega_{m0}$, $m = 1, 2, \cdots$, one of the higher order oblique modes is amplified;

$$\frac{\widehat{P}_0}{\delta^2 K} = -\frac{2t}{\Omega_{m0}} \cos(\Omega_{m0}t) \cos(2m\pi y) \cos\left(\frac{\pi}{2}x\right) \tag{2.19}$$

where the dots again refer to bounded modes. Given that $p = 1 + M\widehat{P}$, the amplified solutions are of limited value on the time scale $Mt = O(1)$, which happens to be the characteristic time of fluid to pass through the semi-confined container.

### 2.3.3 Discussion of Results

Table 2.1 (see p. 12) contains results for a system where $t'_A = L'/c'_0 = 10^{-3}$s, and $\delta = 5$, so that dimensional frequencies can be considered. When $\omega' = 125$ Hz the response, shown in Fig. 2.1 (see pp. 13–16 for figures in this chapter) for $\widehat{P}_0/K \cos(\pi x/2)$ is bounded and is composed almost entirely of the purely axial mode and the $y$-independent part of the quasi-steady solution in (2.17). Beats are observed in Fig. 2.2 when $\omega' \approx 242$ Hz, the response arising primarily from the same modes as in the previously discussed case. Linear monotonic amplitude amplification is seen in Fig. 2.3 for the purely axial mode in (2.18) when $\omega' \approx 250$ Hz.

The bounded result in Fig. 2.4 for $\omega' \approx 2500$ Hz at $y = 0.1$ is primarily due to the purely axial mode in (2.15) but includes some small but important higher frequency response arising from $y$-dependent parts of the quasi-steady part of the solution.

Quite elongated beats are seen in Fig. 2.5 for $\omega' \approx 4992$ Hz, which arise from an interaction of the first oblique mode with the second mode in the quasi-steady solution. The modulation in the response is due to the purely axial wave.

Finally, when $\omega' \approx 5000$ Hz the amplified oblique mode in (2.19) is found in Fig. 2.6 at $y = 0.1$.

The results demonstrate that relatively simple boundary driven disturbances can produce a complex acoustic wave response in a semi-confined geometry. At or near the resonant driving frequencies explicit modal amplification occurs. Even in the case of beats, amplitudes can become large enough during the growth phase to render the perturbation approximation invalid. Clearly one must resort to a weakly nonlinear theory to describe acoustic evolution on a longer time.

Higher order linear acoustic theory shows that in addition to modal amplification arising from boundary driving, other sources of instability include quadratic and cubic acoustic wave interactions and refraction of the basic acoustics by the shear flow. The latter effect creates yet more wave complexity of the type described by Wang and Kassoy (1992a,b).

The results described here are limited by the simplified boundary condition at the open end of the geometry in (2.13) and by the lack of feedback between the transient wall injection and the pressure field, which could be described by a wall admittance function of some type. The pressure node boundary condition is of some importance because it implies that no work is done at the exit boundary. As a result the acoustic energy evolution in the cavity depends only upon the work done on the injection surfaces.

It is noted that the acoustic field does not satisfy the no-slip boundary conditions on the sidewalls. However that deficiency can be easily overcome by describing a weakly viscous boundary layer adjacent to the injection surfaces. This layer, resembling an injected Stokes boundary layer, is significantly thicker than a traditional acoustic boundary layer because the normal velocity arising from injection is "large" given the magnitude of $U'_m$ (e.g., $v'_{w0} \gg U'_m/R_e^{1/2}$). Price and Flandro (1991) have described limited aspects of this boundary layer structure. A related discussion occurs in Chapter 3 of this report.

Each of the limitations noted here will be examined in future endeavors. In particular, it is necessary to focuse on a fully interactive formulation of the model problem which includes a responsive thermally active boundary layer (Kassoy 1979) that mimics the effects of the combustion of solid propellant.

Table 2.1: Acoustic Response Properties for Several Forcing Frequencies

| $\omega$ | $\omega'$ (Hz) | Properties | Primary Response |
|---|---|---|---|
| $\pi/4$ | 125 | stable | axial + $y$-independent quasi-steady modes |
| $\pi/2 - 0.05$ | $\Delta\omega' \approx 8$ Hz | beats | (same) |
| $\pi/2$ | 250 | axial amplification | linear growth |
| $5\pi \approx \Omega_{10}/2$ | 2500 | stable | axial + smaller high frequency modes |
| $\Omega_{10} - 0.05$ | $\Delta\omega' \approx 8$ Hz | beats | first oblique mode + quasi-steady mode with axial wave modulation |
| $\Omega_{10}$ | 5000 | oblique amplification | linear growth of first oblique mode + axial wave modulation |

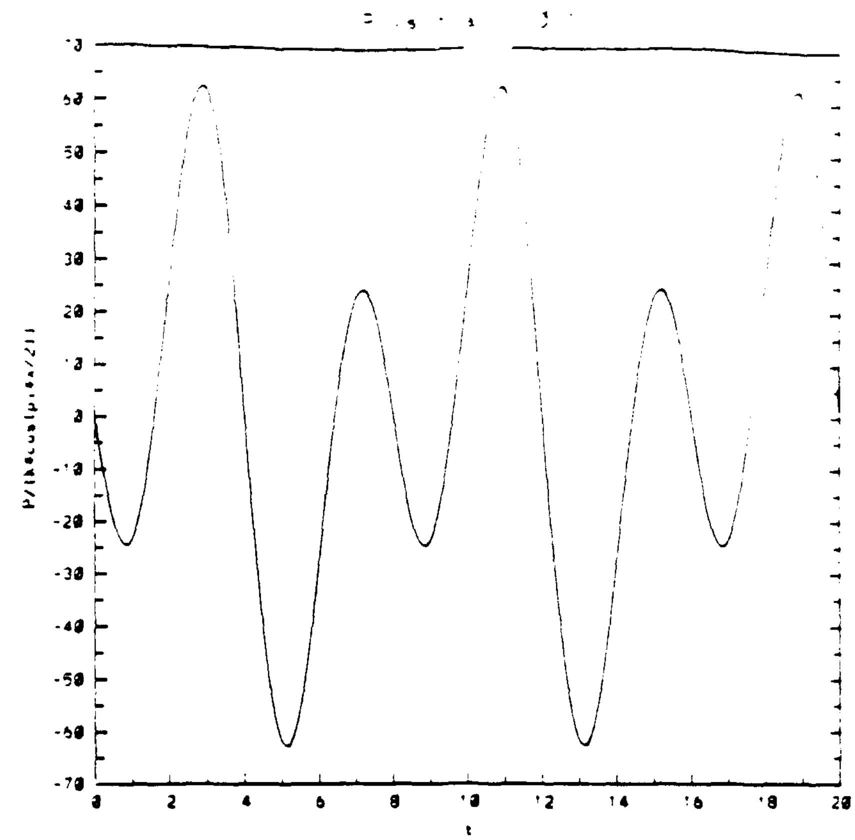

Fig. 2.1 The pressure-time response for w'=125Hz.

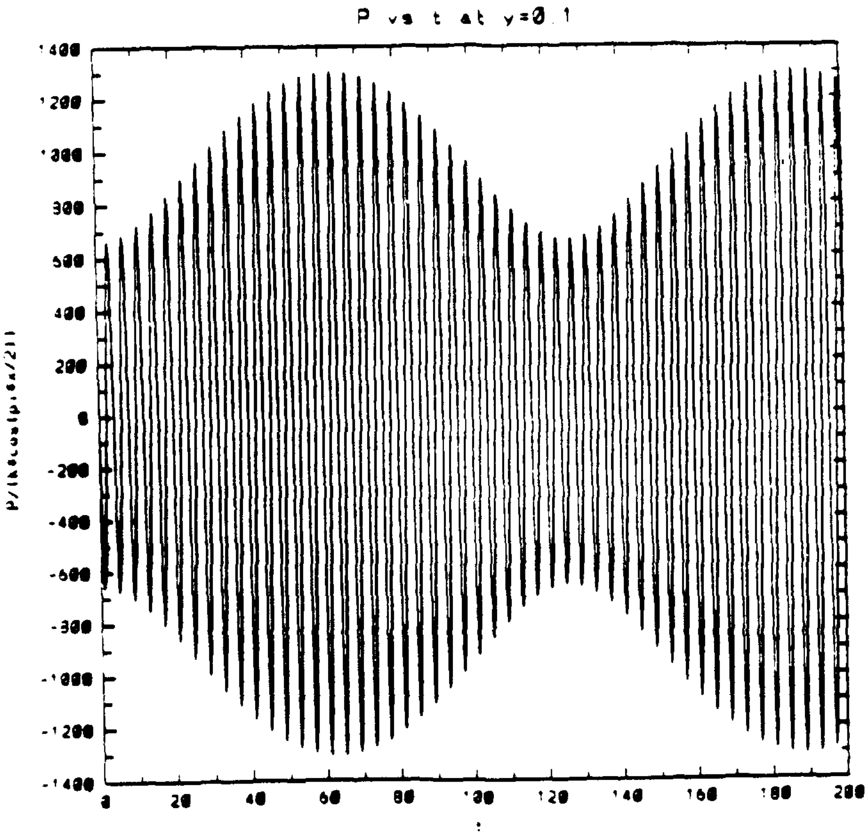


Fig. 2.2 The pressure-time response for w'=242HZ.

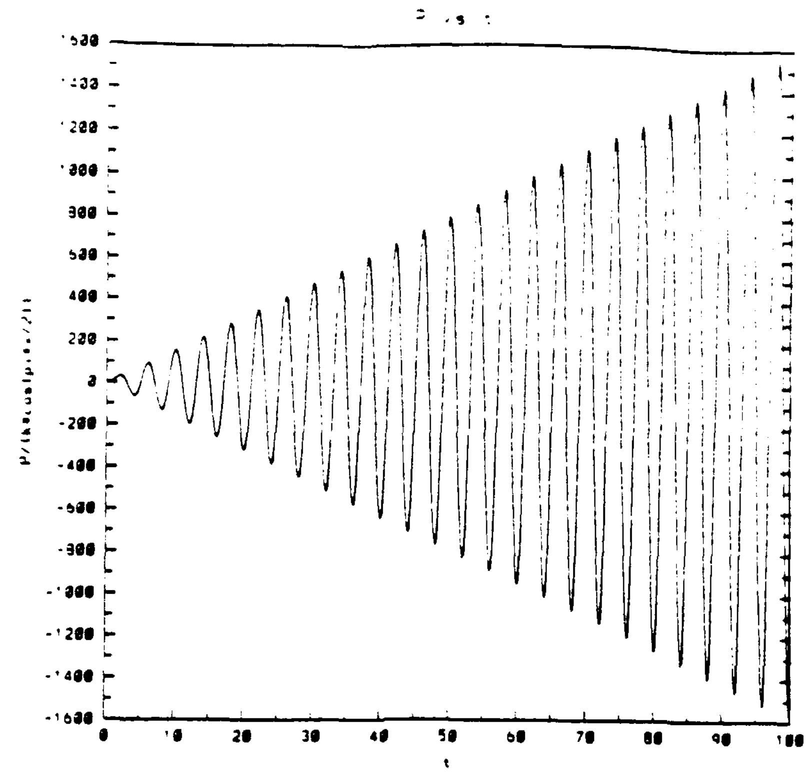


Fig. 2.3 The pressure-time response for w'=250Hz.

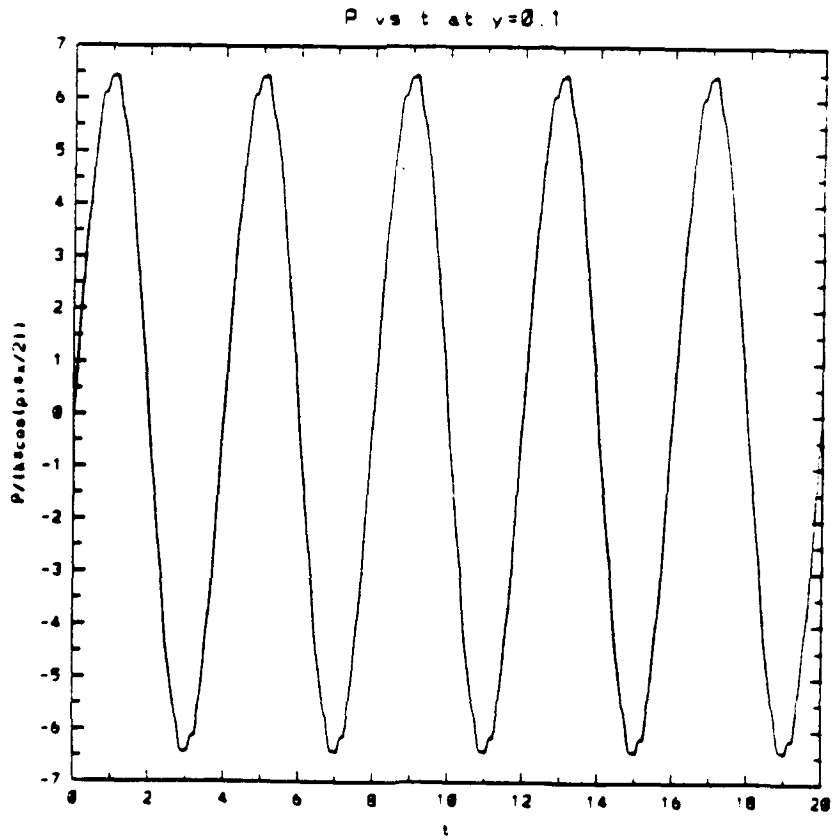


Fig. 2.4 The pressure-time response for w'=2500Hz.

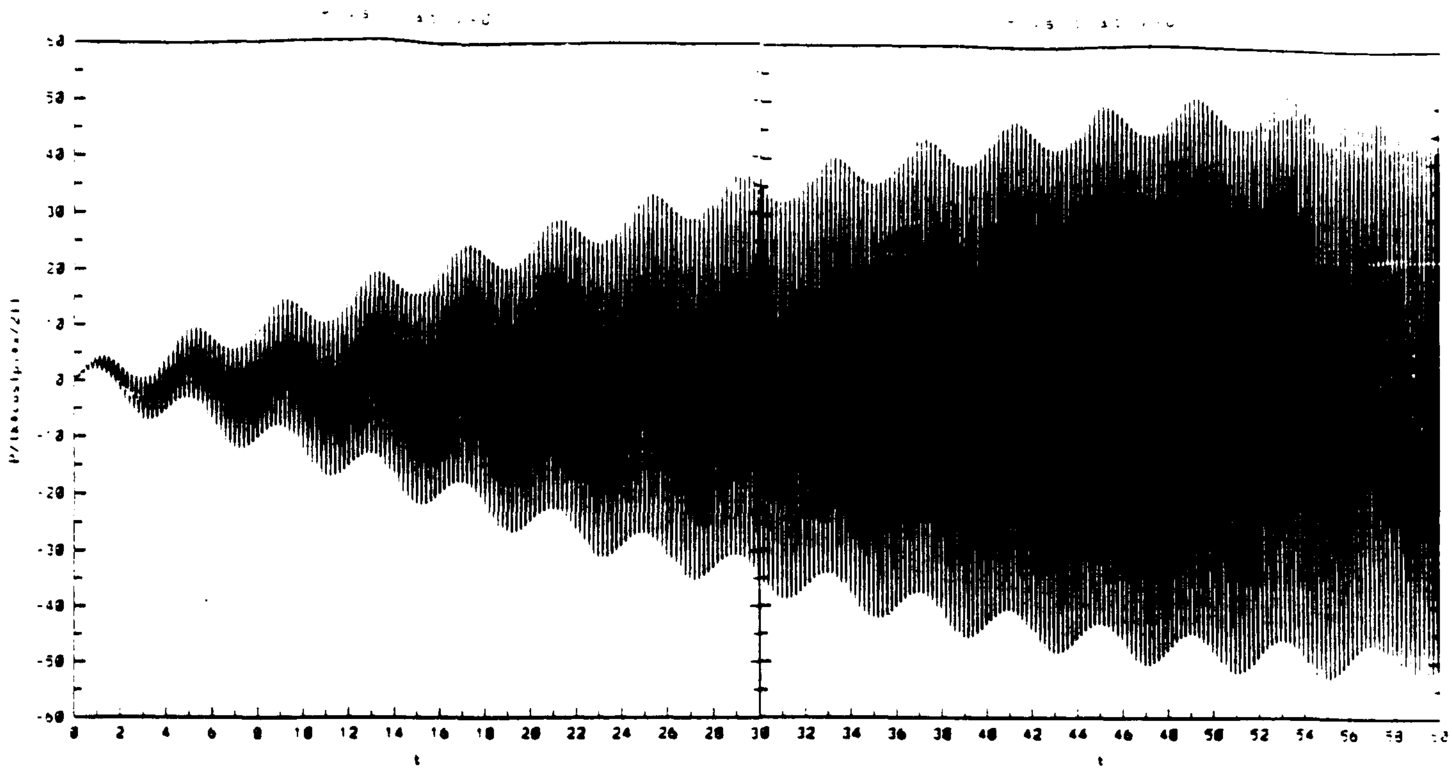


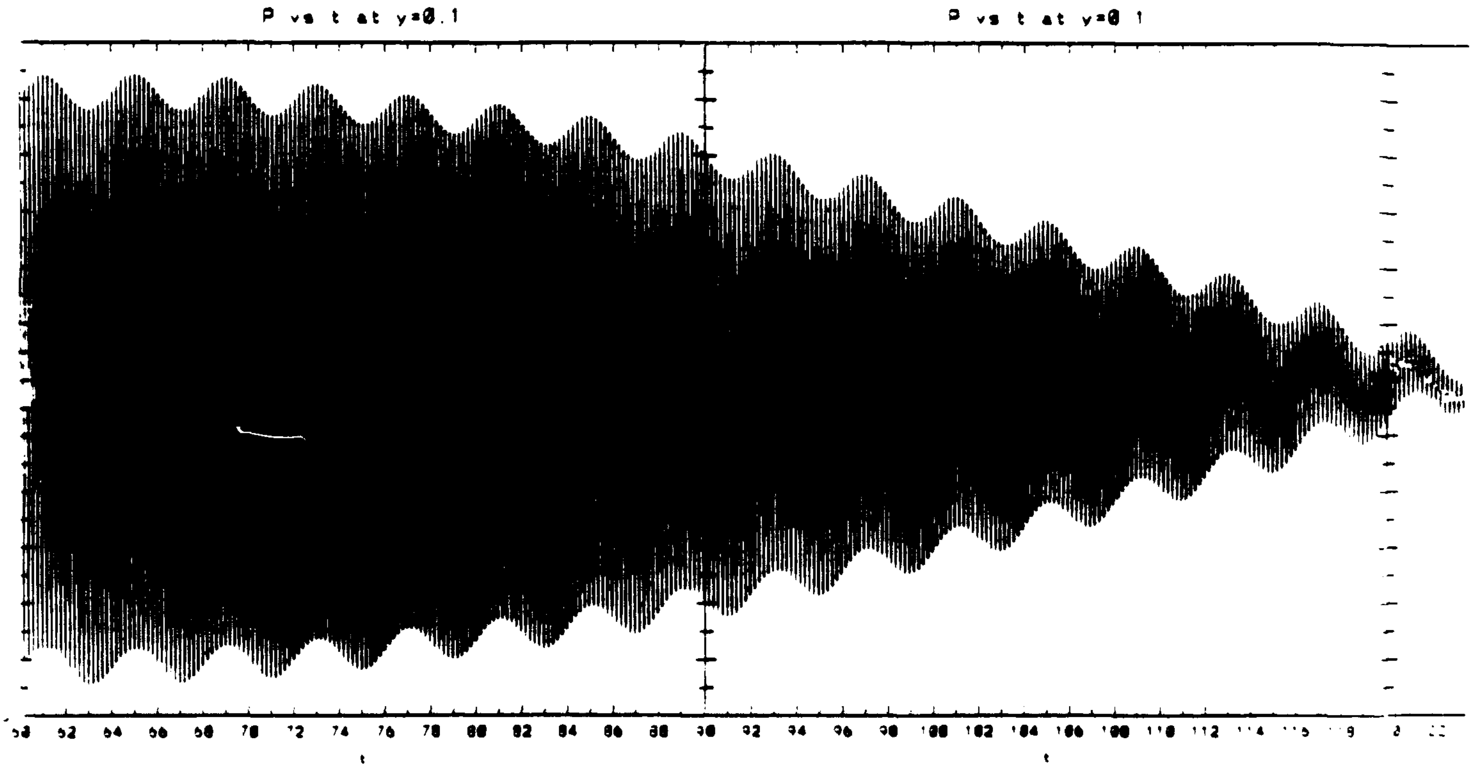


Fig. 2.5 The pressure-time response for w'=4992Hz.

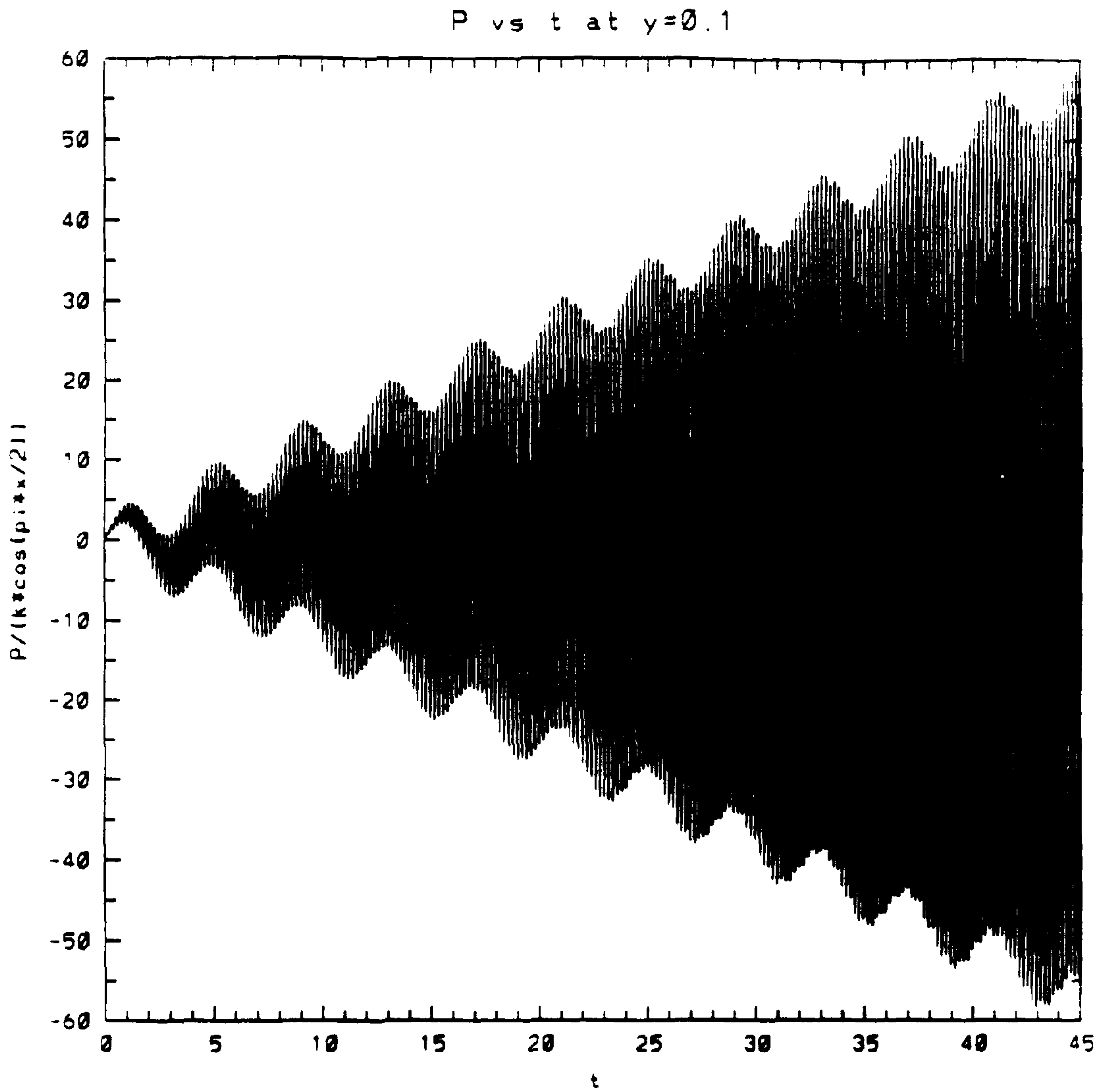


Fig. 2.6 The pressure-time response for w'=5000Hz.

# Chapter 3

# Acoustic Response to Boundary Disturbances in a Self-Induced Low Mach Number Shear Flow in a Cylinder

## 3.1 Problem Statement

Research has been conducted to study acoustic disturbances in a low Mach number ($M \ll 1$) internal flow within an open ended cylindrical chamber of length $L'$ and diameter $D'$. The mean flow is generated by prescribed side wall mass addition and the disturbances are introduced by either end wall transients or side wall injection transients. The objective of this initial-boundary value analysis is to find the complete acoustic response arising from boundary forcing, including all possible resonant modes.

## 3.2 Mathematical Model

Perturbation methods are used to derive the analytic form of the mathematical model. The complete set of fluid mechanics equations is nondimensionalized with respect to the characteristic scales of the variables describing the flow in the open ended cylindrical chamber with low Mach number ($M \ll 1$) and large Reynolds number ($Re \gg 1$).

$$\frac{\partial \rho}{\partial t} + M\left[\frac{1}{r}\frac{\partial(\rho r V_r)}{\partial r} + \frac{1}{r}\frac{\partial(\rho V_\theta)}{\partial \theta} + \frac{\partial(\rho V_z)}{\partial z}\right] = 0, \tag{3.1}$$

$$\rho\left[\frac{DV_r}{Dt} - M\frac{V_\theta^2}{r}\right] = -\delta^2\frac{1}{\gamma M}\frac{\partial P}{\partial r}, \tag{3.2}$$

$$\rho\left[\frac{DV_\theta}{Dt} + \frac{V_r V_\theta}{r}\right] = -\delta^2\frac{1}{\gamma M r}\frac{\partial P}{\partial \theta}, \tag{3.3}$$

$$\rho\frac{\partial V_z}{\partial t} = -\frac{1}{\gamma M}\frac{\partial P}{\partial z}, \tag{3.4}$$

$$\rho\frac{DT}{Dt} = -(\gamma - 1)MP\left[\frac{1}{r}\frac{\partial(rV_r)}{\partial r} + \frac{1}{r}\frac{\partial V_\theta}{\partial \theta} + \frac{\partial V_z}{\partial z}\right], \tag{3.5}$$

$$P = \rho T \tag{3.6}$$

where

$$\frac{D}{Dt} = \frac{\partial}{\partial t} + M\left(V_r\frac{\partial}{\partial r} + \frac{V_\theta}{r}\frac{\partial}{\partial \theta} + V_z\frac{\partial}{\partial z}\right).$$

The transport terms are neglected since $(\frac{L'}{D'})^2\frac{M}{Re} \ll 1$ for most of the situations. The axial velocity component is nondimensionalized with respect to $V'_{zm} = V'_w\delta$ where $\delta = \frac{L'}{D'}$. The azimuthal and radial velocities are nondimensionalized with respect to $V'_w$ which is the characteristic side wall injection speed. Time $t'$ is nondimensionalized with respect to axial acoustic time $t'_a = \frac{L'}{C'_0}$ where $C'_0$ is the characteristic sound speed. Parameters $M$ and $Re$ are defined with respect to $V'_{zm}$. The mathematical model can describe a combination of an inviscid rotational steady flow with a similar size acoustic flow. However, the description of viscous phenomena requires more general equation.

## 3.3 Steady State Flow

A steady state mean flow is generated by time independent mass addition at the side wall that mimics propellant burning. In the parameter range of $(\frac{D'}{L'})^2 Re \gg 1$, and $M \ll 1$, which means large side wall injection, all the variables are written in the following forms:

$$P_i = 1 + M^2 P_{i0}, \qquad V_i = V_{i0}, \qquad i = 1,2,3, \tag{3.7}$$

with $P_i$ representing pressure, density and temperature respectively and $V_i$ representing radial, azimuthal and axial velocity components respectively. The leading order equations and boundary conditions describe an inviscid rotational flow that satisfies the no-slip boundary conditions on the side wall. Analytical solutions for the radial and axial velocity, as well as the pressure distribution for $\frac{L'}{D'} \gg 1$ are:

$$V_{0r} = -\frac{V_m(z)}{r}\sin(\frac{\pi}{2}r^2), \quad V_{0z} = \pi\int_0^z V_m(\tau)d\tau\cos(\frac{\pi}{2}r^2), \tag{3.8}$$

$$P_0 = -\pi^2\gamma\int_0^z\int_0^t V_m(\tau)d\tau V_m(z)dz, \tag{3.9}$$

where $-V_m(z)$ is the time-independent side wall injection distribution. Related solutions can be found in Price and Flandro (1991). A similar analytic solution can be found for the case of constant side wall injection when $\frac{L'}{D'} = O(1)$. The flow field has to be obtained numerically for any other form of the side wall injection.

## 3.4 Leading Order and Higher Order Acoustics

A study is made of two common disturbance sources which cause an unsteady flow;

1. The $O(M)$ end wall disturbance for $\frac{L'}{D'} \gg 1$.

2. Transient $O(M)$ side wall injection for $\frac{L'}{D'} = 1$.

The asymptotic expansions for all the variables are:

$$P_i = 1 + M(P_{i0} + MP_{i1}), \qquad V_i = V_{i0} + MV_{i1}, \quad i = 1,2,3, \tag{3.10}$$

where $P_i$ represent thermodynamic variables and $V_i$ represent the velocity components in $r, \theta, z$ direction respectively.

### 3.4.1 End Wall Effects: $\frac{L'}{D'} \gg 1$

#### Leading Order Solution

The unsteady part of the leading order equations can be combined into a planar wave equation in terms of the axial velocity component:

$$\frac{\partial^2 \tilde{V}_{z0}}{\partial t^2} = \frac{\partial^2 \tilde{V}_{z0}}{\partial z^2} \tag{3.11}$$

The corresponding initial and boundary conditions are given by

$$t = 0, \quad \tilde{V}_{z0} = 0, \quad \frac{\partial \tilde{V}_{z0}}{\partial t} = 0, \tag{3.12}$$

$$z = 0, \quad \tilde{V}_{z0} = \sin \omega t; \tag{3.13}$$

$$z = 1, \quad \frac{\partial \tilde{V}_{z0}}{\partial z} = 0. \tag{3.14}$$

It is assumed that the endwall boundary conditions are independent of $r$ and $\theta$.

The simplicity of the equation can be attributed to the large $\frac{L'}{D'}$ ratio. The prescribed velocity at $z = 0$ has a magnitude similar to the mean axial flow velocity. The boundary condition at the exit is derived from a condition of zero pressure perturbation there.

The general solution for $\tilde{V}_{z0}$ is :

$$\begin{aligned} \tilde{V}_{z0}(z,t) &= \sin \omega t \\ &+ \sum_{n=0, n\neq n^*}^{\infty} \left\{ -\frac{2\omega}{b_n^2} \left[ \left( \frac{b_n^2}{b_n^2 - \omega^2} \right) \sin(b_n t) - \frac{b_n \omega}{b_n^2 - \omega^2} \sin(\omega t) \right] \right\} \sin(b_n z) \\ &- \left\{ \left( \frac{1}{b_{n^*}} \right) \sin(b_{n^*} t) + t \cos(b_{n^*} t) \right\} \sin(b_{n^*} z), \end{aligned} \tag{3.15}$$

where $b_n = (n + \frac{1}{2})\pi$, and the last term represents a resonant effect present only when $\omega = b_{n^*}$. A careful look into the solution provides us with some insight into the properties of the acoustical flow.

- The first term itself and the second part of the nonresonant Fourier series represent quasi-steady motion oscillating at the driving frequency. The other Fourier series terms can be decomposed into two counter-propagating planar travelling waves.

- If the driving frequency $\omega$ equals none of the natural frequencies $b_n$, the solution is bounded. If $\omega$ is very close to one of those natural frequencies, then beat will appear due to the interaction between the quasi-steady motion and one pair of travelling waves.

- Resonance occurs if $\omega$ is equal to one of the $b_n$, and the amplitude of one mode grows linearly with time.

### Discussion of Results

Table 3.1 contains results for a system where $t'_A = \frac{L'}{C'_0} = 10^{-3}$ s so that dimensional frequencies can be considered. When $\omega' \approx 159$ Hz, the response shown in Fig. 3.1 (see pp. 33–35 for figures in this chapter) for $\tilde{V}_{z0}$ is bounded, and the contributions are mainly from the first harmonic term and the first few Fourier modes in (3.15). Beats are observed in Fig. 3.2 where $\omega' \approx 238$ Hz, due to the interaction between the quasi-steady modes and the first axial mode. The period of the beat is approximately 90 s. The linear monotonic amplitude growth seen in Fig 3.3 is primarily due to the resonant axial mode in (3.15) when $\omega' = 250$ Hz.

Table 3.1: Acoustic Response Properties for Several Driving Frequencies

| $\omega$ | $\omega'$(Hz) | Properties | Primary Response |
|---|---|---|---|
| 1 | 159 | stable | axial + quasi-steady modes |
| 1.5 | 238 | beats | quasi-steady modes<br>with axial wave modulation |
| $\pi/2$ | 250 | axial amplification | linear growth |

### Boundary Layer Correction

The leading order core acoustic solution does not satisfy the no-slip boundary condition. A viscous layer adjacent to the walls with multiple scale structure is needed to accom. date the no-slip boundary condition at the side wall. Experimental data (Price and Flandro 1991) implies that the viscous damping thickness is large compared to the scale of spatial oscillation within the thin layer. A multiple scale perturbation scheme based on the thickness of the boundary layer and the characteristic spatial length of the oscillation inside the boundary layer is carried out. The acoustic solution in the core provides an outer boundary condition and the no-slip condition on the side wall provides an inner boundary condition .

The leading order acoustic core solution shows that all the terms can be classified into the following two forms: $\bar{V}(z)e^{i\Omega t}$ with $\Omega = \omega$ or $b_n$, or $-t\cos(b_n t)\sin(b_n z)$.

The viscous layer solution for the outer boundary condition $V_{z0} = \bar{V}(z)e^{i\Omega t}$ is of the following form:

$$V_{z0}(\xi, \eta, z, t) = -\bar{V}(z)\left\{\exp\left[-\frac{\bar{\mu}\Omega^2}{V_w^3(z)}\eta - \frac{i\Omega}{(V_w(z))}\xi\right] - 1\right\} e^{i\Omega t}, \qquad (3.16)$$

where $-V_w(z)$ is the steady side wall injection velocity, $\bar{\mu}$ is the dimensionless viscosity.

The variable $m$ describing spatial oscillations within the viscous layer and $n$ describing viscous layer thickness are defined as:

$$\xi = \frac{1-r}{\alpha}, \qquad \eta = \frac{1-r}{\beta} \tag{3.17}$$

where $\alpha = M$ and $\beta = Re(\frac{D'}{2L'})^2 M^2$. The solution corresponding to resonant outer boundary condition $V_{z0} = -t\cos(b_n t)\sin(b_n z)$ is:

$$\begin{aligned} V_{z0}(\xi,\eta,z,t) &= -t\sin(b_n z)\sin(b_n t) \\ &+ \{t\sin(k\xi)\sin(b_n t) + b_n t\cos(k\xi)\cos(b_n t) \\ &- \left[\frac{\bar{\mu}\eta}{(1+b_n)}\cos(k\xi) + \frac{b_n\xi}{2k^2(1+b_n)}\sin(k\xi)\right]\sin(b_n t) \\ &-\frac{1}{\omega}\left[\frac{V_w^2(z)}{2(1+b_n)}\xi\cos(k\xi) - \left(1 - \frac{\bar{\mu}b_n^2}{1+b_n}\right)\sin(k\xi)\right] \\ &\cos(b_n t)\}\,\frac{1}{b_n}\sin(b_n z)e^{-\frac{\bar{\mu}k^2}{V_w(z)}\eta} \end{aligned} \tag{3.18}$$

where $k = \frac{b_n}{V_w(z)}$.

When $\xi = \eta = 0$, the solutions satisfy the no-slip boundary condition on the wall. On the other hand, when $\xi$ and $\eta \to \infty$, the core solution is recovered in an oscillatory manner since the amplitude of the exponential term goes to zero harmonically. The effective thickness of the boundary layer depends strongly on $\Omega$ and $V_w$. When $\Omega$ gets large, this thickness will become small. For $\Omega = \omega$, if $\omega$ is small, the viscous effect will penetrate deep into the core region; if $\omega$ is large, the viscous effect will be confined in a very thin layer near the side wall. The same effect can be expected for $\Omega = b_n$. Thus the boundary layer thickness is smaller for higher order modes. On the other hand increasing the value of $V_w(z)$ enhances the overall boundary layer thickness.

The theory is valid only for $\Omega^2 \gg V_w^3\beta$ where $\beta \ll 1$. If $\beta$ becomes as large as of O(1) or $\Omega$ is small, then a new multiple scale perturbation technique is needed to find solutions where weak viscous effects fill the entire chamber. This is one of the future research topics.

### Higher Order Acoustics

The $O(M^2)$ equations can be rearranged in terms of $V_{r1}$,$V_{z11}$,$V_{z12}$ and $P_1$, where $V_{r1} = V_{r1}(z,r,t)$, $V_{z1} = V_{z11}(z,t) + V_{z12}(z,r,t)$.

$$\frac{\partial V_{z12}}{\partial t} = g_1(r,z,t), \tag{3.19}$$

$$\frac{1}{r}\frac{\partial(rV_{r1})}{\partial r} = g_2(r,z,t), \tag{3.20}$$

$$\frac{1}{\gamma}\frac{\partial P_1}{\partial t} + \frac{\partial V_{z11}}{\partial z} = f_1(z,t), \tag{3.21}$$

$$\frac{1}{\gamma}\frac{\partial P_1}{\partial z} + \frac{\partial V_{z11}}{\partial t} = f_2(z,t), \tag{3.22}$$

$$P_1 = P_1(z,t) \tag{3.23}$$

where

$$\begin{aligned}
g_1(r,z,t) &= V_{zss}\frac{\partial V_{z0}}{\partial z} \\
g_2(r,z,t) &= \frac{\gamma-1}{2}\frac{\partial \rho_0^2}{\partial t} - V_{zss}\frac{\partial \rho_0}{\partial z} - \frac{\partial V_{z12}}{\partial z} \\
f_1(z,t) &= -\frac{1}{2}\frac{\partial \rho_0^2}{\partial t} - \tilde{V}_{z0}\frac{\partial \rho_0}{\partial z} \\
f_2(z,t) &= -\left[\rho_0\frac{\partial \tilde{V}_{z0}}{\partial t} + \tilde{V}_{z0}\frac{\partial(V_{zss}+\tilde{V}_{z0})}{\partial z} + V_{r0}\frac{\partial V_{zss}}{\partial r} + V_{zss}\frac{\partial V_{zss}}{\partial z}\right].
\end{aligned} \tag{3.24}$$

The initial and boundary conditions are:

$$t = 0, \quad V_{r1} = 0; \quad V_{z1}(z,r,t) = P_1(z,t) = 0, \tag{3.25}$$

$$r = 1, \quad V_{r1} = 0, \tag{3.26}$$

$$z = 0, \quad V_{z1} = 0, \tag{3.27}$$

$$z = 1, \quad P_1 = 0. \tag{3.28}$$

In addition, $V_{r1}$,$V_{z1}$ are required to be finite at $r = 0$.

Unlike the previous lower order acoustic solutions, the radial and axial velocities for this order depend on the radial variable as well as on $z$ and $t$, the result of refraction of the leading order acoustic planar waves by the steady state mean shear flow (Wang and Kassoy 1992a). The driving functions $g_1$(r,z,t) and $g_2(r, z, t)$ include the products of mean flow terms and acoustic terms, and quadratic acoustic wave interaction terms. The latter provide a source for acoustic instabilities in addition to boundary driving sources. This issue will be addressed and discussed in the later part of the report.

### Comments

This study of the acoustic response of an internal flow in a cylinder to $O(M)$ simple harmonic velocity oscillations at the end wall reveals that significant boundary forcing, as large in magnitude as the basic internal flow will cause numerous travelling wave modes as well as a quasi-steady flow motion. Although the quasi-steady motion is predominant for many frequencies, the planar travelling waves can grow significantly if the driving frequency is close enough to any of the natural frequencies. Beats can be seen under those conditions. Resonance will occur in the limiting cases. Higher order acoustic analyses show that in addition to the boundary forcing sources, interactions between the steady mean flow and leading order acoustic waves, and interactions between leading order acoustic modes provide other sources for acoustic instability.

When resonance occurs or beats appear for some cases, the linear study is no longer valid. A weakly nonlinear formulation of the problem is needed because the perturbations are not small for sufficiently long time. Detailed discussion is deferred to later sections.

### 3.4.2 Transient Side Wall Injection: $\frac{L'}{D'} = O(1)$

#### Leading Order Solution

In this case, the end wall velocity is zero and an $O(M)$ transient side wall injection is superimposed on a similar magnitude steady state side wall injection. The induced leading order acoustical flow field in the core is described by the following multi-dimensional wave equation and initial boundary conditions :

$$\frac{\partial^2 P_0}{\partial t^2} = \frac{\partial^2 P_0}{\partial r_1^2} + \frac{1}{r_1}\frac{\partial P_0}{\partial r_1} + \frac{1}{r_1^2}\frac{\partial^2 P_0}{\partial \theta^2} + \frac{\partial^2 P_0}{\partial z^2}, \tag{3.29}$$

$$t = 0, \qquad P_0 = P_{0t} = 0, \tag{3.30}$$

$$0 \le \theta < 2\pi, \qquad P_0(\theta) = P_0(\theta + 2\pi) \tag{3.31}$$

$$r = 0, \qquad |P_0| < \infty, \tag{3.32}$$

$$r_1 = \frac{1}{2\delta}, \qquad \frac{\partial P_0}{\partial r_1} = \delta f(z, \theta, t), \tag{3.33}$$

$$z = 0, \qquad P_{0z} = 0, \tag{3.34}$$

$$z = 1, \qquad P_0 = 0. \tag{3.35}$$

The solution for a general positive transient side wall injection distribution has the following form:

$$\begin{aligned} P_0(r_1, \theta, z, t) &= r_1 \delta f(z, \theta, t) \\ &+ \sum_{l=1}^{\infty}\sum_{m=0}^{\infty}\sum_{n=1}^{\infty}[A_{lmn}(t)\cos m\theta + B_{lmn}(t)\sin m\theta] J_m(\omega_{mn} r_1)\cos(\frac{2l-1}{2})\pi z, \end{aligned} \tag{3.36}$$

where $\omega_{mn}$ satisfy $\frac{dJ_m}{dr_1}(\frac{\omega_{mn}}{2\delta}) = 0$ and $r_1 = \frac{r}{\delta}$. The time dependent coefficients $A_{lmn}(t)$ and $B_{lmn}(t)$ are determined by the system:

$$\frac{d^2 A_{lmn}(t)}{dt^2} + K_{lmn}^2 A_{lmn}(t) = F_{lmn}, \tag{3.37}$$

$$t = 0, \qquad A_{lmn} = g_{Almn}(0); \qquad \frac{\partial A_{lmn}}{\partial t} = g'_{Almn}(0), \tag{3.38}$$

$$\frac{d^2 B_{lmn}(t)}{dt^2} + K_{lmn}^2 B_{lmn}(t) = G_{lmn}, \tag{3.39}$$

$$t = 0, \quad B_{lmn} = g_{Blmn}(0); \quad \frac{\partial B_{lmn}}{\partial t} = g'_{Blmn}(0), \tag{3.40}$$

where $K_{lmn}^2 = (\frac{2l-1}{2}\pi)^2 + \omega_{mn}^2$. $F_{lmn}$, $G_{lmn}$, $g_{Almn}(0)$, $g'_{Almn}(0)$, $g_{Blmn}(0)$ and $g'_{Blmn}(0)$ are quantities that are found from products of Fourier series expansions of each dependent variable.

If $f(z,t) = \cos(\frac{\pi}{2}z)\sin(\omega t)$ is chosen to describe an axial distributed positive transient component of the side wall injection which is superimposed on the steady distribution of the same magnitude, then the solutions are:

- Nonresonant case: $\omega \neq k_n$ for all positive integer $n$,

$$\begin{aligned} P_0 \; = \; & \underbrace{\left[r_1\delta + \frac{f_1}{(\frac{\pi}{2})^2 - \omega^2} + \sum_{n=2}^{\infty}\left(\frac{f_n}{k_n^2 - \omega^2}\right) J_0(\omega_{0n} r_1)\right] \cos(\frac{\pi}{2}z)\sin(\omega t)}_{quasi-steady\ modes} \\ & \underbrace{+\frac{2}{\pi}\left(g_1 - \frac{f_1\omega}{(\frac{\pi}{2})^2 - \omega^2}\right)\sin(\frac{\pi}{2}t)\cos(\frac{\pi}{2}z)}_{axial\ mode} \\ & \underbrace{+\sum_{n=2}^{\infty}\left[\frac{1}{k_n}\left(g_n - \frac{f_n\omega}{k_n^2 - \omega^2}\right)\right]\sin(k_n t)\cos(\frac{\pi}{2}z)J_0(\omega_{0n} r_1)}_{oblique\ modes}. \end{aligned} \tag{3.41}$$

  The first term represents the quasi-steady response of the gas to the boundary forcing; the second term can be rewritten as a pair of counter propagating purely axial travelling waves; and finally, each of the oblique modes can be rewritten as a pair of oblique travelling waves.

- Resonant case:

  1. $\omega = \frac{\pi}{2}$ (axial resonant modes),

$$P_0 = -\frac{f_1}{\pi}t\cos(\frac{\pi}{2}t)\cos(\frac{\pi}{2}z) + \ldots \tag{3.42}$$

where the dots represent the remaining bounded quasi-steady and oblique modes.

2. $\omega = k_{n^*}$, $k_n = \sqrt{(\frac{\pi}{2})^2 + \omega_{0n}^2}$

$$P_0 = -\frac{f_{n^*}}{2\omega} t \cos(\omega t) J_0(\omega_{0n^*} r_1) \cos(\frac{\pi}{2} z) + \ldots, \tag{3.43}$$

with the dots representing the remaining bounded quasi-steady axial and oblique modes.

## Discussion of Results

Table 3.2 contains results for a system where $t_A^{'} = \frac{L^{'}}{C_0^{'}} = 10^{-3}$ s $\delta = 5$ so that dimensional frequencies can be considered. When $\omega^{'} \approx 159$ Hz, the response shown in Fig. 3.4 for $\tilde{V}_{z0}$ is bounded and the main contributions are from the first harmonic oscillation term, the first few axial modes and quasi-steady solution in (3.41). Beats are observed in Fig. 3.5 when $\omega^{'} \approx 238$ Hz. The period of the beat is about 90 s due to the interaction between the quasi-steady modes and the axial mode. Linear monotonic amplitude growth is seen in Fig. 3.6 for the first axial mode in (3.42) when $\omega^{'} = 250$ Hz. Higher forcing frequencies will activate the oblique modes, and similar phenomena as just discussed can be observed if certain range of forcing frequencies are picked.

A more detailed discussion of related solutions for acoustics in an open ended rectangle can be found in Chapter 2.

Table 3.2: Acoustic Response Properties for Several Driving Frequencies

| $\omega$ | $f'$(Hz) | Properties | Primary Response |
|---|---|---|---|
| 1 | 159 | stable | axial + quasi-steady modes |
| 1.5 | 238 | beats | quasi-steady modes<br>with axial wave modulation |
| $\pi/2$ | 250 | axial amplification | linear growth |

### Higher Order Solutions

The higher order analysis is done to discover new sources of acoustic instability above and beyond those arising from the boundary driving resonance just described. The equation system for the higher order pressure is:

$$\frac{\partial^2 P_1}{\partial t^2} = \frac{\partial^2 P_1}{\partial r_1^2} + \frac{1}{r_1}\frac{\partial P_1}{\partial r_1} + \frac{1}{r_1^2}\frac{\partial^2 P_1}{\partial \theta^2} + \frac{\partial^2 P_1}{\partial z^2} + F^1(r, \theta, z, t), \tag{3.44}$$

$$t = 0, \qquad P_1 = P_{1t} = 0, \tag{3.45}$$

$$0 \le \theta < 2\pi, \qquad P_1(\theta) = P_1(\theta + 2\pi), \tag{3.46}$$

$$r_1 = 0, \qquad |P_1| < \infty, \tag{3.47}$$

$$r_1 = \frac{1}{2\delta}, \qquad \frac{\partial P_1}{\partial r_1} = W_1(\theta, z, t), \tag{3.48}$$

$$z = 0, \qquad \frac{\partial P_1}{\partial z} = W_2(r_1, \theta, t), \tag{3.49}$$

$$z = 1, \qquad P_1 = 0. \tag{3.50}$$

There are two nonzero boundary conditions at $r_1 = \frac{1}{2\delta}$ and $z = 0$ respectively.

The solution will have the same general form as the leading order acoustic solution:

$$P_1(r_1,\theta,z,t) = X(r_1,\theta,z,t)$$
$$+\sum_{l=1}^{\infty}\sum_{m=0}^{\infty}\sum_{n=1}^{\infty}[A^1_{lmn}(t)\cos m\theta + B^1_{lmn}(t)\sin m\theta]J_m(\omega_{mn}r)\cos(\frac{2l-1}{2})\pi z \quad (3.51)$$

where

$$\frac{d^2A^1_{lmn}(t)}{dt^2} + K^2_{lmn}A^1_{lmn}(t) = F^1_{lmn}, \quad (3.52)$$

$$t=0, \quad A^1_{lmn} = g^1_{Almn}(0), \quad \frac{\partial A^1_{lmn}}{\partial t} = g^{1'}_{Almn}(0); \quad (3.53)$$

$$\frac{d^2B^1_{lmn}(t)}{dt^2} + K^2_{lmn}B^1_{lmn}(t) = G^1_{lmn}, \quad (3.54)$$

$$t=0, \quad B^1_{lmn} = g^1_{Blmn}(0), \quad \frac{\partial B^1_{lmn}}{\partial t} = g^{1'}_{Blmn}(0); \quad (3.55)$$

$$K^2_{lmn} = (\frac{2l-1}{2}\pi)^2 + \omega^2_{mn}. \quad (3.56)$$

$F^1_{lmn}$, $G^1_{lmn}$, $g^1_{Almn}(0)$, $g^1_{Almn}(0)$, $g^1_{Blmn}(0)$ and $g^{1'}_{Blmn}(0)$ are quantities that are found from products of Fourier series expansions of each dependent variable.

The forcing functions $F^1_{lmn}$ and $G^1_{lmn}$ are the keys to the solution forms of $A^1_{lmn}$ or $B^1_{lmn}$. Resonant growth will occur if $F^1_{lmn}$ or $G^1_{lmn}$ contain any time dependent harmonic functions which have the same frequencies as the natural frequencies. Beats will occur if forcing frequencies are very close to the natural frequencies.

- Nonresonant leading order $\omega \neq K_{lmn}$.

  The forcing functions $F^1_{lmn}$ and $G^1_{lmn}$ contain (a) numerous terms that are products of steady mean flow terms and the leading order acoustic terms. The latter consist of numerous nonresonant modes having the same frequencies as the natural frequencies; (b) quadratic products of the leading order acoustic terms and terms which will cause $O(t)$ growth for 1st order acoustic modes if the sum or the difference of the two leading frequencies or the boundary driving frequency and the leading frequency are equal to one of the natural frequencies. This $O(t)$ growth is not from boundary forcing directly.

- Resonant leading order acoustics $\omega = K_{lmn}$.

  In this case, the leading order solution contains both resonant mode and non-resonant modes. Sources for the time dependent growth of the first order modes can be either refraction phenomena or quadratic modal interactions:

  1. The highest growth rate for the amplitude of the first order acoustic mode is $O(t^2)$ for refraction generated disturbances.

  2. For quadratic modes the contribution to the largest possible growth rate of the first order acoustics can be divided into two categories. The first is from the product of one nonresonant mode and one resonant mode which leads to $O(t^2)$ growth if the sum or the difference of the resonant frquency and the nonresonant frequency are equal to any of the natural frequencies. The second is from the product of two resonant acoustic modes. The consequence is that the first order acoustic modes have at least $O(t^2)$ growth for many frequencies or even $O(t^3)$ growth if one of the natural frequencies is twice any of the other natural frequencies .

The conclusion from the higher order analysis provides the important slow time scales of different conditions so that weakly nonlinear analyses can be carried out properly in the future research.

### Comments

The analysis of the acoustic response of a low Mach number, injection induced flow to large side wall mass transients has been done for the inviscid core region only. A viscous boundary layer is required to accommodate the no-slip boundary condition on the side walls. The general procedure for studying the viscous layer is similar to that used for end wall case.

A weakly nonlinear study of the acoustic core response is of the primary interest because the results will predict the proper long time behavior of the disturbance evolution and these nonlinear core results will provide the correct outer boundary conditions needed for the viscous layer analysis on the longer time scale.

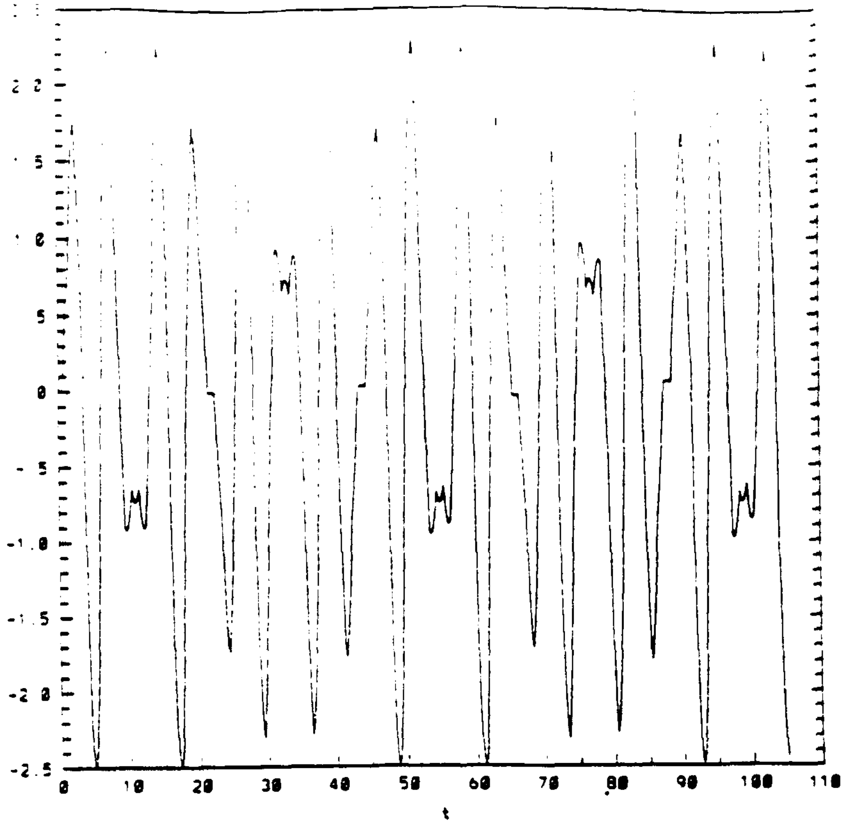

Figure 3.1 Time variation of axial acoustic velocity ($\omega' \approx 159$ Hz, nonresonant).

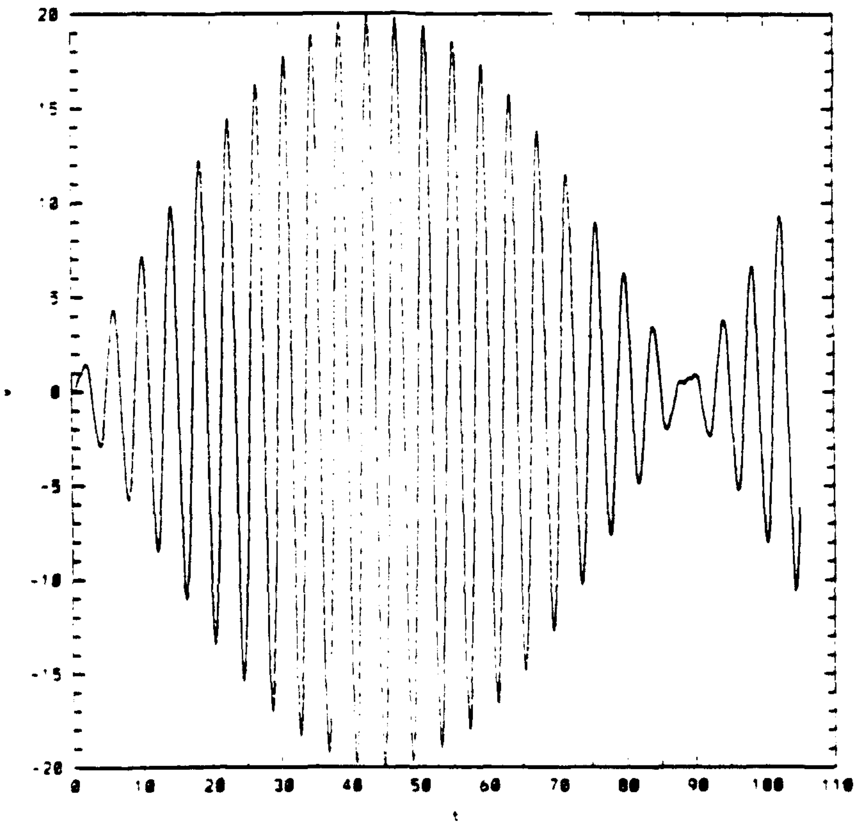

Figure 3.2 Time variation of axial acoustic velocity ($\omega' \approx 238$ Hz, beat).

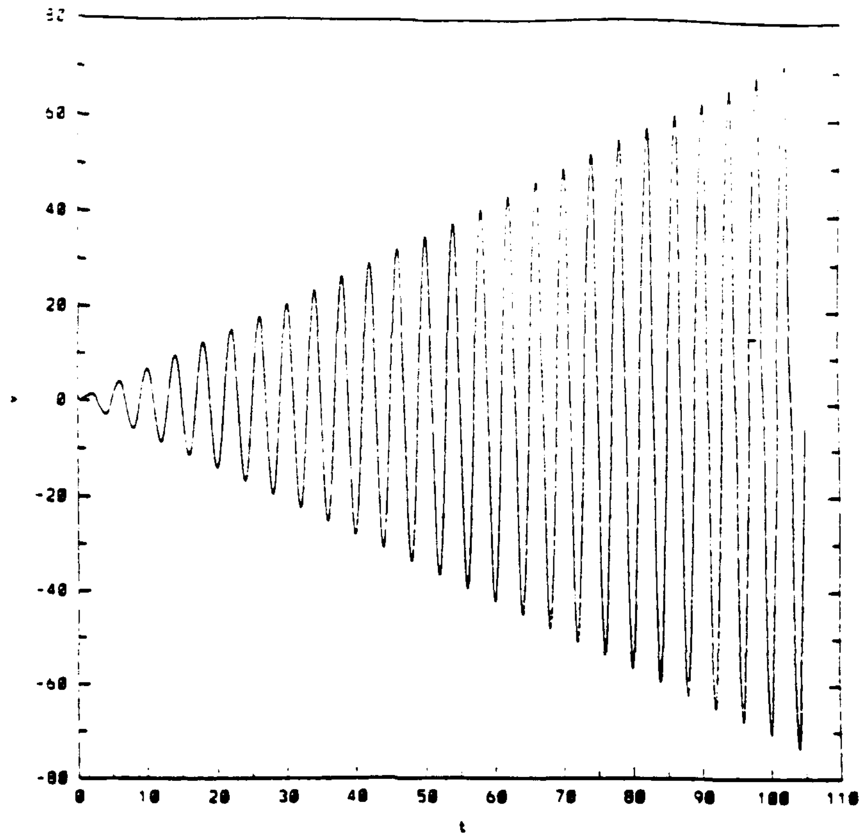

Figure 3.3 Time variation of axial acoustic velocity ($\omega' = 250$ Hz, resonant).

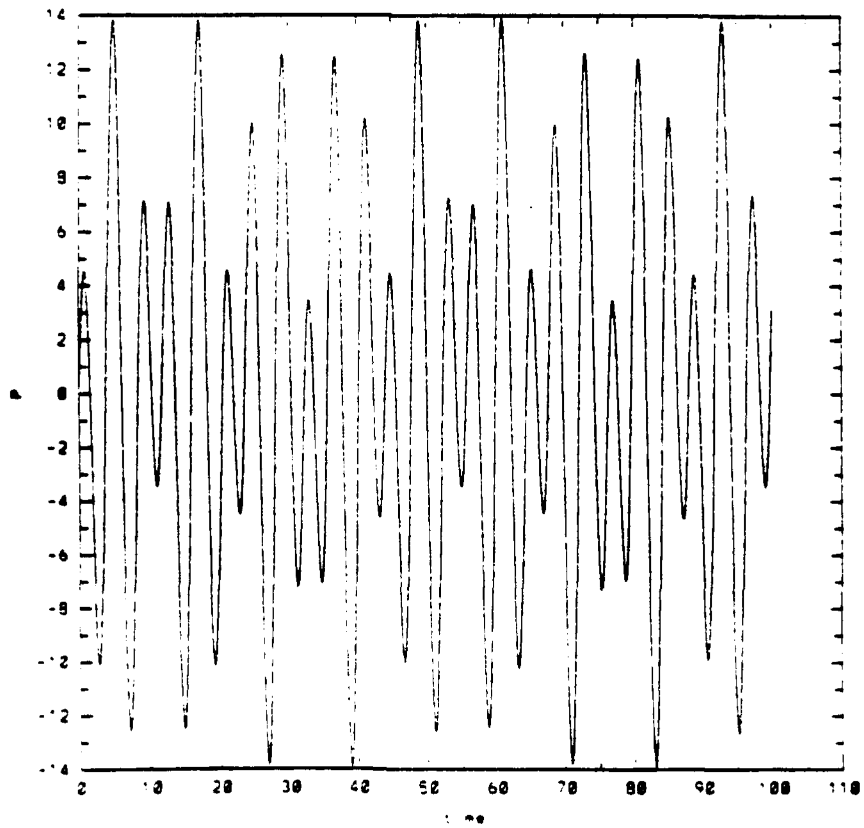

Figure 3.4 Time variation of acoustic pressure ($\omega' \approx 159$ Hz, nonresonant).

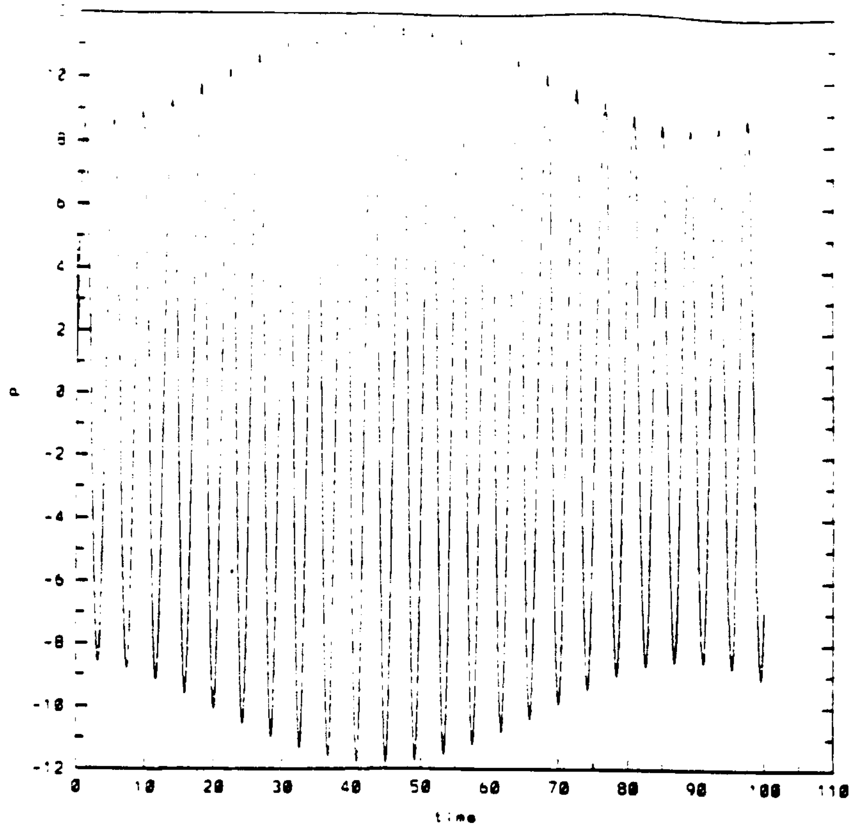

Figure 3.5 Time variation of acoustic pressure ($\omega' \approx 238$ Hz, beat).

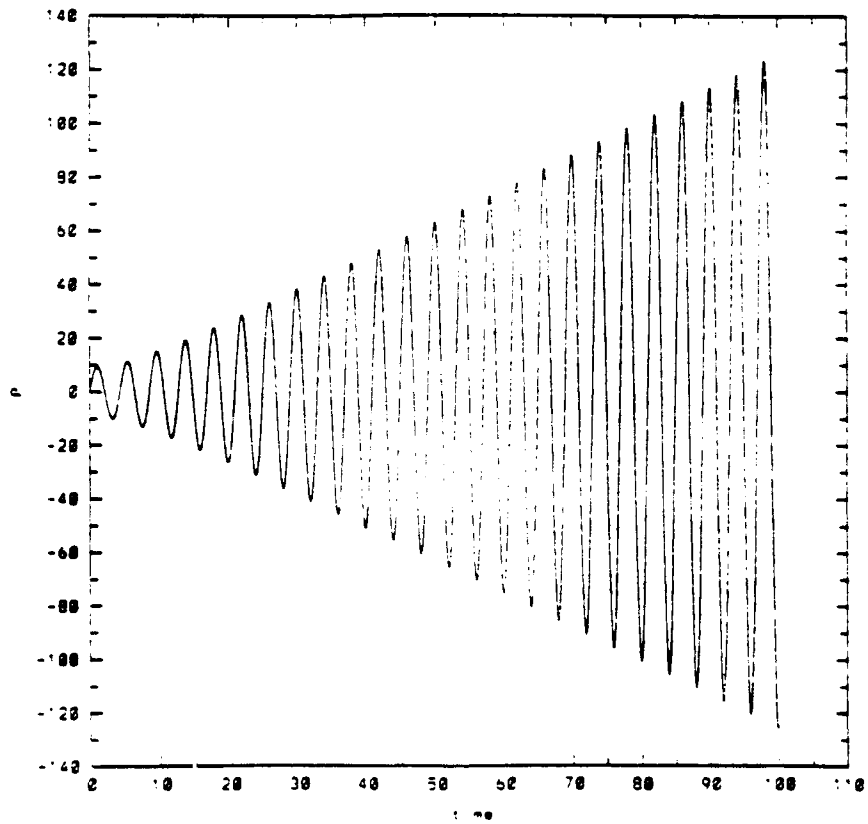

Figure 3.6 Time variation of acoustic pressure ($\omega' = 250$ Hz, resonant).

# Chapter 4

# Effect of Boundary Properties on Resonant Acoustic Oscillations

## 4.1 Motivation

Traditional studies of acoustic instability in solid rocket engines are based upon the concept of normal mode expansion (e.g., Culick 1990; Price and Flandro 1991). Acoustic wave systems are represented mathematically in terms of superpositions of eigenfunctions for a closed chamber with rigid walls. Such a representation ignores the effect of finite acoustic admittance of the burning propellant surface and the sonic nozzle entrance on the acoustic mode shape. The applicability of normal mode representation to rocket combustion chambers, where the velocity fluctuations perpendicular to the bounding surfaces do not usually vanish, has not been carefully examined.

On the other hand, there is an extensive literature on the classical problem of piston-driven acoustic oscillations in a cylinder (e.g., Ochmann 1981; Wang and Kassoy 1990, Seymour and Mortell 1973a,b; Jimenez 1973). Results show that at resonance, the nonlinear limit cycle amplitude and wave shape are strongly dependent upon the imposed boundary conditions on the other end of the cylinder. For periodic piston motions of maximum Mach number $\epsilon$ ($\epsilon \ll 1$) in a closed cylinder, shock formation occurs, and the limit cycle amplitude is of $O(\epsilon^{1/2})$; in an ideally open cylinder where an acoustic pressure node is present at the end, shock waves are less likely to appear, and the limit cycle amplitude is much larger, of $O(\epsilon^{1/3})$. The sharp contrast suggests that boundary conditions have a profound impact on the behavior of an acoustic system.

It is the purpose of this study to explore the effects of different boundary conditions on gasdynamic wave motions in a confined region, and to develop effective mathematical tools capable of handling this type of problems. A simple piston-cylinder configuration is used as a paradigm for extracting the crucial physical pheuomena of interest. Instead of the traditional quasi-steady approach, an initial-boundary value approach is adopted to describe the time-evolution of the amplifying modes to limit cycles under resonant boundary conditions.

## 4.2 Model Problem and Formulation

We consider the one-dimensional acoustic wave motion in a cylinder induced by an oscillating piston at one end. The condition at the other end of the cylinder is specified by an acoustic admittance function, or response function, that relates the disturbance acoustic pressure to the velocity. The piston displacement is assumed small relative to the cylinder length, and the characteristic piston Mach number $\epsilon \ll 1$.

When the Reynolds number is large, the flow and thermodynamic properties of the cylinder gas are governed by the the inviscid Euler equations and the isentropic relations (Wang and Kassoy 1990):

$$\rho_t + (\rho u)_x = 0, \tag{4.1}$$

$$u_t + u u_x = -\rho^{\gamma-2} \rho_x, \tag{4.2}$$

$$p = \rho^{\gamma}, \qquad T = \rho^{\gamma-1}. \tag{4.3}$$

The thermodynamic variables $p$, $\rho$, and $T$ in (4.1)–(4.3) are nondimensionalized with respect to their equilibrium values $p_0$, $\rho_0$ and $T_0$; the velocity $u$ is nondimensionalized with respect to the equilibrium sound speed $c_0'$. The characteristic length and time scales used in the above equations are the cylinder length $L'$ and the acoustic pessage time $t_a = L'/c_0'$, respectively.

The initial and boundary conditions are given by

$$t = 0, \qquad p = \rho = T = 1; \qquad u = 0, \tag{4.4}$$

$$x = -\frac{\epsilon}{\omega}\cos(\omega t), \qquad u = \epsilon\sin(\omega t); \qquad x = 1, \qquad u = \frac{\sigma}{\gamma}(p-1), \tag{4.5}$$

where the dimensionless piston frequency $\omega = \omega' L'/c_0'$. In the second boundary condition the acoustic admittance $\sigma$ is used to provide a general relationship between the velocity fluctuation and the excess (acoustic) pressure on the outflow boundary. For simplicity we assume that $\sigma$ is invariant to frequency and time. One notices that $\sigma = 0$ and $\infty$ correspond to a rigid end and an ideally open end, respectively.

## 4.3 Linear Acoustic Theory

By applying the perturbation expansions

$$u = \epsilon u_1 + \epsilon^2 u_2 + \cdots, \qquad p = 1 + \gamma(\epsilon p_1 + \epsilon^2 p_2 + \cdots), \tag{4.6}$$

to (4.1)–(4.5), the following describing system for the induced leading order acoustic velocity can be derived:

$$u_{1tt} - u_{1xx} = 0, \tag{4.7}$$

$$u_1(t = 0) = u_{1t}(t = 0) = 0, \tag{4.8}$$

$$u_1(x = 0) = \sin(\omega t); \qquad u_{1t}(x = 1) = -\sigma u_{1x}(x = 1). \tag{4.9}$$

This system is most easily solved by using the Laplace transformation technique, and the solution can be split into a quasi-steady part and a transient part:

$$u_1 = u_{1qs} + u_{1tr}, \tag{4.10}$$

$$u_{1qs} = \frac{\{\sin(\omega)\sin[(1-x)\omega] + \sigma^2\cos(\omega)\cos[(1-x)\omega]\}\sin(\omega t)}{\sin^2(\omega) + \sigma^2\cos^2(\omega)} - \frac{\sigma\sin(\omega x)\cos(\omega t)}{\sin^2(\omega) + \sigma^2\cos^2(\omega)}, \tag{4.11}$$

$$u_{1tr} = \sum_n \frac{i\omega}{\lambda_n^2 - \omega^2}\sin(\lambda_n x)\, e^{i\lambda_n t}. \tag{4.12}$$

The quasi-steady solution (4.11) denotes gas oscillations at the piston driving frequency, and is the long-time solution to the entire system provided that the denominator does not vanish. The transient response $p_{2tr}$ given by (4.12) is a summation over all the eigenfunctions multipled by time-dependent coefficients. The eigenvalues $\lambda_n$ are defined by the equation

$$\tan(\lambda_n) = i\sigma. \tag{4.13}$$

They are complex quantities even for real values of $\sigma$, due to the mixed derivatives in the boundary condition (4.9). By writing $\lambda_n$ and $\sigma$ as $\lambda_n = \lambda_{nr} + i\lambda_i$; $\sigma = \sigma_r + i\sigma_i$, (4.12) can be put into a more illuminating form,

$$u_{1tr} = \frac{\omega}{2}e^{-\lambda_i(t+x)}\sum_{n=-\infty}^{\infty}\frac{e^{i[\lambda_{nr}(t+x)-\phi_n]}}{|\lambda_n^2 - \omega^2|} - \frac{\omega}{2}e^{-\lambda_i(t-x)}\sum_{n=-\infty}^{\infty}\frac{e^{i[\lambda_{nr}(t-x)-\phi_n]}}{|\lambda_n^2 - \omega^2|}, \tag{4.14}$$

where

$$\lambda_{nr} = n\pi - \psi, \qquad \lambda_i = -\frac{1}{2}\ln\left|\frac{1-\sigma}{1+\sigma}\right|. \tag{4.15}$$

The quantities $\phi_n$ and $\psi$ are both functions of $\sigma_r$ and $\sigma_i$, whose explicit forms are omitted here for brevity. Clearly, (4.14) represents infinite pairs of counterpropagating waves, whose amplitudes attenuate exponentially if $\lambda_i$ is positive.

Several observations are made regarding the solutions (4.10)–(4.15). First, for real values of acoustic admittance $\sigma$, the imaginary terms of the solution cancel each other and the result is real. Secondly, special result for hard wall boundary ($\sigma = 0$), free boundary ($|\sigma| \to \infty$) and infinitely long cylinder ($\sigma = 1$) can be recovered; in the last case the solution reduces to a simple traveling wave of the form $\sin[\omega(t-x)]$. Thirdly, it can be shown that the transient wave phenomena decays exponentially with time if $\sigma_r$ is positive and less than infinity. This implies that the acoustic energy contained in the initial transients are rapidly radiated through the boundary, and only the acoustic mode oscillating at the piston frequency is sustained by the continuous mechanical energy imput through the piston.

Of particular interest are the conditions for the acoustic system to become resonant. This happens when the denominators in (4.11) and (4.12) are zero, i.e., $\lambda_n^2 - \omega^2 = 0$ or equivalently

$$\sin^2(\omega) + \sigma^2 \cos^2(\omega) = 0. \qquad (4.16)$$

It can be shown that (4.16) has solutions only if (1) $\sigma = 0$ (rigid wall); (2) $|\sigma| \to \infty$ (perfectly open); and (3) $\sigma_r = 0$ ($\sigma$ purely imaginary). When $\sigma$ takes other values, there exist no "right" frequencies to make the system resonant.

When resonance occurs, the linear acoustic theory predicts $O(t)$ growth in the leading order term and faster growth in higher order terms. The solution breaks down after some time elapse and nonlinear theory has to be employed.

## 4.4 Weakly Nonlinear Solutions

A systematic perturbation procedure based on multiple-timescale expansions are employed to obtain the long-time solutions for resonant and nonresonant acoustic processes in the cylinder. This work is currently in progress, and the following is a brief discussion of the preliminary results.

### 4.4.1 Resonance in a Closed Cylinder ($\sigma = 0$)

The linear asymptotic solution at the resonant frequency $\omega = \nu\pi$ ($\nu$ = integer) reveals that

$$u = -\epsilon t\left[\sin(\omega x)\cos(\omega t)\right] + \epsilon^2 t^3 f_2(x,t) + \epsilon^3 t^5 f_3(x,t) + \cdots, \qquad (4.17)$$

where $f_2$ and $f_3$ are bounded functions. The asymptotic expansion breaks down when $t \sim \epsilon^{-1/2}$, $u \sim \epsilon^{1/2}$.

A two-timescale expansion based on the fast acoustic time $t$ and the slow time $\tau = \epsilon^{1/2} t$ are employed to obtain a uniformly valid solution. In this procedure, the time derivatives in the original equations are replaced by derivatives with respect to both $t$ and $\tau$,

$$\left(\frac{\partial}{\partial t}\right)_x = \left(\frac{\partial}{\partial t}\right)_{\tau,x} + \epsilon^{\frac{1}{2}}\left(\frac{\partial}{\partial \tau}\right)_{t,x}, \qquad (4.18)$$

and $u$ and $p$ are expressed asymptotically as

$$u = \epsilon^{\frac{1}{2}} u_1 + \epsilon u_2 + \cdots, \qquad p = 1 + \gamma(\epsilon^{\frac{1}{2}} p_1 + \epsilon p_2 + \cdots). \qquad (4.19)$$

Solutions for the leading order acoustic quantities $u_1$ and $p_1$ consist of summations of standing wave modes with slowly varying amplitudes that are functions of $\tau$. These amplitude functions have to be determined by eliminating resonant terms in the next order solutions. Under null initial conditions and boundary conditions defined by (4.5) where $\sigma = 0$, we obtain

$$u_1 = \sum_{n=1}^{\infty} \alpha_n(\tau)\cos(n\pi t)\sin(n\pi x), \qquad p_1 = -\sum_{n=1}^{\infty} \alpha_n(\tau)\sin(n\pi t)\cos(n\pi x). \qquad (4.20)$$

The Fourier coefficients $\alpha_n(\tau)$ are calculated from

$$\frac{d\alpha_n}{d\tau} = \frac{\gamma+1}{16} n\pi \left(2\sum_{m=1}^{\infty} \alpha_m \alpha_{n+m} - \sum_{m=1}^{n-1} \alpha_m \alpha_{n-m}\right) - \delta_{n\nu}, \qquad (4.21)$$

$$\left.\frac{d\alpha_n}{d\tau}\right|_{\tau=0} = 0, \qquad (4.22)$$

for $n = 1, 2, \cdots$. The quantity $\delta_{n\nu}$ is the Kronecker delta which ensures nontrivial solutions. The above results agree with the solutions obtained by Ochmann (1985), who used the method of averaging.

The infinite mode-coupling system (4.21) provides a mechanism for transfering acoustic energy from the resonant mode $\nu$ to other modes, especially the high frequency modes. As a result, wavefronts steepen to form shock waves in the cylinder. The internal dissipation of the shocks cause strong damping to the amplifying wave field and eventually a limit cycle is approached. Numerical solutions can be obtained by truncating the infinitely coupled equations (4.21) to a desired level of accuracy.

### 4.4.2 Resonance in an Open Cylinder ($|\sigma| \to \infty$)

The eigenvalues corresponding to an open cylinder are given by $\lambda_n = (n - 1/2)\pi$, $n = 1, 2, \cdots$. The $\nu$th mode becomes resonant if the driving frequency $\omega = \lambda_\nu$. In this case, based on the behavior of the linear asymptotic solutions as $t \to \infty$, the correct slow timescale needed to carried out multiple-scale expansions for the weakly nonlinear wave phenomena is $\tau = \epsilon^{2/3}t$, and the limiting amplitude of the velocity and acoustic pressure are of $O(\epsilon^{1/3})$. The larger amplitude arises because there is no shock formation and therefore less energy dissipation prior to $t \sim O(\epsilon^{2/3})$.

The proper asymptotic expansions for $u$ and $p$ on the time scale $\tau$ are thus

$$u = \epsilon^{\frac{1}{3}}u_1 + \epsilon^{\frac{2}{3}}u_2 + \epsilon u_3 + \cdots, \tag{4.23}$$

$$p = 1 + \gamma(\epsilon^{\frac{1}{3}}p_1 + \epsilon^{\frac{2}{3}}p_2 + \epsilon p_3 + \cdots). \tag{4.24}$$

Analogously to the closed cylinder case, the leading order solutions have the form

$$u_1 = \sum_{n=1}^{\infty} [\alpha_n(\tau)\cos(\lambda_n t) + \beta_n(\tau)\sin(\lambda_n t)]\sin(\lambda_n x), \tag{4.25}$$

$$p_1 = \sum_{n=1}^{\infty} [-\alpha_n(\tau)\sin(\lambda_n t) + \beta_n(\tau)\cos(\lambda_n t)]\cos(\lambda_n x), \tag{4.26}$$

where it is required by the initial conditions that $\alpha_n(0) = \beta_n(0) = 0$.

The slowly varying amplitude functions $\alpha_n$ and $\beta_n$ are again to be determined from higher order considerations. Unlike the usual two-scale expansion processes, where the secular equations result from the elimination of resonant terms in the next order, solutions to $O(\epsilon^{2/3})$ are found to be bounded and thus provide no clue in this respect. Derivations have to be carried out to $O(\epsilon)$. Eliminating the resonant terms at this order then leads to the requirement that $\alpha_n$ and $\beta_n$ satisfy an infinitely coupled system of first order differential equations like (4.21). However, the mode coupling terms on the right hand side are cubic rather than quadratic, because quadratic nonlinearity is not cumulative when a pressure node is present at $x = 1$. The exact forms of the amplitude equations are currently being developed.

### 4.4.3 Other Considerations

As discussed in Section 4.3, another type of acoustic resonance can occur when $\sigma$ is purely imaginary and finite. The wave amplification and nonlinearization processes under this catagory possess new features that are also worth studying. This will be undertaken in the future.

Also of interest is the nonlinearization of nonresonant acoustic wave systems. One recognizes that the three types of resonance-prone boundary conditions mentioned earlier are only special cases. In a sense, it is more important to be concerned with near-resonant (beats) and nonresonant situations as well. The crucial issue is to identify the conditions under which shocks form, since the appearance of shock waves introduces an additional damping mechanism–internal dissipation. To this end it is imperative to use the correct eigenfunctions, given the boundary acoustic properties. Multiple-timescale expansion techniques will again be used to describe the wave deformation process due to the nonlinear accumulation, which occurs on a longer time scale in comparison with the resonant cases.

## 4.5 Concluding Remarks

An initial-boundary value problem is formulated to study the linear and nonlinear evolution of acoustic waves in a cylinder driven by a small-amplitude oscillatory piston. The study serves to illustrate the drastic influence of the acoustic properties at the cylinder end upon the time-evolution and limiting amplitudes of the confined wave system. The mathematical technique developed, based on the multiple-timescale perturbation expansion, can be employed in the future to investigate similar boundary effects in more complicated geometries in solid rocket engines.

This study shows that the acoustic mode shape and characteristics are very sensitive to the imposed boundary conditions. Due to the cummulative nature of the quadratic nonlinearity, normal mode approximation always leads to the formation of shock waves. In a shock free system this generates erroneous results and overpredicts damping mechanisms. More exact representations of the system eigenfunctions should be explored in the future, in order to develop reliable prediction capabilities for rocket engine acoustic stability.

# References


Baum, J.D. 1989 Investigation of flow turning phenomena: effects of frequency and blowing rate. AIAA 27th Aerospace Sciences Meeting, AIAA-89-0297.

Culick, F.E.C. 1990 Some resent results for nonlinear acoustics in combustion chambers. AIAA 13th Aeroacoustic Conference, AIAA-90-3927.

Jimenez, J. 1973 Nonlinear gas oscillations in pipes. Part 1. Theory. *J. Fluid Mech.*, **59**, 23-46.

Kassoy, D.R. 1979 The response of a confined gas to a thermal disturbance; I-Slow transients. *SIAM Appl. Math.*, **30**, 624-634.

Ochmann, M. 1985 Nonlinear resonant oscillations in closed tubes-An application of the averaging method. *J. Acoust. Soc. Am.* **77**(1), 61-66.

Price, E.W. and Flandro, G.A. 1991 *Combustion Instability in Solid Propellant Rockets*, book manuscript in preparation.

Seymour, B.R. and Mortell, M.P. 1973a Resonant acoustic oscillations with damping: small rate theory. *J. Fluid Mech.*, **58**, 353-373.

Seymour, B.R. and Mortell, M.P. 1973b Nonlinear resonant oscillations in open tubes. *J. Fluid Mech.*, **60**, 733-749.

Wang, M. and Kassoy, D.R. 1990 Evolution of weakly nonlinear waves in a cylinder with a movable piston. *J. Fluid Mech.*, **221**, 27-52.

Wang, M. and Kassoy, D.R. 1992a Transient acoustic processes in a low Mach number shear flow. *J. Fluid Mech.*, in press.

Wang, M. and Kassoy, D.R. 1992b Standing acoustic waves in a low Mach number shear flow, *AIAA Journal*, to appear in July, 1992.

# Personnel

1. **Principal Investigator:** David R. Kassoy, Professor of Mechanical Engineering and Interim Dean of the Graduate School, University of Colorado, Boulder.

2. **Research Associate:** Dr. Meng Wang, Department of Mechanical Engineering, University of Colorado, Boulder.

3. **Research Assistant:** Qing Zhao, Department of Mechanical Engineering, University of Colorado, Boulder.

# Appendix A

# Transient Acoustic Processes in a Low Mach Number Shear Flow

To Appear in *Journal of Fluid Mechanics.*

# Transient Acoustic Processes in a Low Mach Number Shear Flow

Meng Wang
D.R. Kassoy

Department of Mechanical Engineering
and
Center for Combustion Research
University of Colorado
Boulder, CO 80309

**Abstract**

A systematic perturbation procedure, based on small mean flow Mach number and large duct Reynolds number, is employed to formulate and solve an initial-boundary value problem for acoustic processes in a shear flow contained within a rigid-walled parallel duct. The results describe the general transient evolution of acoustic waves driven by a plane source located at a given duct cross-section. Forced bulk oscillations near the source and oblique wave generation are shown to result from refraction of the basic planar axial disturbance by the shear flow. Refraction also causes the axial waves to exhibit higher order amplitude variations in the transverse direction. As the source frequency approaches certain critical values, specific refraction induced oblique waves evolve into amplifying purely transverse waves. As a result, the magnitude of the refraction effect increases with time, and quasi-steady solutions do not exist. The analysis is extended to the thin acoustic boundary layer adjacent to the solid walls to examine the shear layer structure induced by the variety of acoustic waves in the core flow. Nonlinear effects and acoustic streaming are shown to be negligibly small on a scale measured by a few axial wavelengths.

# 1 Introduction

The effect of shear flow on acoustic wave propagation was first studied analytically by Pridmore-Brown (1958), who derived the following linearized wave equation for propagation in a fully-developed duct flow:

$$\frac{1}{c_0^2}p_{tt} = (1 - M^2)p_{xx} + p_{yy} - \frac{2M}{c_0}p_{xt} + 2\rho_0 c_0 M_y v_x, \tag{1}$$

where $p$ and $v$ are the acoustic pressure and normal velocity, respectively. The sound speed of the mean state ($p_0$, $\rho_0$, $T_0$) is $c_0$, and $M = M(y)$ is the shear flow Mach number. Earlier efforts have been focused on seeking quasi-steady solutions of the type $p = F(y)e^{i(\kappa x - t)}$. Cross-stream eigenfunctions $F$ and eigenvalues $\kappa$ are obtained to describe the shear flow distortion of specific propagating acoustic wave modes. Both asymptotic solutions (Pridmore-Brown 1958) and numerical solutions (Mungur and Gladwell 1969) demonstrate that for a downstream propagating axial wave (the fundamental mode), the acoustic pressure at the wall is significantly larger than the value at the centerline. Calculations for upstream propagation (Hersh and Catton 1971) show a reversed trend of acoustic pressure distribution.

Quasi-steady theory is useful for describing only limited types of acoustic phenomena due to the restrictive nature of the presumed solution form. For example, one cannot use it to track the evolution of an initial disturbance toward the quasi-steady waveform, if it exists. Solutions describing temporal amplitude growth (resonance) are excluded entirely. Furthermore, the quasi-steady solution does not provide the absolute magnitude of a propagating wave and its relation to a specific acoustic source, nor does it include new waves that may be generated by refraction of the given wave. It is also important to note that the solution as well as the formulation exclude the acoustic boundary layer where the wave motion is damped by viscous effects to satisfy no-slip conditions on the duct wall. These limitations can be overcome by develop-ing an initial-boundary value solution for acoustic disturbances in a shear flow. In addition to the acoustic analysis one must consider viscous boundary layer effects adjacent to the duct walls.

Previous oscillatory boundary layer analyses are mostly for incompressible flows. For example, Stokes (1851) studied the long-time quasi-steady response of a viscous fluid to boundary oscillation; Sexl (1930) and Uchida (1956) investigated laminar pipe flow due to oscillatory pressure gradient. The heat transfer process in the pulsating pipe flow was examined by Romie (1956). These studies all demonstrate the velocity overshoot at the edge of the viscous layer, commonly known as Richardson's annular effect (Richardson and Tyler 1929). More recently, Barnett (1970, 1981) studied the pulsating pipe flow process based on linearized turbulent Navier-Stokes equations. Rott's (1980) investigation of acoustic oscillations in an infinite gas region parallel to a flat plate is more closely related to the present study, because he uses a low Mach number compressible gas model. The effect of mean temperature variation along the direction of oscillation is included, but no mean flow is allowed.

In contrast to the traditional quasi-steady linear approach, Baum and Levine (1987) developed numerical solutions to an initial-boundary value problem in order to describe uni-directional acoustic propagation in an axisymmetric cylinder with a coexisting mean shear flow. The code is based on Reynolds-averaged Navier-Stokes equations for compressible flow, coupled with the $k$–$\epsilon$ turbulence model. Acoustic disturbances, generated by a disk-shaped acoustic source of spatially uniform strength, are studied over a few acoustic wavelengths. In this short-time calculation one cannot expect to find the quasi-steady wave structure solution used to solve (1).

The present study is inspired by the limitations of the classical quasi-steady solutions mentioned above, and the lack of long-time results in Baum and Levine's work. The physical system under consideration involves a horizontal parallel duct containing a fully developed low Mach number shear flow (cf. Fig. 1), a two-dimensional duct counterpart to the cylinder considered by Baum and Levine (1987). An initial-boundary value problem is formulated for an acoustic disturbance propagating into the imposed shear flow. The disturbance is initiated by a source located at a given duct cross-section. Such an approach ensures the spontaneous appearance of all types of acoustic waves, including non-axial waves, arising from the refraction of the basic axial wave, and provides an explicit relationship between the driving acoustic source and the evolving wave field.

The analysis is based on a laminar flow model for a viscous, heat conducting fluid. By using a rational approximation procedure, in Section 2, transport effects are shown in a formal manner to be limited to extremely thin acoustic boundary layers adjacent to the duct wall. Perturbation methods, based on the small mean flow Mach number parameter $M$, are employed to find solutions for both the transport-free core region in Section 3 and the viscous layer in Section 4. The solution procedure is especially simplified due to the low Mach number simplifications. Finally, in Section 5, the results are discussed in comparison with the numerical solutions of Baum and Levine (1987), and the major findings of the present work are summarized.

The results demonstrate that refraction, known to distort the pressure distribution of the leading order axial wave, is also the source of new and dispersive acoustic transients. When nonresonant conditions prevail, these transients evolve into oblique propagating waves and a forced bulk response at the acoustic source frequency. The former correspond to the selected higher modes of quasi-steady propagation in duct acoustics, while the bulk response is composed of an infinite number of attenuated modes that decay rapidly away from the plane acoustic source. The quasi-steady axial wave solution agrees with those from the classical studies (Pridmore-Brown 1958; Hersh and Catton 1971). Resonance occurs in one of the propagated modes if the duct width is some integer multiple of the driving acoustic wavelength. In this case purely transverse waves with growing amplitude are found to exist that cause a drastic increase in refraction effects.

In the viscous, heat-conducting acoustic boundary layers, a complex response arises from the variety of acoustic waves in the core. The transverse velocity in the acoustic boundary layer is much larger and more complicated than that predicted by Rott (1980), because it must match with the core solution that contains refraction effects. The refraction magnitude and the acoustic boundary layer thickness obtained from the perturbation solutions are found to be comparable with those of Baum and Levine (1987).

# 2 Mathematical Formulation

The complete dimensionless equations describing the compressible fluid motion in a planar duct shown in Fig. 1 can be written in the form,

$$p = \rho T, \tag{2}$$

$$\rho_t + M\left[(\rho u)_x + (\rho v)_y\right] = 0, \tag{3}$$

$$\rho\left[u_t + M(uu_x + vu_y)\right] = -\frac{1}{\gamma M}p_x + \frac{M}{\Omega R_e}\left(u_{yy} + \frac{4}{3}\Omega^2 u_{xx} + \frac{1}{3}\Omega^2 v_{xy}\right), \tag{4}$$

$$\rho\left[v_t + M(uv_x + vv_y)\right] = -\frac{1}{\gamma M\Omega^2}p_y + \frac{M}{\Omega R_e}\left(\Omega^2 v_{xx} + \frac{4}{3}v_{yy} + \frac{1}{3}u_{xy}\right), \tag{5}$$

$$\begin{aligned}\rho\left[T_t + M(uT_x + vT_y)\right] &= -M(\gamma-1)p(u_x + v_y) + \frac{M\gamma}{\Omega P_r R_e}\left(T_{yy} + \Omega^2 T_{xx}\right)\\ &+\frac{M^3}{\Omega R_e}\gamma(\gamma-1)\left[\left(u_y + \Omega^2 v_x\right)^2 + 2\Omega^2\left(u_x^2 + v_y^2\right) - \frac{2}{3}\Omega^2\left(u_x + v_y\right)^2\right],\end{aligned} \tag{6}$$

where for convenience the thermophysical properties are assumed constant. The nondimensional variables are defined in terms of dimensional quantities by

$$(p, \rho, T) = \frac{(p', \rho', T')}{(p_0', \rho_0', T_0')}, \qquad u = \frac{u'}{U_c'}, \qquad v = \frac{v'}{v_R'},$$

$$t = \frac{t'}{t'_R}, \qquad x = \frac{x'}{x'_R}, \qquad y = \frac{y'}{d'}. \tag{7}$$

Quantities $p'_0$, $\rho'_0$, and $T'_0$ are thermodynamic properties of the gas at mean state, $d'$ is the width of the duct and $U'_c$ the characteristic velocity of the mean flow. The characteristic time scale is defined as the inverse of the circular frequency of the axial acoustic wave, $t'_R = 1/\omega'$, so that the wavelength gives the proper axial length scale $x'_R = c'/\omega'$. The characteristic transverse velocity $v'_R = M\omega' d'$. The dimensionless groups in (2)–(6) defined by

$$M = \frac{U'_c}{c'}, \qquad R_e = \frac{U'_c d'}{\nu'}, \qquad P_r = \frac{\nu'}{\alpha'}, \qquad \Omega = \frac{\omega' d'}{c'}, \tag{8}$$

are the maximum mean flow mach number, the mean flow Reynolds number, the Prandtl number, and the normalized axial acoustic frequency, respectively. One notices that $\Omega$ is the ratio of the transverse acoustic time in the duct to the wave period.

In the present study solutions to the above described system are sought in the limit $1/R_e \to 0$ and $M \to 0$, where it is assumed that $1/R_e \ll M$. Additionally, one assumes that the Prandtl numder is an order one quantity and $\Omega \leq O(1)$.

As in previous studies (Pridmore-Brown 1958; Mungur and Gladwell 1969; Hersh and Catton 1971), the basic steady flow in the duct is assumed to be fully-developed. It is driven by a pressure gradient which is inversely proportional to the Reynolds number of the flow. One can easily derive from (2)–(5) that

$$u = U(y), \qquad v = 0, \qquad dp/dx = O(M^2/R_e). \tag{9}$$

Obviously, on the length scale $x'_R$ the variation of $p$ is negligibly small.

Since the Reynolds number is very large, it is observed from (2)–(6) that except for the extremely thin acoustic boundary layers adjacent to the solid surfaces, which will be discussed in detail in Section 4, the wave motion in the core region is basically unaffected by transport effects. In this limiting case, the state, continuity and energy equations (cf. (2), (3) and (6)) can be combined to give the familiar results,

$$p = \rho^{\gamma} + O\left(\frac{M}{\Omega R_e}\right), \qquad T = \rho^{\gamma-1} + O\left(\frac{M}{\Omega R_e}\right). \tag{10}$$

These isentropic relations, together with the inviscid version of (3)-(5), suffice to describe the acoustic wave motion in the core.

When the fully developed duct flow is disturbed by an $O(\epsilon)$ acoustic velocity,

$$u = U(y) + \epsilon\hat{u}, \qquad v = \epsilon\hat{v}, \tag{11}$$

it can be shown that the thermodynamic corrections are always $O(M\epsilon)$, in order to balance the acoustic components in the governing equations (3)-(5). Accordingly, $p$, $\rho$ and $T$ are put into the following form:

$$p = 1 + (M\epsilon)\gamma\hat{p}, \qquad \rho = 1 + (M\epsilon)\hat{\rho}, \qquad T = 1 + (M\epsilon)\hat{T}. \tag{12}$$

The continuity equation (3) can be rewritten in terms of acoustic variables as

$$\hat{\rho}_t + \hat{u}_x + \hat{v}_y + MU(y)\hat{\rho}_x + (M\epsilon)\left[(\hat{\rho}\hat{u})_x + (\hat{\rho}\hat{v})_y\right] = 0. \tag{13}$$

Similarly, the $x$ and $y$ momentum equations become

$$\hat{u}_t + M\left[U(y)\hat{u}_x + \hat{v}U'(y)\right] + (M\epsilon)(\hat{u}\hat{u}_x + \hat{v}\hat{u}_y) = -\frac{\hat{p}_x}{1 + (M\epsilon)\hat{\rho}}, \tag{14}$$

$$\hat{v}_t + MU(y)\hat{v}_x + (M\epsilon)(\hat{u}\hat{v}_x + \hat{v}\hat{v}_y) = -\frac{\hat{p}_y}{\Omega^2\left[1 + (M\epsilon)\hat{\rho}\right]}. \tag{15}$$

In (13)-(15) terms containing $U(y)$ represent the shear flow interaction with the acoustic field. They are $O(M)$ quantities. The nonlinear product terms are of $O(\epsilon M)$. There are three interesting asymptotic limits that can be applied to (13)-(15) for low Mach number shear flows:

*1) The parameters satisfy the inequality $\epsilon \ll M \ll 1$, and the asymptotic limit $\epsilon \to 0$, $M$ fixed is used.* The nonlinear terms can be ignored since their magnitudes are small relative to $M$. A combination of (13), (14) and (15) generates a leading order acoustic equation equivalent to (1). This demonstrates that the previous quasi-steady analyses by Pridmore-Brown (1958), Mungur and Gladwell (1969), and Hersh and Catton (1971) are asymptotically accurate for extremely small amplitude acoustics relative to the characteristic shear flow Mach number.

*2) The parameters satisfy the inequality $O(\epsilon) = M \ll 1$, and the asymptotic limit $M \to 0$ is used.* If $O(M^2)$ terms in (13)-(15) are uniformly ignored relative to $O(M)$ terms in the asymptotic limit, their analogue to (1) contains no $O(M^2)$ term. This shows that the Pridmore-Brown results are formally valid to $O(M)$ where $M \ll 1$. Numerical studies by Baum and Levine (1987) are primarily concerned with this regime.

*3) The parameters satisfy the inequality $M \ll \epsilon \leq O(1)$, and the asymptotic limit $M \to 0$, $\epsilon$ fixed is used.* An examination of (13)-(15) shows that the nonlinear terms and the refraction producing terms containing $U(y)$ are of the same magnitude, $O(M)$, in the limit. As a result, (1) which is purely linear cannot describe acoustic phenomena when the pressure disturbance in (12) is $O(M)$.

The following analysis is focused formally on Case 2 described above, although the solutions for acoustic variables are equally valid for Case 1 since both cases yield identical truncated versions of (13)-(15) to $O(M)$. The initial state of the disturbance quantities is described by

$$t = 0, \qquad \hat{u} = \hat{v} = \hat{p} = 0. \tag{16}$$

Acoustic waves are excited at $x = 0$ by imposing a periodic horizontal disturbance velocity

$$x = 0, \qquad \hat{u} = A\sin(t), \tag{17}$$

where the amplitude $A$ is in general $y$-dependent, although the simpler case of constant amplitude is emphasize here. The normal velocity component generated in the viscous acoustic boundary layer is of much smaller magnitude relative to the core flow magnitude, as will be shown later. Hence, so far as the acoustic core region is concerned, the impermeable condition

$$y = 0, 1; \qquad \hat{v} = 0. \tag{18}$$

can be applied directly to describe the acoustic behavior close to the duct walls.

# 3 Core Solution

## 3.1 Acoustic Transients due to Axial Wave Refraction

First, the acoustic quantities are expanded asymptotically in terms of $M$ in the following manner:

$$\hat{\Psi} = \Psi_1 + M\Psi_2 + O(M^2), \qquad \Psi = (u, v, p, \rho, T). \tag{19}$$

In order to account for the small changes in the absolute wave propagation speed due to the $O(M)$ mean flow, it is necessary to use a strained coordinate

$$\bar{x} = \frac{x}{1 + M\tilde{U}_0 + \cdots}, \tag{20}$$

where

$$\tilde{U}_0 = \int_0^1 U(y)dy \tag{21}$$

is the bulk shear flow velocity area-averaged across the duct. One finds from (13)–(15) ordered sets of equations,

$$\rho_{1t} + u_{1x} + v_{1y} = 0, \tag{22}$$

$$u_{1t} + p_{1x} = 0, \tag{23}$$

$$v_{1t} + \frac{1}{\Omega^2}p_{1y} = 0, \tag{24}$$

and

$$\rho_{2t} + u_{2\bar{x}} + v_{2y} = -U(y)\rho_{1\bar{x}} + \tilde{U}_0 u_{1\bar{x}}, \tag{25}$$

$$u_{2t} + p_{2\bar{x}} = \tilde{U}_0 p_{1\bar{x}} - U(y)u_{1\bar{x}} - U'(y)v_1, \tag{26}$$

$$v_{2t} + \frac{1}{\Omega^2}p_{2y} = -U(y)v_{1\bar{x}}. \tag{27}$$

Additionally, the isentropic relations (10) imply that

$$p_1 = \rho_1, \qquad p_2 = \rho_2. \tag{28}$$

Equations (22)-(24) are combined to generate the linear, homogeneous wave equation for $p_1$,

$$p_{1tt} - \left(p_{1\bar{x}\bar{x}} + \frac{1}{\Omega^2}p_{1yy}\right) = 0. \tag{29}$$

The leading order acoustic equation is seen to be unaffected by the mean shear flow, except for the bulk convection effect incorporated into the variable $\bar{x}$. If the boundary velocity oscillation has a constant amplitude, $A = 1$ in (17), the solution satisfying (16)-(18) describes a wave train propagating axially into a quiescent gas,

$$p_1 = u_1 = \sin(t - \bar{x}), \qquad v_1 = 0. \tag{30}$$

Note that ahead of the wavefront, when $\bar{x} \geq t$, all the acoustic quantities are zero.

In order to study the explicit effect of the shear flow velocity gradient on the acoustic field, (25)-(27) are combined to give the second order analogue of (29),

$$p_{2tt} - \left(p_{2\bar{x}\bar{x}} + \frac{1}{\Omega^2}p_{2yy}\right) = -2\tilde{U}_0 p_{1\bar{x}\bar{x}} - 2U(y)p_{1\bar{x}t} + 2U'(y)v_{1\bar{x}}. \tag{31}$$

The forcing function, representing the interactions between the shear flow and the leading order acoustics, are simplified for the case considered here, i.e., when the boundary oscillation is $y$-independent. Upon inserting (30) into (31), the latter can be rewritten as

$$p_{2tt} - \left(p_{2\bar{x}\bar{x}} + \frac{1}{\Omega^2}p_{2yy}\right) = -2\left[U(y) - \tilde{U}_0\right]\sin(t - \bar{x}) \tag{32}$$

for $\bar{x} \leq t$. The initial and boundary conditions necessary to solve (32) are derived by a proper combination of the preceding results in this section with (16)-(18). They are given by

$$t = 0, \qquad p_2 = p_{2t} = 0, \tag{33}$$

$$\bar{x} = 0, \qquad p_{2\bar{x}} = \left[U(y) - \tilde{U}_0\right] \cos(t); \qquad \bar{x} \to \infty, \qquad p_2 = \text{finite}, \tag{34}$$

$$y = 0; 1, \qquad p_{2y} = 0. \tag{35}$$

The hyperbolic equation system (32)-(35) can be solved by a combination of Laplace transform and Fourier series method, as outlined below. If $Q$ and $s$ are used to denote the transformed variables of $p_2$ and $t$, respectively, a Laplace transform of (32)-(35) with respect to time $t$ yields

$$Q_{\bar{x}\bar{x}} + \frac{1}{\Omega^2} Q_{yy} - s^2 Q = 2\left[U(y) - \tilde{U}_0\right] \frac{e^{-s\bar{x}}}{1 + s^2}, \tag{36}$$

$$\bar{x} = 0, \qquad Q_{\bar{x}} = \left[U(y) - \tilde{U}_0\right] \frac{s}{s^2 + 1}; \qquad \bar{x} \to \infty, \qquad Q = \text{finite}, \tag{37}$$

$$y = 0; 1, \qquad Q_y = 0. \tag{38}$$

The homogeneous boundary condition (38) suggests that a Fourier series solution of the form

$$Q = a_0(\bar{x}, s) + \sum_{n=1}^{\infty} a_n(\bar{x}, s) \cos(n\pi y) \tag{39}$$

is obtainable. Once the shear flow velocity $U(y)$ is Fourier decomposed into

$$U(y) = \tilde{U}_0 + \sum_{n=1}^{\infty} \tilde{U}_n \cos(n\pi y), \tag{40}$$

where the bulk part $\tilde{U}_0$ is given by (21), and

$$\tilde{U}_n = 2\int_0^1 U(y) \cos(n\pi y) dy, \tag{41}$$

it becomes clear immediately from (36)-(38) that $a_0 = 0$. The $n$th Fourier coefficient, for $n = 1, 2, \cdots$, is governed by

$$a_n'' - (s^2 + q_n^2) a_n = 2\tilde{U}_n \frac{e^{-s\bar{x}}}{1 + s^2}, \tag{42}$$

where the parameter $q_n$ is defined as

$$q_n = \frac{n\pi}{\Omega}. \tag{43}$$

The solution to (42), which satisfies

$$a_n'(0) = \tilde{U}_n \frac{s}{s^2+1} \tag{44}$$

and has a finite value as $\bar{x} \to \infty$ is obtained as

$$a_n = \tilde{U}_n \left(\frac{2}{q_n^2} - 1\right) \frac{s}{s^2+1} \frac{e^{-\sqrt{s^2+q_n^2}\,\bar{x}}}{\sqrt{s^2+q_n^2}} - \frac{2\tilde{U}_n}{q_n^2} \frac{e^{-s\bar{x}}}{1+s^2}. \tag{45}$$

Upon using (45) in (39), and taking the inverse Laplace transform by means of an extended Laplace transform table (Oberhettinger and Badii 1973) and the convolution theorem, one finally obtains

$$\begin{aligned} p_2 \;\; &= \;\; -\sin(t-\bar{x}) \sum_{k=1}^{\infty} \frac{2\tilde{U}_k}{q_k^2} \cos(k\pi y) \\ &+ \;\; \sum_{n=1}^{\infty} \tilde{U}_n \left(\frac{2}{q_n^2} - 1\right) \int_{\bar{x}}^{t} \cos(t-\xi)\, J_0\left(q_n\sqrt{\xi^2 - \bar{x}^2}\right) d\xi \cos(n\pi y). \end{aligned} \tag{46}$$

where $J_0$ is the zeroth order Bessel function of the first kind.

The first term on the right side of (46) represents a quasi-steady, axial traveling wave (fundamental duct mode), with $y$-dependent amplitude given by the summation. It is an $O(M)$ correction to the leading order axial wave (cf. (30)) and thus describes the effect of shear flow induced refraction on the propagating axial wave. As predicted by the classical theory, the axial wave acoustic pressure redistributes itself nonuniformly across the duct. The $y$-dependent amplitude function grows rapidly with driving acoustic frequency (cf. (46) and (43)) and varies with shear flow velocity profile. It is, within a constant, equivalent to the result of Hersh and Catton's (1971) perturbation study, if the latter is rewritten in Fourier decomposed form. However.

here the amplitude is completely defined because the solution is obtained from an initial-boundary value problem.

A second fundamental advantage of studying linear acoustic refraction phenomena in terms of an initial-boundary value problem is that the transient (non quasi-steady) evolution of the acoustic refraction and its absolute magnitude can be found explicitly, a result not available from the classical studies (Pridmore-Brown 1958; Mungur and Gladwell 1969; Hersh and Catton 1971). The complete second term in (46) represents acoustic transients initiated by the passage of the leading order axial wave through the shear flow, including dispersive effects. The transients evolve into oblique waves (higher propagated modes) and forced bulk vibration consisting of infinite numbers of attenuated modes, as will be shown soon.

The $O(M)$ axial and transverse acoustic velocities can be obtained by integrating (26) and (27), respectively. They are listed below:

$$u_2 = -\sin(t-\bar{x})\sum_{k=1}^{\infty}\left(\frac{2}{q_k^2}-1\right)\tilde{U}_k\cos(k\pi y)+\sum_{n=1}^{\infty}\tilde{U}_n\left(\frac{2}{q_n^2}-1\right)\bar{x}\,h_n(t,\bar{x})\cos(n\pi y), \tag{47}$$

$$\begin{aligned} h_n = {} & \int_{\bar{x}}^{t}\frac{J_0\left(q_n\sqrt{\zeta^2-\bar{x}^2}\right)}{\zeta}d\zeta \\ & -\int_{\bar{x}}^{t}\int_{\bar{x}}^{\zeta}\left[\frac{\sin(\zeta-\xi)}{\xi}-\frac{\cos(\zeta-\xi)}{\xi^2}\right]J_0\left(q_n\sqrt{\xi^2-\bar{x}^2}\right)d\xi d\zeta, \end{aligned} \tag{48}$$

$$\begin{aligned} v_2 = {} & [\cos(t-\bar{x})-1]\sum_{k=1}^{\infty}\frac{2\tilde{U}_k}{k\pi}\sin(k\pi y) \\ & +\sum_{n=1}^{\infty}\frac{2\tilde{U}_n}{n\pi}\left(1-\frac{q_n^2}{2}\right)\int_{\bar{x}}^{t}\int_{\bar{x}}^{\zeta}\cos(\zeta-\xi)\,J_0\left(q_n\sqrt{\xi^2-\bar{x}^2}\right)d\xi d\zeta\ \sin(n\pi y). \end{aligned} \tag{49}$$

The two terms in both $u_2$ and $v_2$ expressions again represent the quasi-steady axial wave and other transient phenomena, corresponding to those in (46). For large $\bar{x}$, one can show from (48) that $h_n \sim O(\bar{x}^{-1})$, so that $u_2$ remains bounded despite the explicit $\bar{x}$ proportionality.

## 3.2 The Evolution to Quasi-steady Propagation

Insightful results for the long-time properties of $p_2$ can be obtained from the asymptotic properties of the integral

$$I_n(t,\bar{x}) = \int_{\bar{x}}^{t} \cos(t-\xi)\, J_0\left(q_n\sqrt{\xi^2-\bar{x}^2}\right) d\xi. \tag{50}$$

When $q_n \neq 1$, (50) converges for large values of $t$ such that

$$\lim_{t\to\infty} I_n = \begin{cases} \frac{\cos(t)\, e^{-\bar{x}\sqrt{q_n^2-1}}}{\sqrt{q_n^2-1}} & q_n > 1 \\ \frac{\sin\left(t-\sqrt{1-q_n^2}\,\bar{x}\right)}{\sqrt{1-q_n^2}} & q_n < 1 \end{cases} \tag{51}$$

when $\bar{x} = O(1)$ (Gradshteyn and Ryzhik 1980). It follows from (46) and (51) that the nonresonant long-time solution for the refractive acoustic pressure can be written as

$$\begin{aligned} p_2 \;=\; & -\sin(t-\bar{x})\sum_{k=1}^{\infty}\frac{2\tilde{U}_k}{q_k^2}\cos(k\pi y) \\ & +\sum_{n=1}^{N}\tilde{U}_n\left(\frac{2}{q_n^2}-1\right)\frac{\sin\left(t-\sqrt{1-q_n^2}\,\bar{x}\right)}{\sqrt{1-q_n^2}}\cos(n\pi y) \\ & +\cos(t)\sum_{n=N+1}^{\infty}\tilde{U}_n\left(\frac{2}{q_n^2}-1\right)\frac{e^{-\sqrt{q_n^2-1}\,\bar{x}}}{\sqrt{q_n^2-1}}\cos(n\pi y). \end{aligned} \tag{52}$$

where $N$ is defined such that $q_N < 1 < q_{N+1}$.

The second full term in (52) contains $N$ Fourier modes, or higher propagated modes in classical acoustics terms. Each mode can be rewritten as a pair of oblique traveling waves. This is illustrated by rewriting the $n$th mode, denoted by $P_n$, as

$$P_n = \frac{\tilde{U}_n\,(2-q_n^2)}{2q_n^2\sqrt{1-q_n^2}}\left[\sin(t-z_{n1})+\sin(t-z_{n2})\right], \tag{53}$$

where

$$z_{n1} = \sqrt{1-q_n^2}\,\bar{x} - n\pi y, \qquad z_{n2} = \sqrt{1-q_n^2}\,\bar{x} + n\pi y, \tag{54}$$

represent a pair of oblique paths for the traveling waves, shown in Fig. 2. The wave reflects repeatedly from both duct walls as it travels along. Upon each reflection, it switches from one path to the other. If the transverse coordinate is rescaled by $Y = \Omega y$, so that both $Y$ and $x$ are normalized using the same characteristic length scale $x'_R = c'/\omega'$, one easily finds that the phase speed of the $n$th mode along the $z_{n1}, z_{n2}$ paths is unity, while the phase speed along the $x$-axis varies from 0 to $\infty$, depending on the angle of incidence $\theta_n = \sin^{-1}\left(\sqrt{1 - q_n^2}\right)$. The latter is identical to the angle of reflection because of the rigid-wall assumption. It is to be noted that when $q_n$ is close to 1, one pair of large amplitude oblique waves become nearly transverse, so that a form of wave trapping appears. This type of result, to be discussed in full in Section 3.3, implies that a resonance occurs when $q_n \to 1^-$ and amplitude growth with time can be expected.

The oblique traveling waves exist only when $q_n < 1$. In dimensional terms, this implies that $n < 2d'/\lambda'$ ($\lambda'$ is the wavelength) must be satisfied in order for the waves to propagate. The number of non-axial traveling wave modes is thus proportional to the duct width and inversely proportional to the acoustic wavelength. This is well known in quasi-steady duct acoustics (see, for example, Morse and Ingard 1968). However, the present transient analysis demonstrates explicitly that refraction of a basically axial wave is the direct source of the oblique propagating waves. These oblique waves will also interact with the shear flow as they propagate along, to generate more complex refraction effects. The latter are not included in the $p_2$ solution because they are $O(M)$ smaller.

The last term in (52) describes a bulk response of the gas, driven at the frequency of the acoustic source. These so called attenuated modes ($q_n > 1$) decay exponentially along the $\bar{x}$-axis, and thus normally affect only a small region close to the surface of the acoustic source. The penetration depth is proportional to $(q_n^2 - 1)^{-1/2}$. Given

(43), one finds that small mode number $n$ and high frequency $\Omega$ lead to deeper penetration. Resonance can also be viewed as occurring in the limit $q_n \to 1^+$, so that the first attenuated mode in (52) penetrates asymptotically far into the field, up to the basic axial wavefront. In practical terms, only the first few attenuated modes from the second infinite summation are needed, because of the rapid decay of the Fourier coefficients with the mode number $n$.

The transition to the quasi-steady solution (52) can be illustrated by numerically evaluating the second order acoustic pressure from the general formula (46). Since the Fourier series converges fairly rapidly, only the first 20 terms are used in each summation. A comparison of the results with those from summations of 40 or more terms shows agreement to within three decimal places. The integral $I_n$ is computed by calling the QDAG integration subroutine from the IMSL software library, which uses a globally adaptive scheme based on Gauss-Kronrod rules. Representative examples of results for various acoustic frequencies and different types of duct mean flows are discussed below.

Figs. 3 and 4 show the acoustic refraction effect in a fully developed laminar duct flow, described by $U = 4y(1-y)$. In Figs. 3a and 4a, the time variations of $p_2$, evaluated from (46), are plotted for the cases of $\Omega = 2$ and 8 respectively, on a duct cross-section located at $x = 2\pi$, one wavelength downstream from the plane acoustic source. The solid lines represent the second order acoustic pressures at the wall, while the dashed lines denote those at the center-plane of the duct. For comparison the axial wave contribution to $p_2$ (the first term in (46), henceforth denoted as $p_{2a}$) corresponding to the conditions in Figs. 3a and 4a are depicted in Figs. 3b and 4b, respectively. The mean flow Mach number employed in the calculations is 0.1.

Since the mean flow is symmetric with respect to the duct center-plane, the Fourier coefficient $\tilde{U}_n = 0$ for $n = odd$ (cf. (41)). Thus the first oblique wave pair for

$p_2$ corresponds to the $n = 2$ mode, whose cut-off frequency $\Omega = 2\pi$ ($\lambda' = d'$ in dimensional terms). The driving acoustic frequency is below the cut-off frequency for the $n = 2$ mode in Figs. 3, so that only the propagating axial wave exists in the quasi-steady state. The $p_2$ curves are thus similar to those for $p_{2a}$. The small discrepency, caused by the acoustic transients induced in the gas medium when the wavefront first passes the given location, is seen to die out gradually as the solution converges to the quasi-steady solution (52). The effect of attenuated modes is negligibly small at $x = 2\pi$. Calculations conducted at other frequencies for which oblique waves are absent show that the transient phenomenon is more prominent and disappears more slowly for lower frequency cases than for higher frequency cases.

The situation depicted in Figs. 4 is quite different. Here $\Omega = 8$, higher than the cut-off frequency for the $n = 2$ mode. The second order acoustic pressure shown in Fig. 4a is a superposition of both the axial wave and one oblique wave pair, in addition to the small transient effect. As a result, it is dramatically different, both in amplitude and phase, from the pure axial wave solution presented in Fig. 4b.

Fig. 5 depicts the time variation of $p_2$ in a "turbulent" mean flow field emulated by $U = (1 - |2y - 1|)^{1/7}$. The other plotting conditions are identical to those used in producing Fig. 3a, the laminar flow counterpart of Fig. 5. The refraction induced acoustic pressure is observed to be much smaller in amplitude in the latter, because the mean flow represented by the one-seventh power law has a relatively small velocity gradient in most parts of the duct. The high velocity gradient regions, concentrated near the two duct walls, are too narrow to promote acoustic refraction on a global scale.

The bulk convection of the acoustic wave by the mean flow can also be observed from Figs. 3–5. The wavefront emitted from the plane acoustic source arrives at $x = 2\pi$ after approximately 5.9 dimensionless time units, which is less than $2\pi$, the time required for a wave to travel the same distance in a static medium.

The pressure curves in Figs. 3 and 5 suggest that a simple relation exists for quasi-steady acoustic refraction at relatively low driving frequency. If $\Omega < 2\pi$, so that non-axial waves are absent from (52), and if one is sufficiently far away from the plane acoustic source, where the effect of the attenuated modes is negligible, the entire quasi-steady solution contains axial waves only (cf. (19), (30) and (52)). In this case the total acoustic pressure normalized by its value at the duct center-plane provides a quantitative measure of the global refraction effect:

$$\frac{\hat{p}_s}{\hat{p}_{sc}} \cong 1 + M \sum_{k=1}^{\infty} \frac{2\tilde{U}_k}{q_k^2} \left[ \cos\left(\frac{k\pi}{2}\right) - \cos(k\pi y) \right], \tag{55}$$

where the subscripts $s$ and $c$ denote quasi-steady state and center-plane respectively. Eqn. (55) is in fact the ratio of the amplitude functions for the fundamental mode, equivalent to those found in earlier studies (Pridmore-Brown 1958; Mungur and Gladwell 1969; Hersh and Catton 1971) in the low frequency range.

In Fig. 6 (55) is plotted for the case $\Omega = \pi$ and $M = 0.1$, for three types of mean flow conditions: $U = 1 - |2y - 1|$, $U = 4y(1 - y)$, and $U = (1 - |2y - 1|)^{1/7}$. The familiar results are presented in decibels to follow convention. Obviously, the acoustic energy of the downstream propagating axial wave train is channeled towards the walls. The linear and parabolic mean flows cause acoustic refraction effects of similar magnitudes, while the shear flow represented by the one seventh power law generates the smallest refraction for the reason explained previously.

It must be emphasized that (55) or curves like those in Fig. 6 are accurate representations of acoustic refraction phenomena in quasi-steady state, when the duct geometry only allows purely axial wave propagation for the given driving acoustic frequency. For $\Omega > 2\pi$, like the case depicted in Fig. 4, refraction of the planar axial wave also generates oblique traveling waves. The ratio of local acoustic pressure to that at the center-plane is both $t$ and $x$ dependent, and is not a useful representation of the transverse variation of the refraction effect.

### 3.3 Resonant Amplification of Refraction Phenomena

The above discussions have been focused on nonresonant situations. The refractive pressure response is dramatically different if $q_{n^*} = 1$, or in physical terms, $d' = n^*\lambda'/2$, where $n^*$ denotes the resonant mode. The resonance occurs because the frequencies of $J_0(\xi)$ and the harmonic function in (50) are nearly identical for $\xi \gg 1$ when $q_{n^*} = 1$. As a result, the integral becomes unbounded when $t \to \infty$, and no quasi-steady solutions exist. When the time is large, $\bar{x} \leq O(1)$, one can show that

$$I_{n^*}(t \gg 1, \bar{x}) \sim \sqrt{\frac{2t}{\pi}} \cos\left(t - \frac{\pi}{4}\right). \tag{56}$$

In particular, at $\bar{x} = 0$ (50) can be evaluated exactly (Gradshteyn and Ryzhik 1980) to give

$$I_{n^*}(t, 0) = \int_0^t \cos(t - \xi) J_0(\xi) d\xi = t J_0(t), \tag{57}$$

which agrees with (56) if the asymptotic property of $J_0$ for large $t$ is used. By using (56) the resonant Fourier mode in (46) can be written asymptotically as

$$P_{n^*}(t \gg 1, \bar{x}) \sim \tilde{U}_{n^*} \sqrt{\frac{t}{2\pi}} \left[\cos\left(t - \Omega y - \frac{\pi}{4}\right) + \cos\left(t + \Omega y - \frac{\pi}{4}\right)\right]. \tag{58}$$

It shows clearly the pair of purely transverse waves trapped in the duct with growing amplitudes.

Numerical evaluations of (50) for $q_n = 1$ are shown in Fig. 7, where the horizontal coordinate is the characteristic coordinate $t - \bar{x}$ for easier comparison. As the $\bar{x}$ value is increased, similar trends of growth with $t$ are observed. However, the solutions at $t = 60$ still exhibit strong $x$-dependence because the asymptotic results described by (56) have yet to be reached.

The effect of resonance on acoustic refraction is explicitly demonstrated in Fig. 8, where the variations of $p_2$ on the duct wall $y = 0$, at three separate axial locations are plotted against time. The shear flow profile is parabolic as used earlier. The driving frequency $\Omega = 2\pi$, so that the $n = 2$ mode in the second term of (46) is resonant. All the pressure curves show growth in amplitude after sufficient time elapses, when the growing resonant mode embedded in the second summation dominates the system in (46). For relatively short time, however, the resonant mode amplitude is not large compared with that of the fundamental mode (the entire first term in (46)). The amplitude of $p_2$ may initially decrease with time, as in the cases for $\bar{x} = 2\pi$ and $3\pi$, due to destructive interference.

Calculations for $\Omega$ values slightly below and above the resonant frequency $2\pi$ show similar trends of growth for $p_2$. However, the amplitudes eventually approach large but finite limiting values predicted by (52).

The resonant result illustrates a fascinating mechanism for exciting and amplifying purely transverse waves in the duct through axial wave-shear flow interaction. This shows yet another distinct advantage of the present analytical based initial-boundary value study. Numerical investigations for traveling wave refraction (Baum and Levine 1987) are limited to a few wave cycles only, due to difficulties associated with non-reflective outflow boundary conditions. The results in Fig. 8 show that short-time solution behavior cannot be used to determine if resonant amplifications of refractive pressure are occurring. The classical quasi-steady solutions (e.g. Pridmore-Brown 1958), on the other hand, cannot describe the resonant mode at all.

Due to the $t^{1/2}$ growth of the resonant or near-resonant mode in $p_2$, one concludes that for such systems the perturbation expansion (19) breaks down as $t \sim O(M^{-2})$. A new derivation will be needed to predict its long-time behavior, which will contain the resonance-enhanced refraction effects (the transverse waves) in the leading order.

It should also be noted that the validity of the above developed perturbation solutions depends on the value of $\Omega$. In general, once the dimensionless frequency $\Omega$ becomes as large as $O(M^{-1/2})$, the magnitude of $Mp_2$ becomes comparable with that of $p_1$ (cf. (30), (46) and (43)), causing the breakdown of the asymptotic expansion (19). The actual size of $Mp_2$ nevertheless also depends upon the magnitude of $\tilde{U}_n$. For mean duct flows symmetric with respect to the center-plane $y = 1/2$, the largest terms in the Fourier summations in (46) and (52) vanish because $\tilde{U}_n = 0$ for $n = odd$. As shown in the example calculations, $p_2$ remains $O(1)$ when the value of $\Omega$ is as large as 8.

In the high frequency limit $\Omega \gg 1$, when acoustic refraction effects are no longer small correction terms of $O(M)$, a new theory needs to be developed which includes refraction in the leading order acoustics.

## 3.4 Acoustic Transients due to $y$-dependent Boundary Disturbance

In this section non-axial acoustic transients generated by source oscillations with $y$-dependent amplitude is discussed.

If the velocity oscillation at the source ($\bar{x} = 0$) is given by $\hat{u} = A(y)\sin(t)$, (29) must be solved subject to the following conditions:

$$t = 0, \qquad p_1 = p_{1t} = 0, \tag{59}$$

$$\bar{x} = 0, \qquad p_{1\bar{x}} = -A(y)\cos(t); \qquad \bar{x} \to \infty, \qquad p_1 = \text{finite}, \tag{60}$$

$$y = 0; 1, \qquad p_{1y} = 0. \tag{61}$$

A solution procedure identical to that used to solve (32)–(35) can be employed to obtain

$$p_1 = \tilde{A}_0 \sin(t - \bar{x}) + \sum_{n=1}^{\infty} \tilde{A}_n I_n(t, \bar{x}) \cos(n\pi y), \qquad \bar{x} \le t, \tag{62}$$

where $I_n$ is the same integral as defined in (50). The Fourier coefficients $\tilde{A}_0$ and $\tilde{A}_n$ are defined by

$$A(y) = \tilde{A}_0 + \sum_{n=1}^{\infty} \tilde{A}_n \cos(n\pi y). \tag{63}$$

Equation (62) consists of a propagating axial wave mode of constant amplitude $\tilde{A}_0$, and an infinite number of dispersive higher modes. Note that unlike the $O(M)$ higher modes due to refraction considered earlier, here the higher modes, generated directly by the acoustic source, are of the same order of magnitude as the fundamental mode. After sufficient time elapses, in the absence of resonance, the solution may again be expressed into the quasi-steady form,

$$\begin{aligned} p_1 \;=\;& \tilde{A}_0 \sin(t - \bar{x}) + \sum_{n=1}^{N} \frac{\tilde{A}_n}{\sqrt{1-q_n^2}} \sin\left(t - \sqrt{1-q_n^2}\,\bar{x}\right) \cos(n\pi y) \\ &+ \cos(t) \sum_{n=N+1}^{\infty} \frac{\tilde{A}_n}{\sqrt{q_n^2 - 1}} e^{-\sqrt{q_n^2-1}\,\bar{x}} \cos(n\pi y). \end{aligned} \tag{64}$$

As an example, the boundary disturbance $\hat{u}(x=0) = y\sin(t)$ in a laminar mean flow field with bulk velocity $\tilde{U}_0 = 2/3$, is considered. This bulk velocity corresponds to $U = 4y(1-y)$, although the explicit form of $U(y)$ is not needed for the leading order calculation. The maximum mean flow Mach number is assumed to be 0.1. Figs. 9a–9d exemplify the characteristic acoustic pressure signals at $x = 2\pi$ ($x' = \lambda'$), under four different driving acoustic frequencies, as evaluated numerically from (62). In each figure, the time variations of $p_1$ on both duct walls ($y = 0, 1$) and at the center-plane ($y = 1/2$) are depicted. In Fig. 9a $\Omega = 2$, lower than the cut-off frequency for the first oblique propagated mode in the duct. The resulting wave field is basically an axial one. Thus the pressure signals at three different $y$-locations on the same duct cross-section are almost the same, whose amplitudes are approximately 1/2 ($\tilde{A}_0$ in (63)). The small deviations are again attributed to the initial transients that diminish as time progresses. Fig. 9b corresponds to $\Omega = \pi$, the resonant frequency for the first acoustic mode ($n = 1$), which causes $p_1$ to grow with time. The wave field is no longer purely axial because of the appearance of the transverse waves associated with the resonant mode. The results in Fig. 9c for $\Omega = 4$ contain both the fundamental mode and the first propagated oblique mode. The pressure curves vary with the $y$-coordinate but are bounded. Finally, in Fig. 9d the driving acoustic frequency is high enough to allow the third propagated oblique mode to appear in the duct, in addition to the fundamental and the first modes (note that the even modes do not appear because $A(y)$ is an odd function of $y$). The acoustic pressure curves differ dramatically from those in the previous three figures.

Additional numerical evaluations of $p_1$ show that when the acoustic frequency is varied within the range that allows a fixed number of propagated modes, the character of the wave field remains similar though the results vary in a quantitative sense. However, whenever the cut-off frequency of a new mode is crossed, there is a qualitative change in the wave phenomena.

The $O(M)$ refraction effect of this more general acoustic system could be studied by using the first order results in (31). This is deferred to a future endeavor.

# 4 Acoustic Boundary Layer Solution

## 4.1 Boundary Layer Formulation

In the acoustic boundary layer near the wall at $y = 0$, thermodynamic perturbations must be of the same order of magnitude as those found at the edge of the core flow. Therefore,

$$p = 1 + M^2\gamma\tilde{p}, \qquad \rho = 1 + M^2\tilde{\rho}, \qquad T = 1 + M^2\tilde{T}, \tag{65}$$

where the tilded variables denote acoustic quantities superimposed on the mean state. A stretched boundary layer coordinate pointing away from the wall,

$$\eta = \frac{y}{\delta}, \tag{66}$$

is needed in order to describe the structure of the extremely slender acoustic boundary layer. A balance between diffusion and other important physical mechanisms in the general governing equations (2)-(6) can be obtained if

$$\delta = \left(\frac{M}{\Omega R_e}\right)^{\frac{1}{2}}, \tag{67}$$

which provides the scale of the acoustic boundary layer thickness. In dimensional terms, one finds the well known result $\delta' \sim (\nu'/\omega')^{1/2}$, indicating explicitly the dependence of boundary layer thickness upon the fluid viscosity and the frequency of the traveling acoustic waves. The proper scaling for fluid velocities in the layer, obtained by examining the asymptotic behavior of (11) when $y \to 0$ for $\epsilon = M$, are given by

$$u = M\tilde{u} + \delta\eta U'(0) + \cdots, \qquad v = (M\delta)\tilde{v}. \tag{68}$$

The $O(\delta)$ contribution to $u$ arises from the Taylor series expansion for $U(y)$ in the boundary layer, which is much smaller in magnitude than the horizontal acoustic velocity $M\tilde{u}$, given the assumption made in Section 2 that $M \gg 1/R_e$. Consequently, the independent variable $x$, rather than $\bar{x}$, is an appropriate horizontal coordinate.

If the new dependent and independent variables defined in (65)-(68) are used, (2)-(6) can be transformed into

$$\gamma\tilde{p} - \tilde{\rho} - \tilde{T} = M^2\tilde{\rho}\tilde{T}, \tag{69}$$

$$\tilde{\rho}_t + \tilde{u}_x + \tilde{v}_\eta = -M^2\left[(\tilde{\rho}\tilde{u})_x + (\tilde{\rho}\tilde{v})_\eta\right] + O(M\delta), \tag{70}$$

$$\tilde{u}_t - \tilde{u}_{\eta\eta} + \tilde{p}_x = -M^2(\tilde{\rho}\tilde{u}_t + \tilde{u}\tilde{u}_x + \tilde{v}\tilde{u}_\eta) + O(M^4) + O(M\delta), \tag{71}$$

$$\tilde{p}_\eta = O(\delta^2), \tag{72}$$

$$\tilde{T}_t - \frac{\gamma}{P_r}\tilde{T}_{\eta\eta} + (\gamma-1)(\tilde{u}_x + \tilde{v}_\eta) = M^2\left\{\gamma(\gamma-1)\left[\tilde{u}_\eta^2 - \tilde{p}(\tilde{u}_x + \tilde{v}_\eta)\right]\right.$$
$$\left. -(\tilde{\rho}\tilde{T}_t + \tilde{u}\tilde{T}_x + \tilde{v}\tilde{T}_\eta)\right\} + O(M^4) + O(M\delta). \tag{73}$$

The above equations are accurate representations of (2)–(6) in the acoustic boundary layer up to $O(M^2)$. The orders of magnitude of terms not written explicitly are indicated in each equation. It is interesting to notice that nonlinear product terms. which are responsible for acoustic streaming phenomena (Rott 1964), again turn out to be of $O(M^2)$ relative to leading order acoustics. Terms of $O(M\delta)$ result from the residue mean flow velocity in the boundary layer (cf. (68)). These are higher-order small quantities, of comparable size with $O(M^4)$ terms under flow conditions described by, for example, $M = 0.1$ and $R_e = 10^6$.

In the following solution development correction terms of $O(M^2)$ and smaller in (69)–(73) are ignored. For convenience the same variable names (with an implicit zero subscript) will be used to describe the basic acoustic variations in the asymptotic series. Notice that although $O(M)$ terms do not appear in (69)–(73), the results are valid to $O(M)$, and are matched with the core solutions to the same order. The general matching conditions are expressed mathematically as

$$\Psi_{b.l.}(x,t,\eta \to \infty) \sim \Psi_{core}(x,t,y \to 0), \qquad \Psi = (u,v,p,\rho,T). \tag{74}$$

On the duct wall the no-slip condition and the appropriate thermal conditions must be imposed.

## 4.2 Transient Solutions

The acoustic pressure is seen from (72) to be basically uniform across the boundary layer, equal to that at the edge of the layer. Thus

$$\tilde{p} = \tilde{p}(t, \bar{x}; y \to 0). \tag{75}$$

When the small correction terms on the right side of (71) are truncated, the resulting equation, which describes the transient diffusion process of the horizontal velocity perturbation driven by the acoustic pressure, is seen to be decoupled from the others. It must be solved subject to the no-slip condition at $\eta = 0$. At $t = 0$, $\tilde{u}$ must vanish because there is no acoustic motion in the core. Following a standard Laplace transform procedure, the solution is obtained in integral form:

$$\tilde{u} = -\int_{\bar{x}}^{t} \tilde{p}_x(\xi, \bar{x})\, erf\left(\frac{\eta}{2\sqrt{t-\xi}}\right) d\xi. \tag{76}$$

Eqns. (30), (46) and (62) can be used in (75) and (76) to evaluate the corresponding boundary layer velocity.

It is also of interest to study the transverse acoustic velocity and other thermodynamic variables in the acoustic boundary layer. To this end (69), (70) and (73) are combined to find

$$\tilde{T}_t - \frac{1}{P_r}\tilde{T}_{\eta\eta} = (\gamma - 1)\tilde{p}_t, \tag{77}$$

which is a diffusion equation with a compressibility forcing function, valid to $O(M)$. An appropriate thermal condition needs to be specified at the duct wall, to obtain solutions for $\tilde{T}$ as well as $\tilde{\rho}$ and $\tilde{v}$. For simplicity two idealized types of thermal conditions, i.e., the adiabatic condition and the isothermal condition, are considered, with the understanding that practical situations usually lie in-between.

*1) Adiabatic Wall ($\tilde{T}_\eta(\eta = 0) = 0$).* A formal solution to (77) subject to zero initial condition and the adiabatic wall condition yields the isentropic relations

$$\tilde{T} = (\gamma - 1)\tilde{p}, \qquad \tilde{\rho} = \tilde{p} \tag{78}$$

if (69) is used. This indicates that no thermal diffusion exists, and all the thermodynamic quantities are uniform across the acoustic boundary layer. Eqn. (70) can be integrated to $O(M)$ by using (76) and (78) to give

$$\tilde{v} = -\tilde{p}_t \eta + \frac{\partial}{\partial x}\left[\int_{\bar{x}}^{t} \tilde{p}_x(\xi, \bar{x}) \int_0^{\eta} erf\left(\frac{\zeta}{2\sqrt{t-\xi}}\right) d\zeta d\xi\right], \tag{79}$$

which is zero on the wall surface. By employing integration by parts for the error function, the above result is rewritten as

$$\begin{aligned} \tilde{v} \;=\; & \left[-\tilde{p}_t + \frac{1}{1+M\tilde{U}_0} erf\left(\frac{\eta}{2\sqrt{t-\bar{x}}}\right) + \int_{\bar{x}}^{t} \tilde{p}_{xx}\, erf\left(\frac{\eta}{2\sqrt{t-\xi}}\right) d\xi\right]\eta \\ & + \frac{1}{1+M\tilde{U}_0}\frac{2\sqrt{t-\bar{x}}}{\sqrt{\pi}}\left(e^{-\frac{\eta^2}{4(t-\bar{x})}} - 1\right) + \frac{2}{\sqrt{\pi}}\int_{\bar{x}}^{t} \tilde{p}_{xx}\sqrt{t-\xi}\left(e^{-\frac{\eta^2}{4(t-\xi)}} - 1\right) d\xi, \end{aligned} \tag{80}$$

where the factor $1/(1 + M\tilde{U}_0)$ arises from $d\bar{x}/dx$. Eqn. (80) is arranged according to terms that grow with $\eta$ and those that remain $O(1)$ as $\eta \to \infty$. The former are driven by the refraction induced transverse velocity in the core, and can be shown to match with the asymptotic behavior of the corresponding core solution, given the coordinate transformation (66).

*2) Isothermal Wall ($\tilde{T}(\eta = 0) = 0$).* The mathematical system for $\tilde{T}$ is analogeous to that for $\tilde{u}$. The solution can immediately be written down as

$$\tilde{T} = (\gamma - 1)\int_{\bar{x}}^{t} \tilde{p}_\xi(\xi, \bar{x})\, erf\left(\frac{\eta_T}{2\sqrt{t-\xi}}\right) d\xi, \tag{81}$$

where

$$\eta_T = \eta\sqrt{P_r} = \frac{y}{\delta_T} \tag{82}$$

is the vertical coordinate for the temperature boundary layer, of thickness characterized by $\delta_T = (M/(\Omega P_r R_e))^{\frac{1}{2}}$. Eqn. (81) can be transformed into a more meaningful form by integrating the right side by parts, and defining

$$\zeta = \frac{\eta_T}{2\sqrt{t-\xi}}. \tag{83}$$

to give

$$\tilde{T} = (\gamma - 1)\left[\tilde{p}(t, \bar{x}) - \frac{2}{\sqrt{\pi}} \int_{\frac{\eta_T}{2\sqrt{t-\bar{x}}}}^{\infty} \tilde{p}\left(t - \frac{\eta_T^2}{4\zeta^2}, \bar{x}\right) e^{-\zeta^2} d\zeta\right] \tag{84}$$

The second term in the square brackets in (84), arising from conduction effects, describe the deviation in temperature from the isentropic condition represented by $\tilde{p}(t, \bar{x})$. One notices that at $\bar{x} = t$, the instantaneous location of the acoustic wavefront in the core, both $\tilde{p}$ and $\tilde{T}$ are zero to match those quantities in the undisturbed flow field. The acoustic density and transverse velocity for the present case can be derived from (69) and (70), respectively. They are omitted here for brevity.

## 4.3 Quasi-steady Solutions

As shown previously, core solutions for a non-resonant acoustic system as $t - \bar{x}$ becomes large consist of quasi-steady modes only. The corresponding boundary layer solutions are more easily derived by using the complex notation. The acoustic pressure is written as a summation of complex Fourier series,

$$\tilde{p}(t, \bar{x}) = i \sum_{n=0}^{\infty} a_n e^{-i\left(t - \sqrt{1 - q_n^2}\, \bar{x}\right)}. \tag{85}$$

Given (75), a comparison of (85) with the core pressure expressions shows that

$$\begin{aligned} a_0 &= 1 - M \sum_{k=1}^{\infty} \frac{2\tilde{U}_k}{q_k^2}, \\ a_n &= M \frac{\tilde{U}_n (2 - q_n^2)}{q_n^2 \sqrt{1 - q_n^2}}, \qquad n = 1, 2, \cdots \end{aligned} \tag{86}$$

for the **axial wave refraction case** (cf. (30) and (52)), and

$$\begin{aligned} a_0 &= \tilde{A}_0, \\ a_n &= \frac{\tilde{A}_n}{\sqrt{1 - q_n^2}} \qquad n = 1, 2, \cdots \end{aligned} \tag{87}$$

for the non-axial wave case examined in Section 3.3 (cf. (64)), without considering the refraction effect.

The velocities in the acoustic boundary layer are dependent upon the boundary coordinate $\eta$. One can assume that the quasi-steady solution for each horizontal velocity mode is of the form $\tilde{u}_n = b_n(\eta)e^{-i\left(t-\sqrt{1-q_n^2}\,\bar{x}\right)}$. If this expression is substitited into (71) with (85), and the conditions $\tilde{u}_n(\eta = 0) = 0$; $\tilde{u}_n(\eta \to \infty) = O(1)$ are invoked, then the desired solution is

$$\tilde{u} = \sum_{n=0}^{\infty} \tilde{u}_n = \frac{i}{1 + M\tilde{U}_0} \sum_{n=0}^{\infty} a_n \sqrt{1 - q_n^2} \left(1 - e^{-\frac{1-i}{\sqrt{2}}\eta}\right) e^{-i\left(t-\sqrt{1-q_n^2}\,\bar{x}\right)}, \qquad (88)$$

where $a_n$ is given by (86) or (87), depending on the core acoustic solutions. Eqn. (88) can be rewritten in terms of its real part, which is, for the refraction case,

$$\begin{aligned}\tilde{u} \;=\; & \frac{1}{1 + M\tilde{U}_0} \left\{ \left(1 - M \sum_{k=1}^{\infty} \frac{2\tilde{U}_k}{q_k^2}\right) \left[\sin(t - \bar{x}) - e^{-\frac{\eta}{\sqrt{2}}} \sin\left(t - \bar{x} - \frac{\eta}{\sqrt{2}}\right)\right] \right. \\ & + M \sum_{n=1}^{N} \tilde{U}_n \left(\frac{2}{q_n^2} - 1\right) \left[\sin\left(t - \sqrt{1 - q_n^2}\,\bar{x}\right) - e^{-\frac{\eta}{\sqrt{2}}} \sin\left(t - \sqrt{1 - q_n^2}\,\bar{x} - \frac{\eta}{\sqrt{2}}\right)\right] \\ & \left. + M \sum_{n=N+1}^{\infty} \tilde{U}_n \left(\frac{2}{q_n^2} - 1\right) e^{-\sqrt{q_n^2 - 1}\,\bar{x}} \left[\sin(t) - e^{-\frac{\eta}{\sqrt{2}}} \sin\left(t - \frac{\eta}{\sqrt{2}}\right)\right] \right\}. \qquad (89)\end{aligned}$$

As the value of $\eta$ increases, the $\eta$-dependent terms in (89) diminish exponentially, and the result is that of the inviscid core evaluated at $y = 0$.

The first term inside the curly braces in (89) is associated with the fundamental propagated mode in the core. It is the axial traveling wave counterpart of the classical Stokes solution (Stokes 1851). Thus the characteristic behavior of the Stokes solution, including velocity overshoot (Richardson's annular effect) near the edge of the layer, and strong viscous damping near the wall will be observed (cf. Figs. 10). The amplitude of the fundamental mode deviates by $O(M)$ from unity, due to the acoustic refraction effect (the infinite summation in the parentheses) and the bulk convection ($M\tilde{U}_0$) caused by the mean shear flow in the core. In the case of downstream propagation the former effect augments the axial wave amplitude, while the latter damps it. For upstream wave propagation the reversed trend is obtained. Eqn. (89) also shows that the $N$ higher propagated modes behave in the same way as the fundamental mode, except for decreased amplitude and increased phase speed as the mode number $n$ increases. Each mode exhibits Richardson's annular effect, followed by smooth transition to no-slip velocity on the wall. Like the core solution, the effect of attenuated modes are limited to a region close to the acoustic source.

The result given by (89) is illustrated graphically in Figs. 10a and 10b, which depict horizontal velocity profiles across the acoustic boundary layer when $\Omega = 2$ and 7 respectively, for $\pi/4$ intervals over one acoustic period, at a location one and half wavelengths ($x = 3\pi$) downstream the plane acoustic source. This location is sufficiently far from the acoustic source so that the effects of stationary modes (last summation term in (89)) are virtually non-existent. The solid lines denote the horizontal velocity $\tilde{u}$ when a mean flow field, described by $U = 4y(1-y)$ and $M = 0.1$, is present in the core region. The velocity distributions for the case of no mean flow ($M = 0$), which corresponds to the Stokes solution, are also plotted as dashed lines for comparison. It is observed that when $\Omega = 2$, the analogous solid and dashed curves differ only by a constant multiplication factor (cf. (89)), because the only propagated mode in the duct is purely axial. The velocity amplitude is smaller than that of the Stokes solution due to the bulk convection, whose damping effect exceeds the amplifying effect of refraction at this low frequency. It should be pointed out that the pairs of solid and dashed curves in Figs. 10 are plotted at the same relative phase within a cycle begining at their respective maximum velocity. The two solutions are out of phase in the absolute sense because the acoustic wave carried by the mean flow arrives at the given position sooner than that in the static field.

As the driving acoustic frequency becomes higher, the increased refraction amplifies the velocity oscillation. When $\Omega \cong 6$, the refraction effect roughly balances bulk convection effect, and the velocity curves are found to coincide with those derived from Stokes solution. The acoustic system remains dominated by the single fundamental mode until $\Omega \geq 2\pi$, when the second mode ($n = 2$) appears. Fig. 10b depicts such a case where $\Omega = 7$. Here the amplitude of the acoustic velocity is larger than that of the Stokes velocity. The velocity profiles can no longer be obtained by multiplying the corresponding Stokes velocity profiles by a constant, because the addition of the second propagated mode alters the phase of the velocity at each time instant. Additionally, this mode makes the magnitudes of the velocity as well as pressure $x$-dependent because the oblique waves strike the boundary layer nonuniformly along its course of propagation (cf. Fig. 2).

On the acoustic source plane, $x = 0$, it can be shown that (89) takes the form

$$\tilde{u}(\bar{x} = 0) = \sin(t) - e^{-\frac{\eta}{\sqrt{2}}} \sin\left(t - \frac{\eta}{\sqrt{2}}\right). \tag{90}$$

All the $O(M)$ terms disappear because acoustic convection and refraction take place only away from the acoustic source. However, (90) does not satisfy the boundary condition (17) because nonzero $\tilde{v}$ is allowed at $x = 0$. A boundary-layer type of treatment which eliminates the slip velocity along the acoustic source plane will be necessary in order for the extra term in (90) to vanish.

The acoustic temperature and transverse velocity in the quasi-steady state depends on the thermal boundary condition along the duct wall. If the wall is adiabatic, the thermodynamic properties of the boundary layer gas again obey the isentropic relation (78), and the transverse acoustic velocity is integrated from (70) to give

$$\begin{aligned} \tilde{v} \; = \; & \sum_{n=0}^{\infty} a_n \left\{ \left[ \frac{1 - q_n^2}{\left(1 + M\tilde{U}_0\right)^2} - 1 \right] \eta + \frac{1 - q_n^2}{\left(1 + M\tilde{U}_0\right)^2} \frac{1 + i}{\sqrt{2}} \left( e^{-\frac{1-i}{\sqrt{2}}\eta} - 1 \right) \right\} \\ & \times e^{-i\left(t - \sqrt{1 - q_n^2}\, x\right)}. \end{aligned} \tag{91}$$

Figs. 11a and 11b display the transverse velocity profiles, calculated from (91), under conditions identical to those employed in Figs. 10a and 10b respectively. The transverse boundary layer motion for $\Omega = 7$ is quite different from that for $\Omega = 2$, owing to the existence of the oblique acoustic waves in the core in the former case. As $\eta$ becomes large, both cases exhibit growth in velocity amplitude with $\eta$ to match with that in the core, in contrast to the transverse velocity in a Stokes boundary layer whose amplitude approaches a constant as the edge of the layer is approached.

If the wall is kept at constant temperature, the solution for $\tilde{T}$ and $\tilde{v}$ can be derived from (77) and (70) in the same manner. They are expressed below in the complex form:

$$\tilde{T} = i(\gamma-1)\sum_{n=0}^{\infty} a_n \left(1 - e^{-\frac{1-i}{\sqrt{2}}\eta_T}\right) e^{-i\left(t-\sqrt{1-q_n^2}\,x\right)}, \tag{92}$$

$$\tilde{v} = \sum_{n=0}^{\infty} a_n \left\{ \left[ \frac{1-q_n^2}{\left(1+M\tilde{U}_0\right)^2} - 1 \right] \eta + \frac{1-q_n^2}{\left(1+M\tilde{U}_0\right)^2} \frac{1+i}{\sqrt{2}} \left(e^{-\frac{1-i}{\sqrt{2}}\eta} - 1\right) + \frac{\gamma-1}{\sqrt{P_r}} \frac{1+i}{\sqrt{2}} \left(e^{-\frac{1-i}{\sqrt{2}}\eta_T} - 1\right) \right\} e^{-i\left(t-\sqrt{1-q_n^2}\,x\right)}. \tag{93}$$

The similar forms of (92) and (88) suggest that in the thermal boundary layer adjacent to an isothermal wall, the temperature diffuses in the same way as the horizonal velocity does in the viscous boundary layer. The first two terms in the curly braces of (93) are identical to those in (91), representing the effect of momentum diffusion driven by the acoustic waves in the core. In addition, thermal expansion of the gas due to nonuniform temperature distribution across the layer also contributes to the transverse fluid motion. This effect is represented by the last term in the curly braces of (93).

The fundamental mode in (92)-(93) can be shown to agree with the results obtained by Rott (1980) where the effect of the mean shear flow is removed. An important contribution of the mean shear flow is to generate a variety of acoustic waves that all contribute to the larger transverse velocity, represented in the acoustic boundary layer by the term proportional to $\eta$ in (91) and (93). In the limit $\eta \to \infty$, the magnitude of this term exceeds that of all the others. thus (91) and (93) have the same asymptotic behavior which can be shown to match with that of the core solution.

# 5 Discussion and Conclusions

In this study a systematic analysis has been developed to discover the effect of a low Mach number shear flow on acoustic wave propagation in a planar duct. Two distinct flow regions are considered: the inviscid, non-heat conducting core region and the thin acoustic boundary layer near the wall of the duct. The mathematical analysis is carried out in the limit $M \to 0$ for $R_e \gg O(1/M)$, when the axial wavelength is longer than or comparable in the order of magnitude sense with the duct width.

Solutions for the acoustic pressure and velocity describe both short-time acoustic transients and long-time evolution for both nonresonant and resonant cases. This study bridges the recent transient numerical study of Baum and Levine (1987) and earlier quasi-steady studies (Pridmore-Brown 1958, for example) and, more importantly, provides new results not available in those investigations. More physical insights into the refraction mechanism are obtained by demonstrating explicitly the interactions between the mean flow and the various types of acoustic waves represented by Fourier modes whose summation describes the global variations in acoustic quantities.

It is of interest to compare the present perturbation results with the numerical solutions of Baum and Levine (1987), to shed light on a number of issues raised in their initial-boundary value numerical study valid over a few acoustic periods.

*1) Acoustic Refraction Magnitude.* The following examples are used to demonstrate that the present linear analysis yields refraction magnitudes comparable with those from numerical solutions to the Navier-Stokes equations (Baum and Levine

1987). In a duct of width $d' = 0.1$ m, with a symmetric mean flow described by the one-seventh power law, a center-plane Mach number $M = 0.1$ and sound speed $c' = 340$ m/s, the dimensionless frequency corresponding to $f' = 3000$ Hz is $\Omega \cong 2.772$, less than the cut-off frequency for the first oblique wave. The quasi-steady axial wave solution is thus representative of the acoustic refraction phenomena since the transient effects are relatively small. The pressure amplitude near the wall, as calculated from (55), is 4.5% larger than that at the center-plane. This result compares well with the numerical result of 6.4% by Baum and Levine (1987), who employed the same conditions except that $d'$ is the diameter of an infinite cylinder. When the acoustic frequency is changed to 1000 Hz ($\Omega = 0.924$), the linear asymptotic solution and nonlinear numerical solution yield near-wall acoustic pressure increases of 0.50% and 0.55% respectively, relative to the centerline pressures. They are again in good agreement. The above comparisons should of course be interpreted in the qualitative sense, in view of the different geometries (parallel duct vs. circular cylinder) and flow models (laminar vs. turbulent $k$–$\epsilon$ model) used in the two studies. Nonetheless they demonstrate that linear studies can predict refraction effects accurately, and that the two types of solutions are in qualitative agreement if comparisons are made in the same parameter range. In the light of these conclusions, it is likely that the differences between linear and nonlinear results noted by Baum and Levine (1987) result from comparisons in inappropriate parameter regimes.

*2) Acoustic Boundary Layer Thickness and Structure.* The boundary layer structure described in the perturbation solution, including the Richardson's annular effect and the substantial viscous damping, also agrees qualitatively with that found by Baum and Levine (1987). In particular, it is of interest to compare the boundary layer thickness predicted by the analysis with that from the numerical work.

The effective thickness of the velocity boundary layer, as defined by Lighthill

(1978), is given by $5\delta = 5(M/(\Omega R_e))^{1/2}$. According to Figs. 10, this corresponds to the distance away from the solid wall for which the amplitude of $\tilde{u}$, after the overshoot, approaches its asymptote of constant value to within approximately 2.7%. For acoustic waves of frequency 1000 Hz traveling in air contained within a duct of width 0.1 m, under standard conditions (one atmospheric pressure and room temperature), the calculated boundary layer thickness is approximately 0.25% the width of the duct. This result should also hold for wave motion in a circular cylinder of diameter equal to the duct width, because the curvature effect is negligible in the extremely thin layer. If the same criterion of 2.7% deviation is applied to Fig. 14 of Baum and Levine (1987), one finds a boundary layer thickness of approximately 0.35% of the diameter of the cylinder. This result is actually larger than, but agrees well in the order of magnitude sense with, the linear perturbation prediction. Similar agreement is observed in terms of the maximum velocity overshoots and the locations where they occur. Thus we do not agree with the conclusion of Baum and Levine (1987) that linear theory significantly overpredicts the boundary layer thickness.

*3) Nonlinear Effect and Acoustic Streaming.* In the present work, through a systemmatic rational approximation and perturbation procedure, it has been demonstrated in (13)–(15) that the convective nonlinear terms are $O(M)$ smaller than those responsible for acoustic refraction when $x = O(1)$. Although the former can have an accumulative effect which eventually leads to waveform deformation and weak shock formation, the nonlinearization process becomes prominent only after the wave travels a distance of $x = O(M^{-2})$ (Kevorkian and Cole 1981; Wang and Kassoy 1990). Nonlinearity cannot have a profound influence on either the acoustic or the overall flow quantities, on the $O(1)$ time and length scales considered by Baum and Levine (1987). In the acoustic boundary layer the nonlinear terms are again shown to be $O(M^2)$, relative to the basic variations occurring there (cf. (69)–(73)). Acoustic streaming associated with the nonlinear convective terms is thus insignificant relative to the amplitude of refraction effects. The relatively good agreements between the present fundamentally linear solutions and the fully nonlinear numerical soultions in terms of refraction size and acoustic boundary layer structure, discussed above, also attest to the insignificance of the nonlinear phenomena.

The major findings of the present study can be summarized as follows: When a plane acoustic source of uniform strength is placed across a duct containing an undisturbanced shear flow, it induces leading order purely axial and quasi-steady acoustic waves propagating at a speed which is modified by $O(M)$ due to bulk convection. Second order acoustic quantities, including $y$-dependent axial and oblique propagating waves, as well as bulk forced oscillations that affect only a narrow region near the plane acoustic source, are generated as a result of leading order axial wave refraction by the mean flow velocity gradient. The propagated and attenuated wave modes exhibit transient phenomena initially, and evolve gradually, in the absence of resonance, into their respective quasi-steady state long after the passage of the axial wavefront.

Resonance occurs when the duct width is an integer multiple of the the driving acoustic wavelength. Then, the refraction of the axial wave induces an amplifying purely transverse wave. In general, the refraction effect increases with the driving frequency as well as the mean flow Mach number, and decreases with the wave amplitude. The refraction induced $O(M)$ wave phenomena become increasingly complex as the number of propagated modes, which is proportional to the driving frequency for given duct geometry, increases. At low frequency, when the driving acoustic wavelength is greater than the duct width, the only propagating waves are axial, and the net effect of acoustic refraction is to distort the pressure distribution across the wave by $O(M)$. The quasi-steady solutions agree with the classical axial wave solutions.

In the thin acoustic boundary layer, typically with thickness of less than 1% of the duct width, the acoustic pressure is basically uniform across the layer, equal to that at the outer edge of the layer. The boundary layer responds to all the acoustic modes existing in the core region, generating complex velocity and temperacture responses. Quasi-steady solutions again exist when resonance is absent, after an initial transient period. The horizontal velocity component for each acoustic mode exhibits Richardson's annular effect, followed by smooth transition to no-slip boundary condition on the wall. The total horizontal velocity deviates by $O(M)$ from the Stokes solution, because of the acoustic refraction and convection effects generated in the core. The transverse velocity grows with the transverse boundary layer coordinate, and is matched by the core solution outside the layer.

## Acknowledgements

This work was supported by Air Force Office of Scientific Research through a grant AFOSR 89-0023.

# References


Barnett, D.O. 1970 *An Analytical Investigation of Heat Transfer in Pulsating Turbulent Flow in a Tube*, Ph.D. Dissertation, Auburn University.

Barnett, D.O. 1981 The effect of pressure pulsations and vibrations in fully developed pipe flow. AEDC-TR-80-31 Report, Arnold Engineering Development Center.

Baum, J.D. and Levine, J.N. 1987 Numerical investigation of acoustic refraction. *AIAA Journal*, **25**(12), 1577–1586.

Gradshteyn, I.S. and Ryzhik, I.M. 1980 *Table of Integrals, Series, and Products*, corrected and enlarged edition, Academic Press.

Hersh, A.S. and Catton, I. 1971 Effect of shear flow on sound propagation in rectangular ducts. *J. Acoust. Soc. Am.*, **50**(3), 992–1003.

Kevorkian, J. and Cole, J.D. 1981 *Perturbation Methods in Applied Mathematics*. Springer-Verlag.

Lighthill, M.J. 1978 Acoustic streaming. *J. Sound Vib.*, **61**(3), 391–418.

Morse, P.M. and Ingard, K.U. 1968 *Theoretical Acoustics*. McGraw-Hill, Inc.

Mungur, P. and Gladwell, G.M.L. 1969 Acoustic wave propagation in a sheared fluid contained in a duct. *J. Sound Vib.*, **9**(1), 28–48.

Oberhettinger, F. and Badii L. 1973 *Tables of Laplace Transforms*, Springer-Verlag.

Pridmore-Brown, D.C. 1958 Sound propagation in a fluid flowing through an attenuating duct. *J. Fluid Mech.*, **4**, 393–406.

Richardson, E.G. and Tyler, E. 1929 The transverse velocity gradient near the mouths of pipes in which an alternating or continuous flow of air is established. *Proc. Phys. Soc. Lond.*, **42**, 1–15.

Romie, F.E. 1956 *Heat Transfer to Fluids Flowing with Velocity Pulsations in a Pipe*, Ph.D. Dissertation, UCLA.

Rott, N. 1964 Theory of time-dependent laminar flows. Princeton University Series, *High Speed Aerodynamics and Jet Propulsion*, Princeton University Press, Vol. **IV**, 395–438.

Rott, N. 1980 Thermoacoustics. *Advances in Applied Mechanics*, **20**, 135–175.

Schlichting, H. 1979 *Boundary Layer Theory*, Seventh edition, McGraw-Hill, N.Y.

Sexl, T. 1930 Annular effect in resonators observed by E.G.Richardson. *Zeitschrift für Physik*, **61**, 349–362.

Stokes, G.G. 1851 On the effect of the internal friction of fluids on the motion of pendulums. *Trans. Camb. Phil. Soc.*, **9**(II), 8–106.

Uchida, S. 1956 The pulsating viscous flow superposed on the steady laminar motion of incompressible fluid in a circular pipe. *ZAMP*, **7**, 403–422.

Wang, M. and Kassoy, D.R. 1990 Evolution of weakly nonlinear waves in a cylinder with a movable piston. *J. Fluid Mech.*, **221**, 27–52.

# List of Figures

8. Time variations of the second order acoustic pressure $p_2$ on the duct wall $y = 0$, at three axial locations, at resonant frequency $\Omega = 2\pi$. Other conditions are identical to those in Figs. 3a.

9. Time variations of the first order acoustic pressure $p_1$ at three $y$-locations on the duct cross-section $x = 2\pi$, as calculated from (62). The acoustic waves are generated by the $y$-dependent velocity perturbation $\hat{u}(x = 0) = y\sin(t)$ in a mean flow field described by $U = 4y(1 - y)$, $M = 0.1$. The dimensionless frequencies are (a) $\Omega = 2$; (b) $\Omega = \pi$; (c) $\Omega = 4$; and (d) $\Omega = 10$.

10. Profiles of quasi-steady horizontal velocity across the acoustic boundary layer at $x = 3\pi$, for $\pi/4$ intervals over one acoustic period, when the mean flow in the core is described by $U = 4y(1-y)$ and $M = 0.1$, and the acoustic disturbance is $\hat{u}(x = 0) = \sin(t)$. The dashed lines correspond to the Stokes solution ($M = 0$). The dimensionless frequencies are (a) $\Omega = 2$; and (b) $\Omega = 7$.

11. Profiles of quasi-steady transverse velocity across the acoustic boundary layer adjacent to an adiabatic duct wall, at $x = 3\pi$, for $\pi/4$ intervals over one acoustic period, under conditions identical to those in Figs. 10. The dimensionless frequencies are (a) $\Omega = 2$; and (b) $\Omega = 7$.

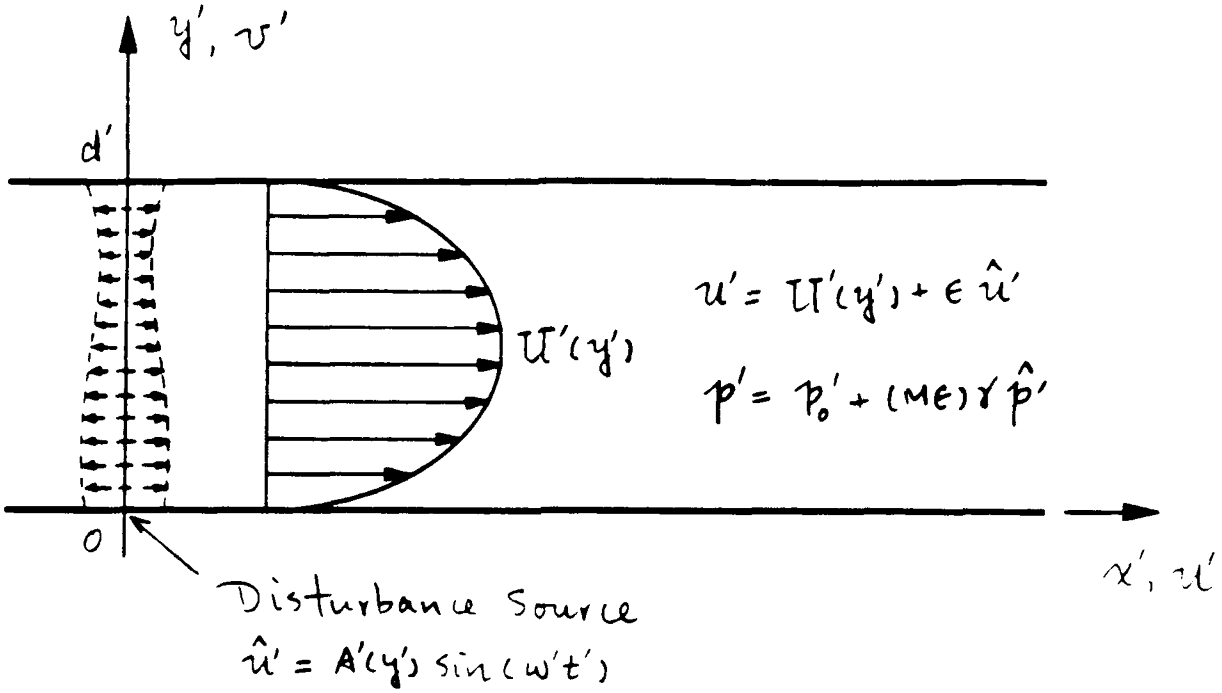
$y', v'$
$d'$
$0$
$u' = U'(y') + \epsilon \hat{u}'$
$U'(y')$
$p' = p_0' + (M\epsilon)\gamma \hat{p}'$
$x', u'$
Disturbance Source
$\hat{u}' = A'(y') \sin(\omega' t')$

Fig. 1

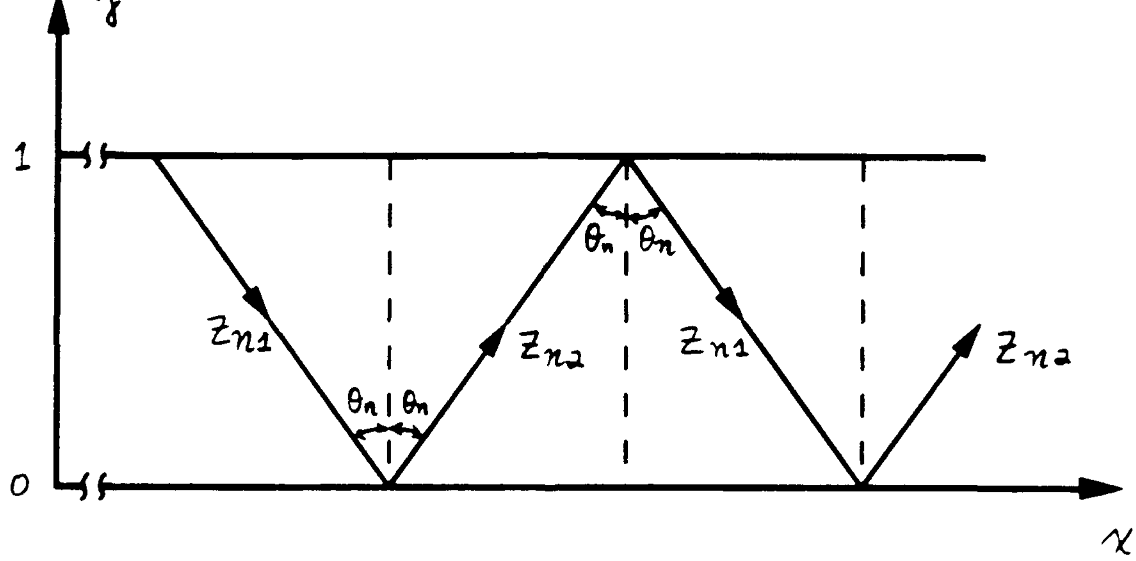


Fig. 2

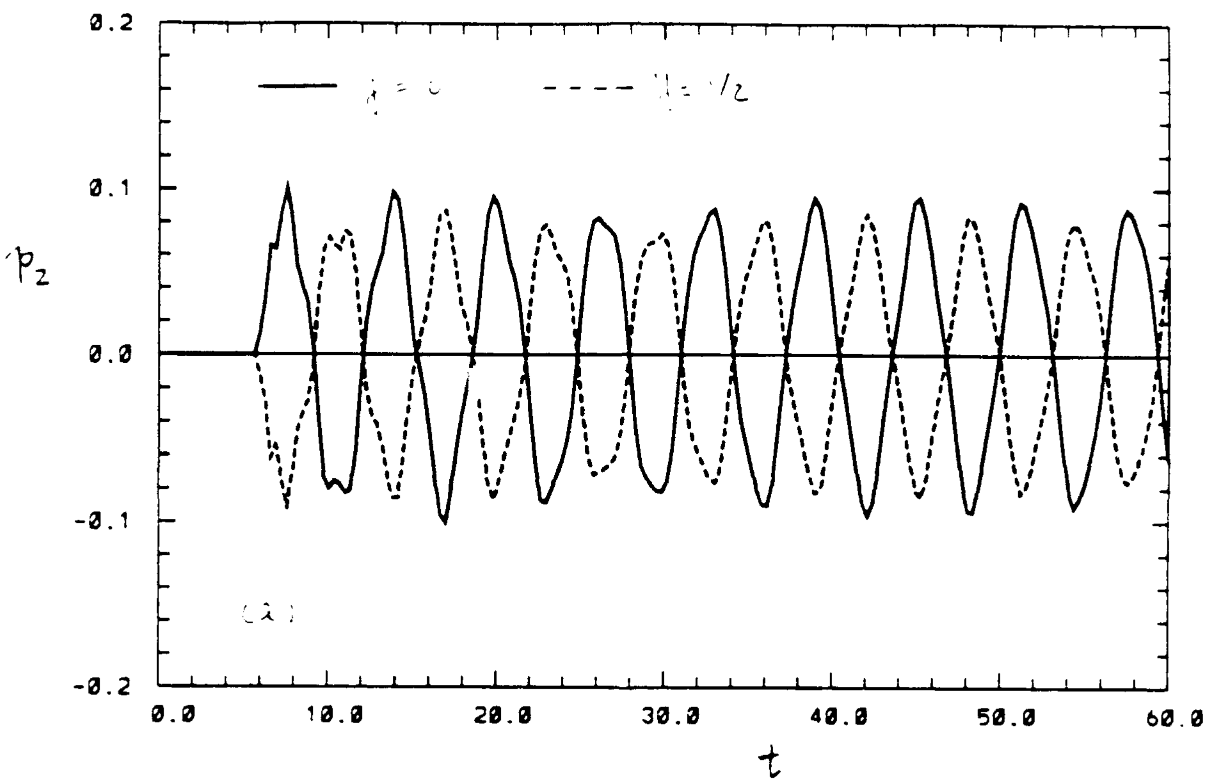


Fig. 3a

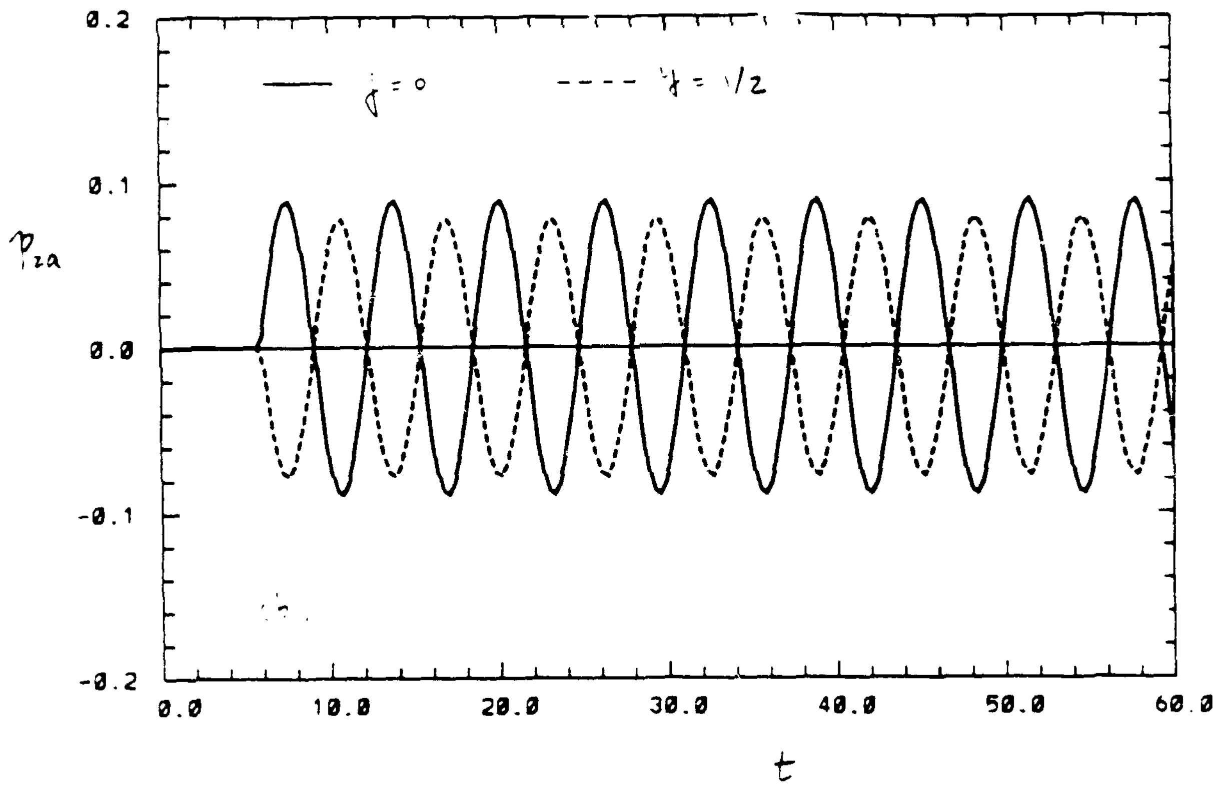


Fig 3b

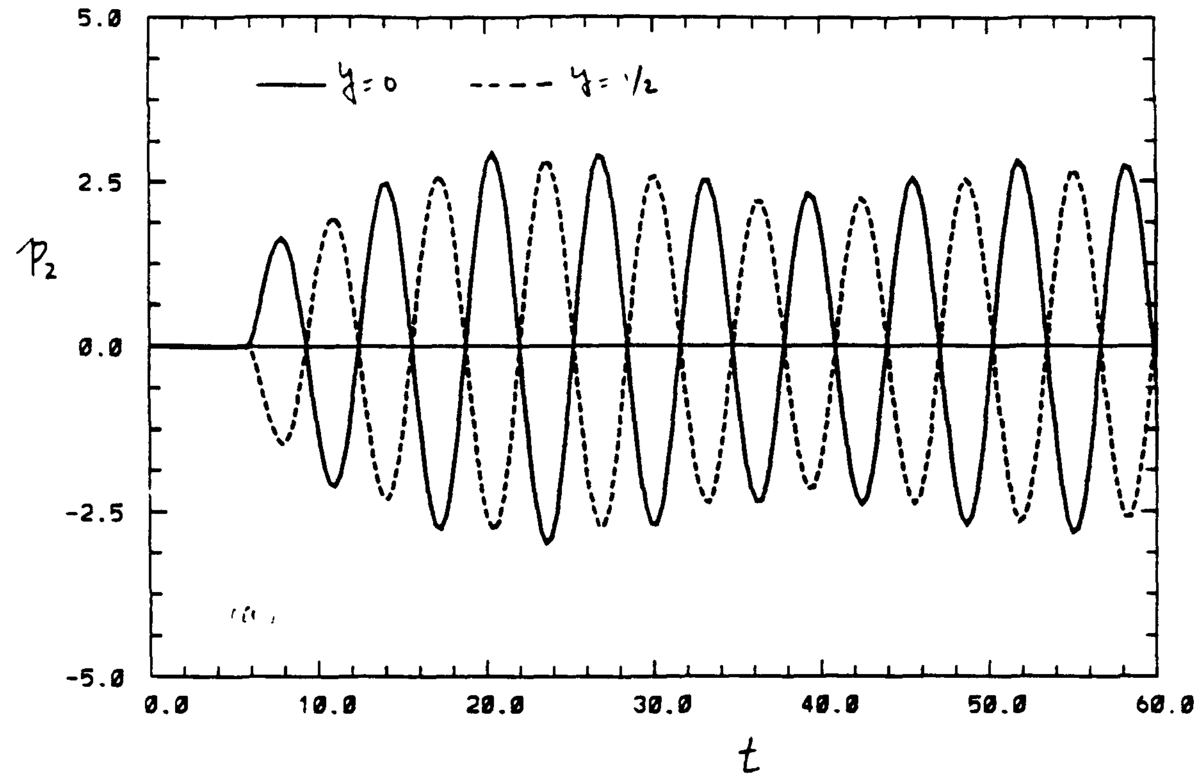


Fig 4a

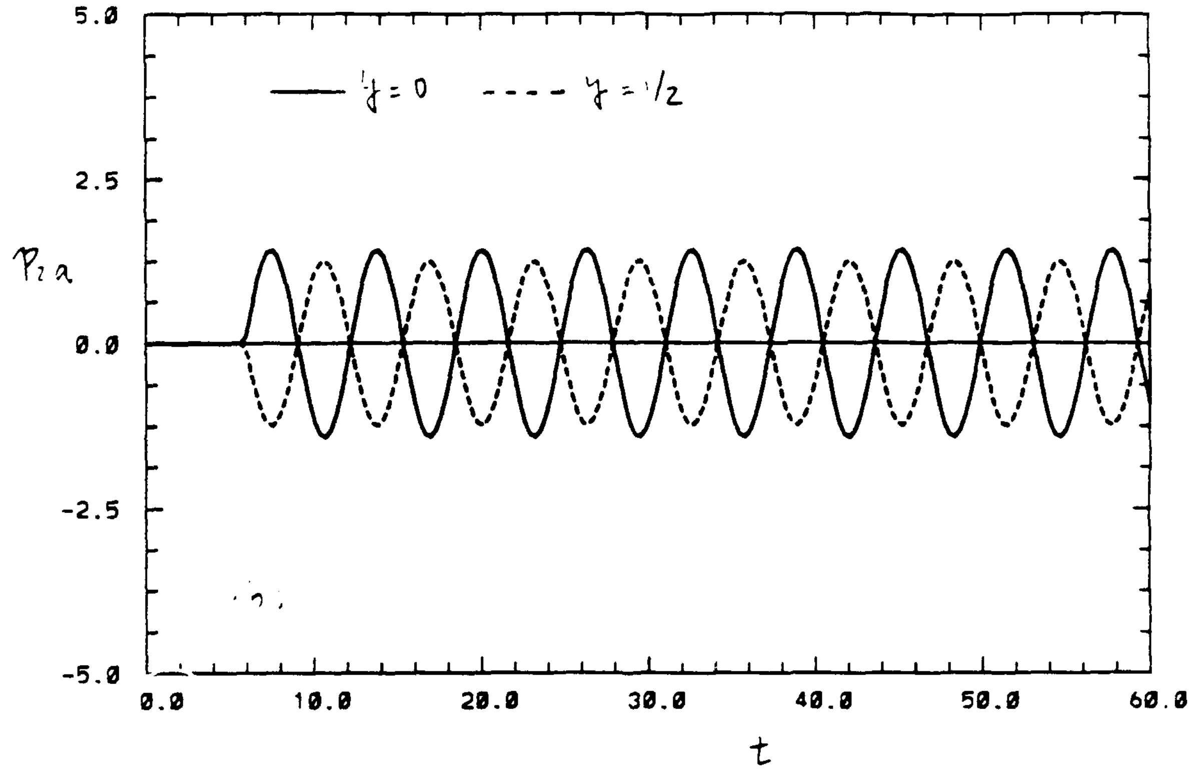


Fig. 4b

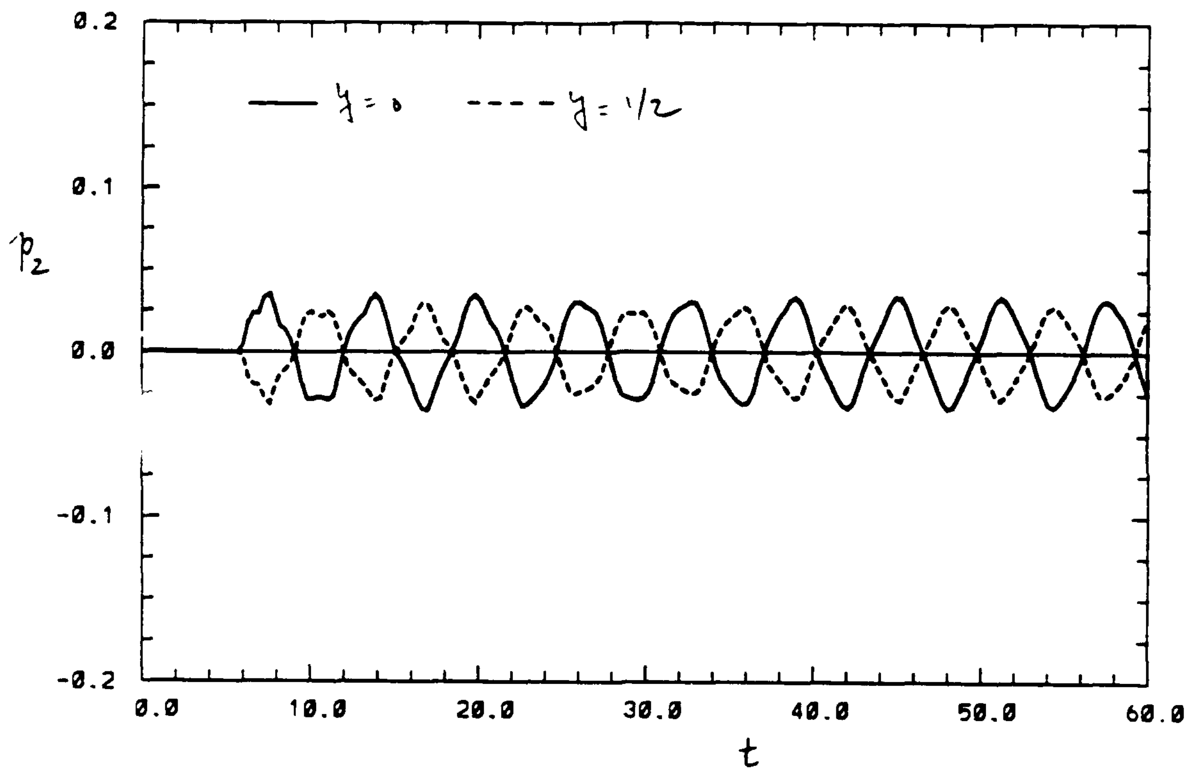


Fig. 5

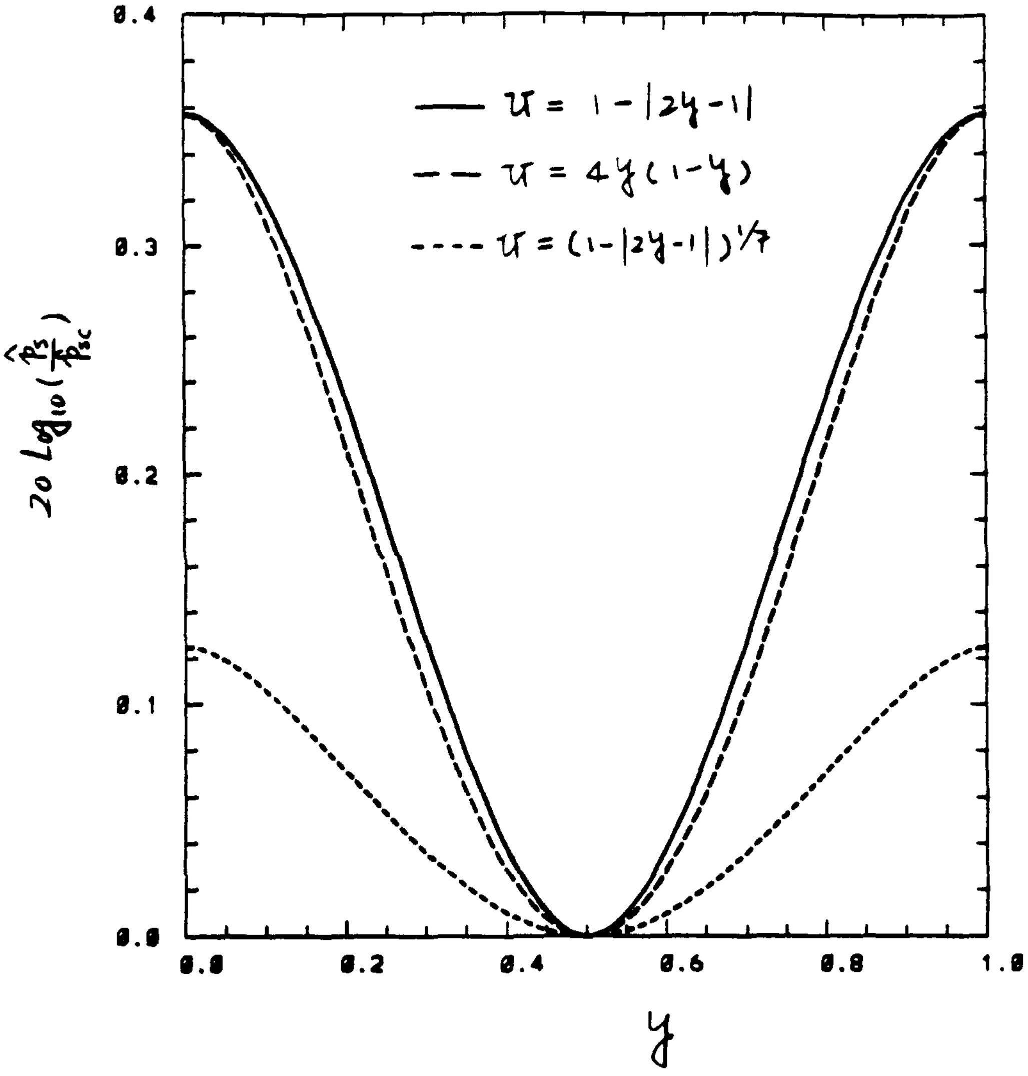

0.4
0.3
0.2
0.1
0.0
0.0
0.2
0.4
0.6
0.8
1.0
$U = 1-|2y-1|$
$U = 4y(1-y)$
$U = (1-|2y-1|)^{1/7}$
$20\,Log_{10}(\hat{p}_s/\hat{p}_{sc})$
$y$


Fig. 6

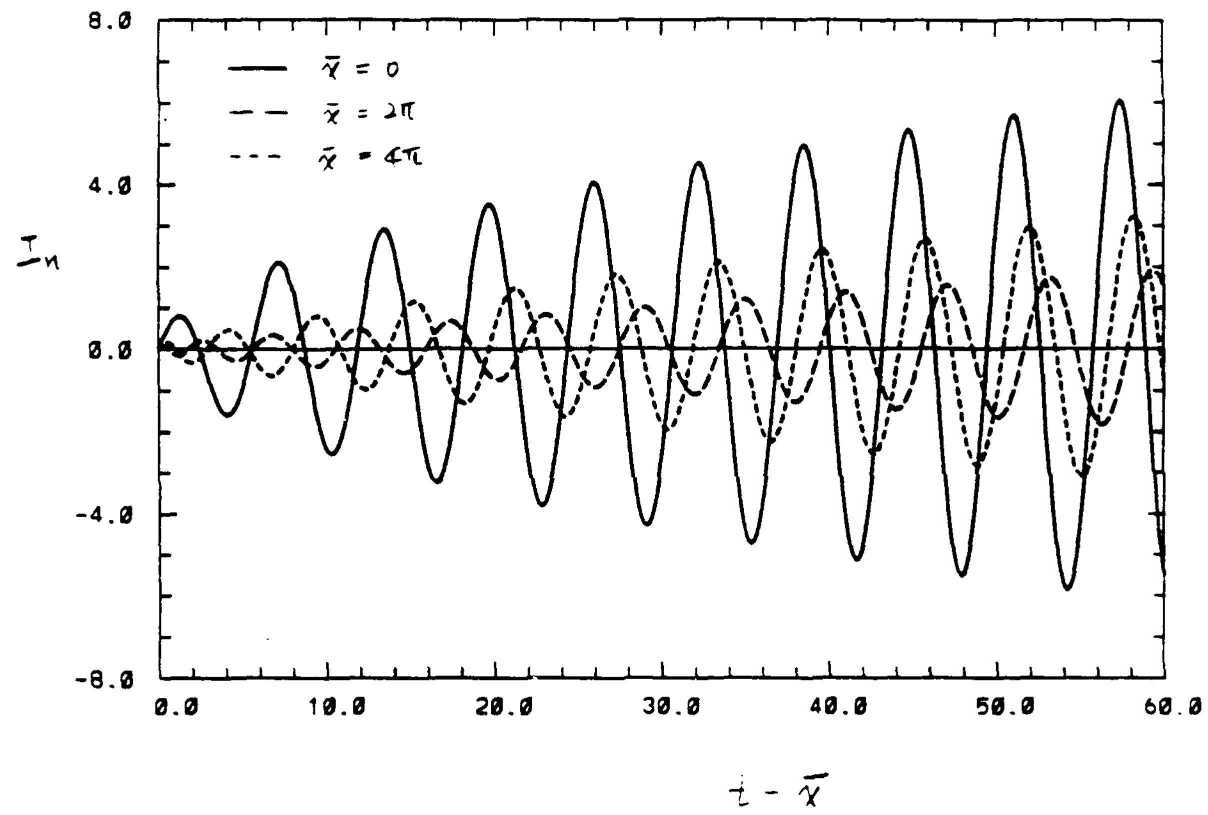

8.0
4.0
0.0
-4.0
-8.0
$\bar{x} = 0$
$\bar{x} = 2\pi$
$\bar{x} = 4\pi$
$I_n$
0.0
10.0
20.0
30.0
40.0
50.0
60.0
$t - \bar{x}$


Fig. 7

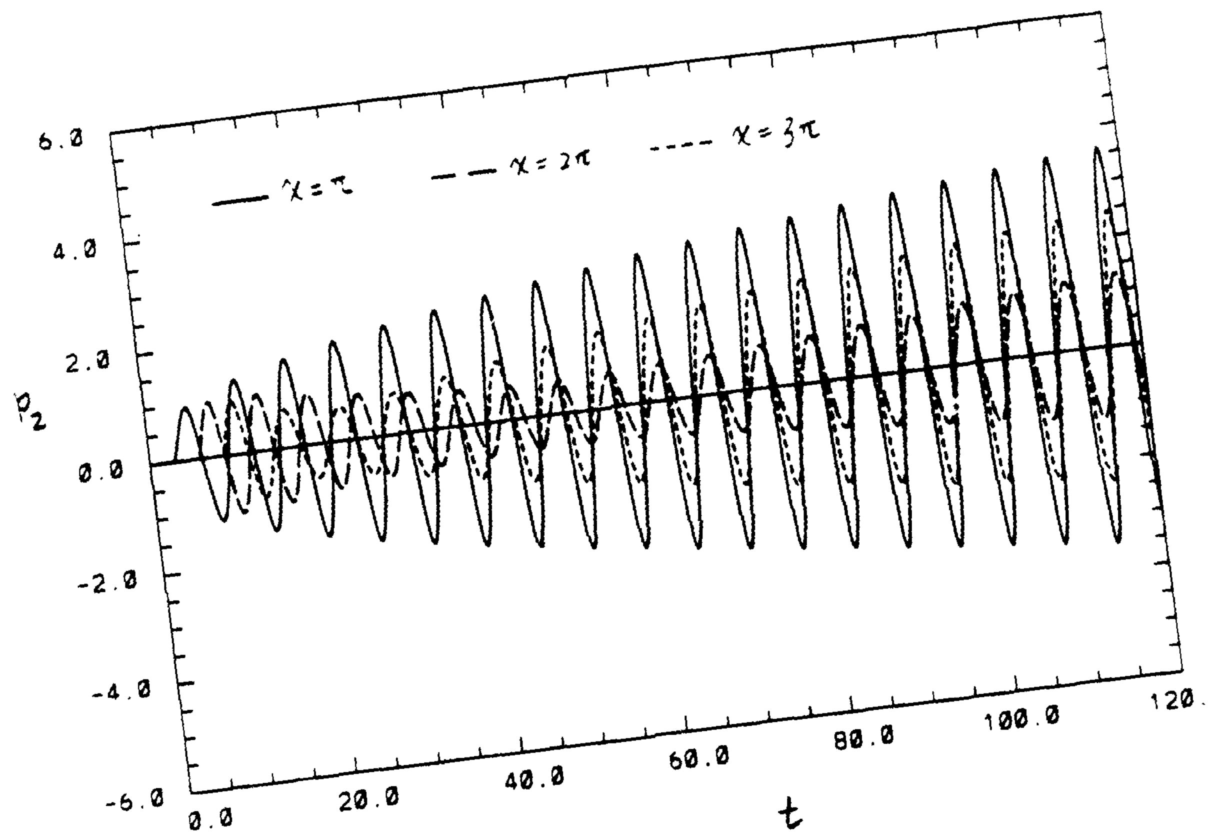


Fig. 8

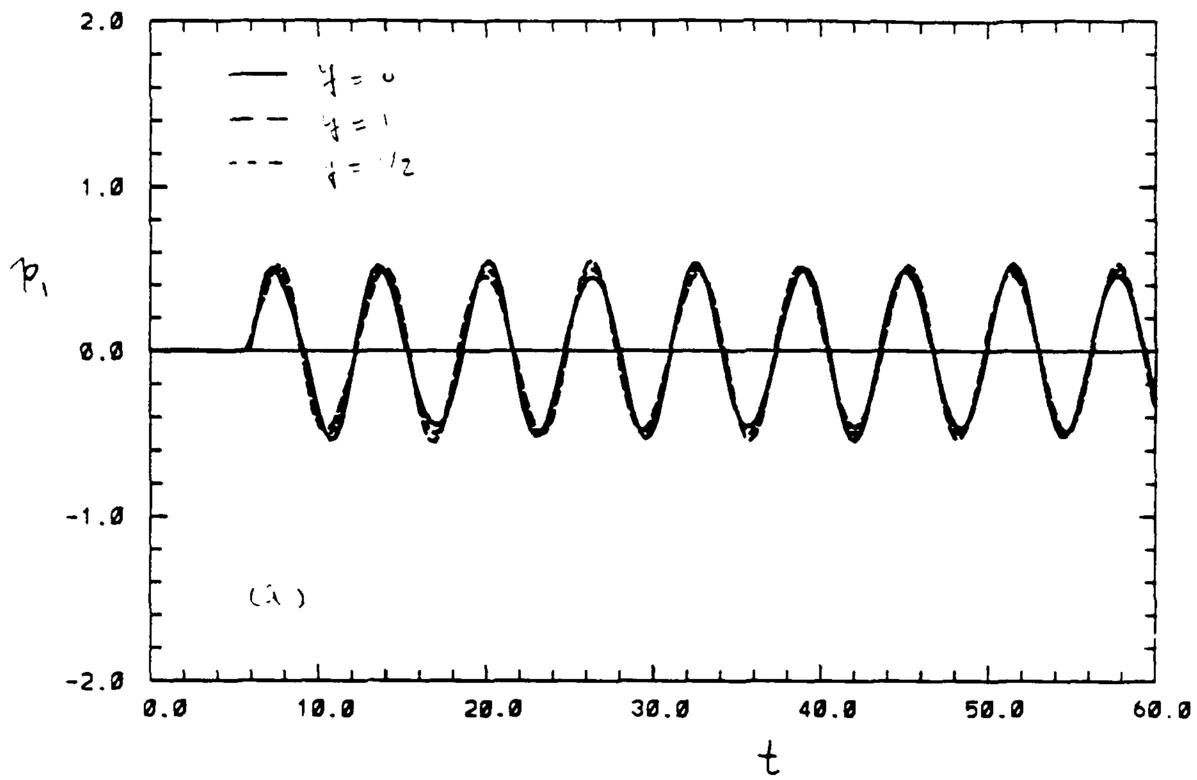


Fig. 7.2

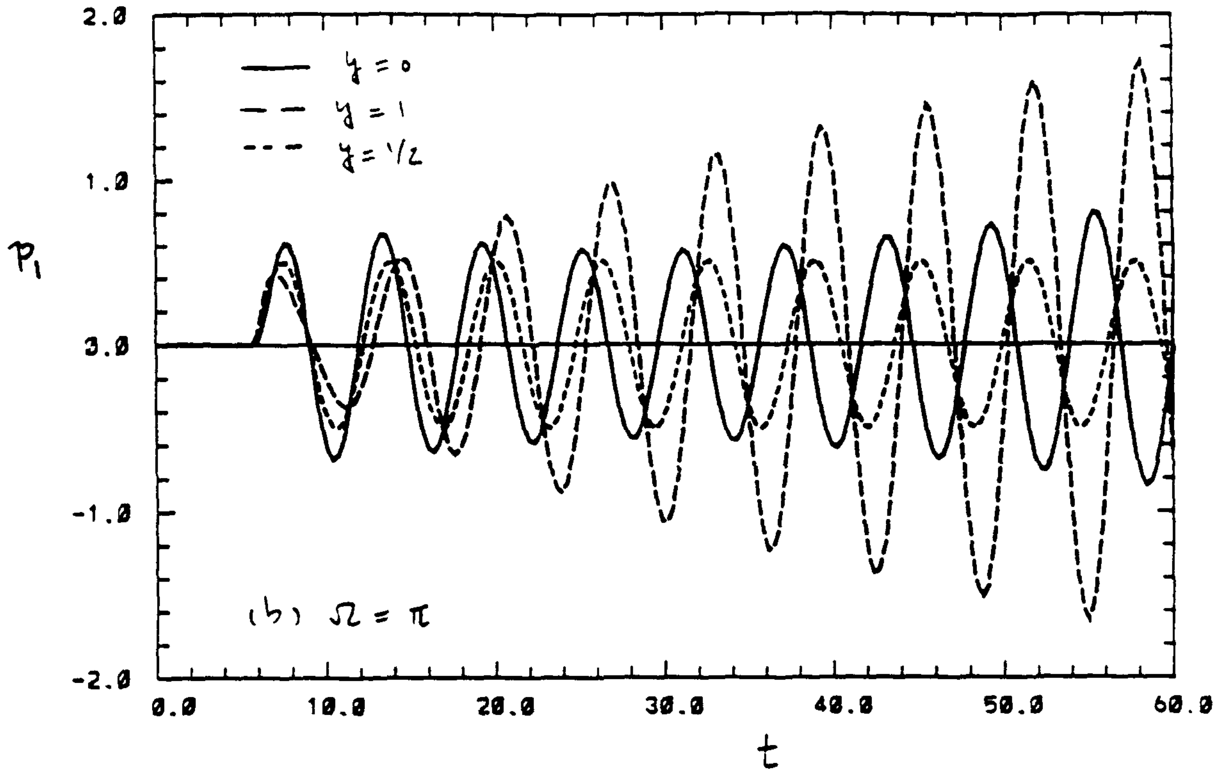


Fig. 9b

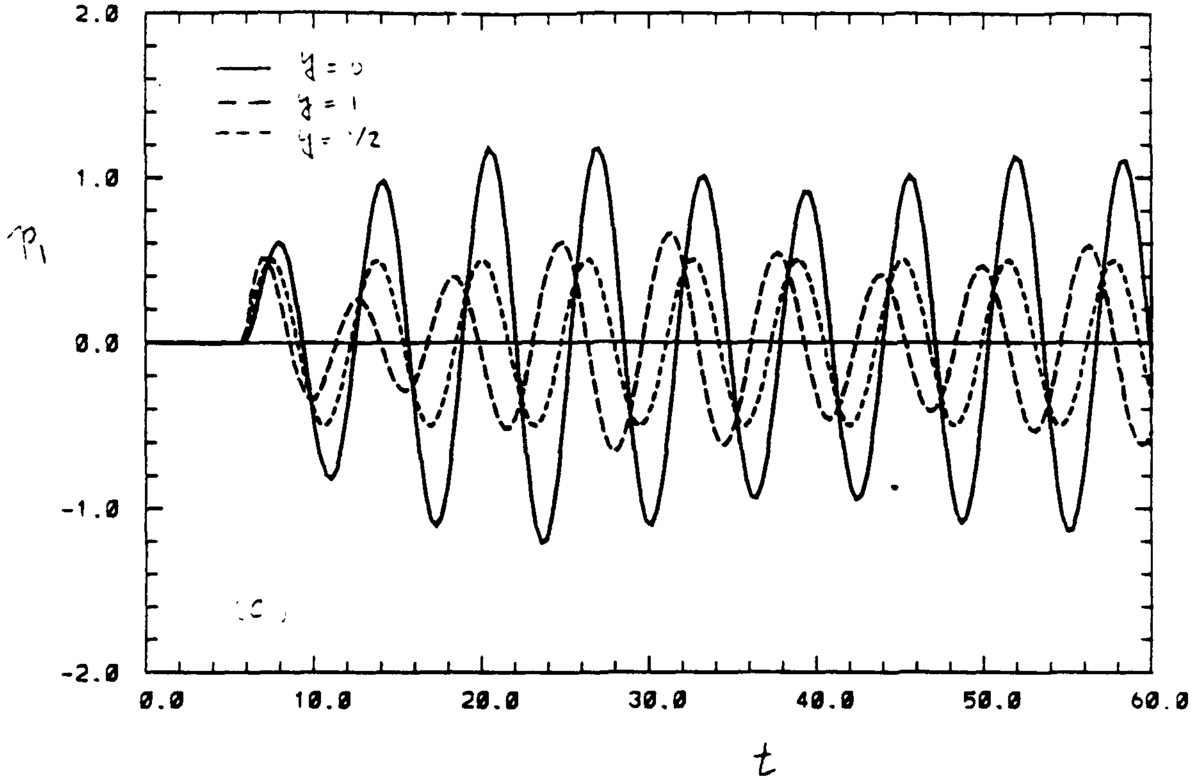


Fig 7c

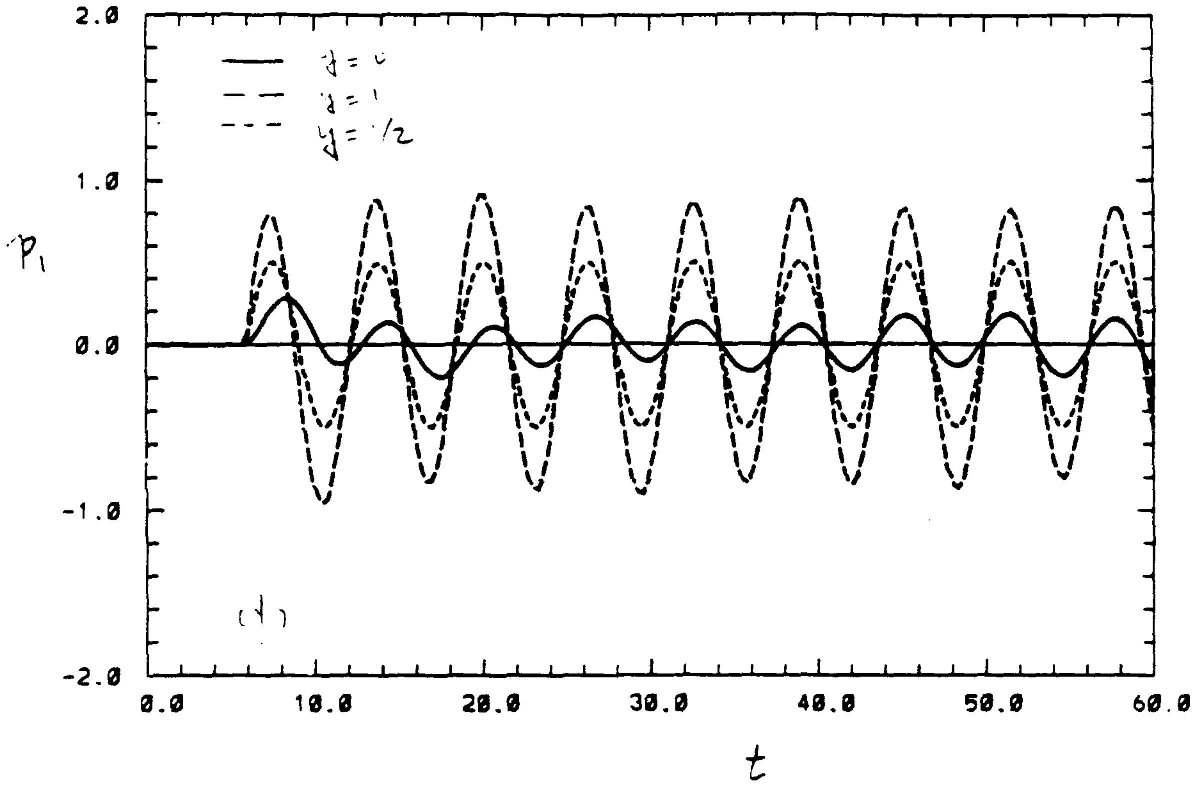


Fig. 14

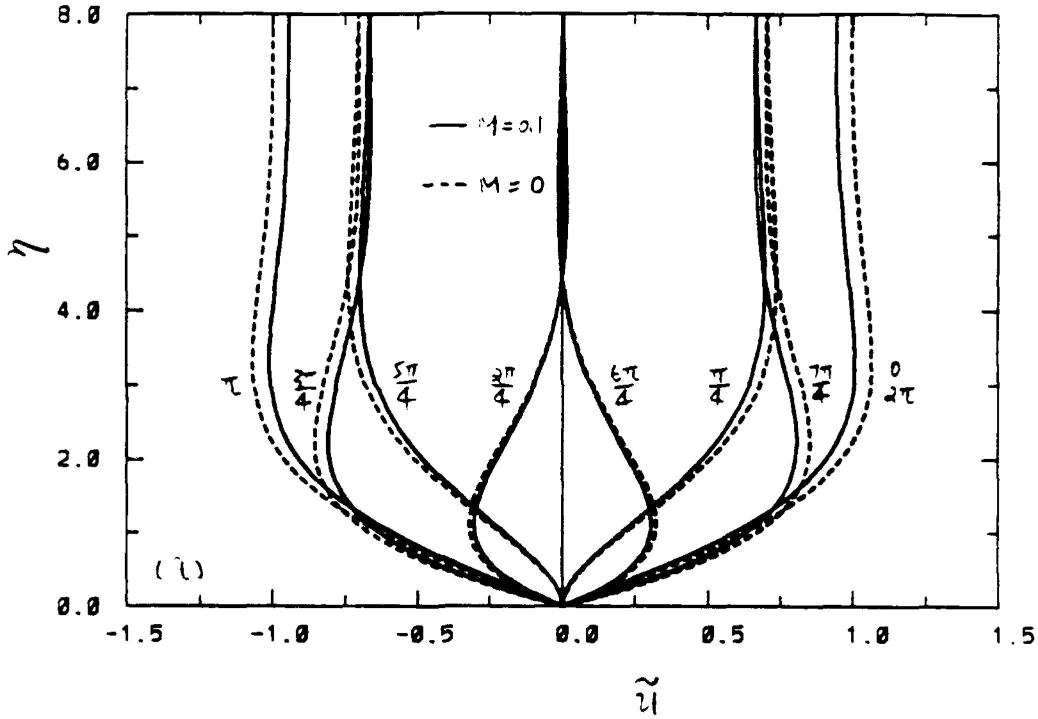


Fig. 10a

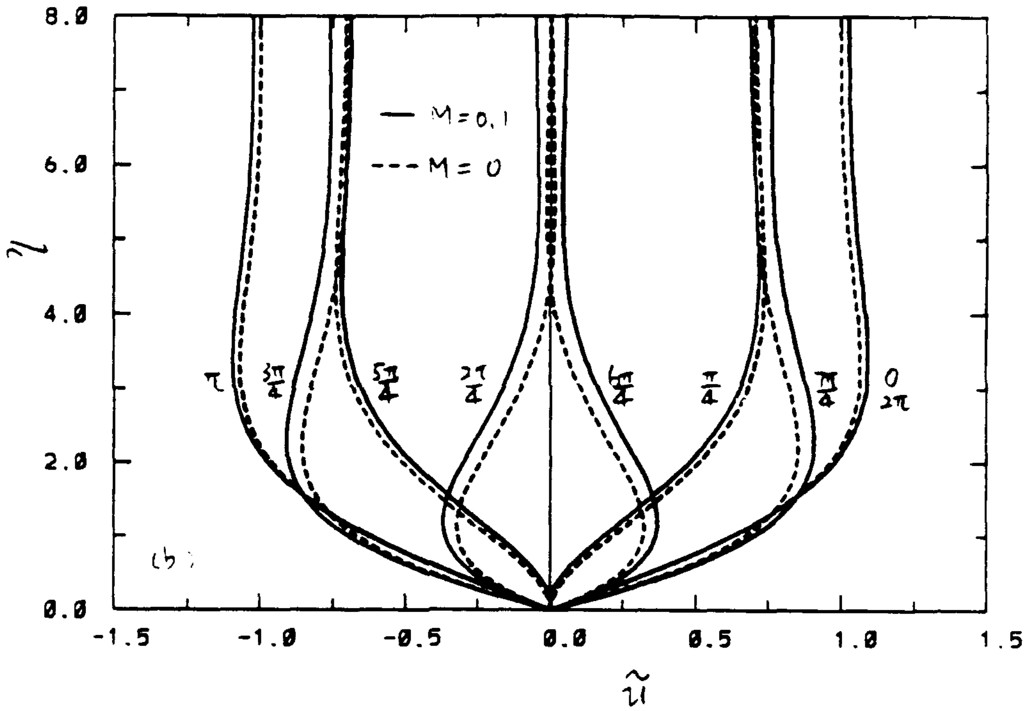

8.0
6.0
4.0
2.0
0.0
η
— M = 0.1
- - - M = 0
π
3π/4
5π/4
3π/4
6π/4
π/4
7π/4
0
2π
(b)
-1.5
-1.0
-0.5
0.0
0.5
1.0
1.5
ũ


Fig. 6b

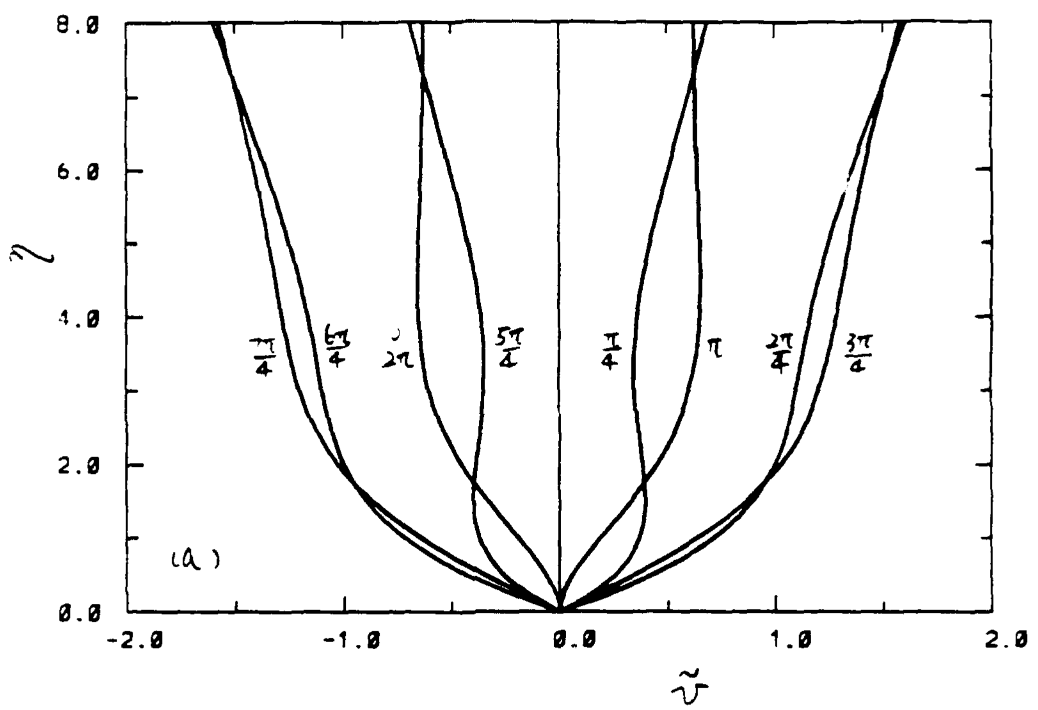

8.0
6.0
4.0
2.0
0.0
-2.0
-1.0
0.0
1.0
2.0
$\eta$
$\tilde{v}$
$\frac{7\pi}{4}$
$\frac{6\pi}{4}$
$2\pi$
$\frac{5\pi}{4}$
$\frac{\pi}{4}$
$\pi$
$\frac{2\pi}{4}$
$\frac{3\pi}{4}$
(a)


Fig 11a

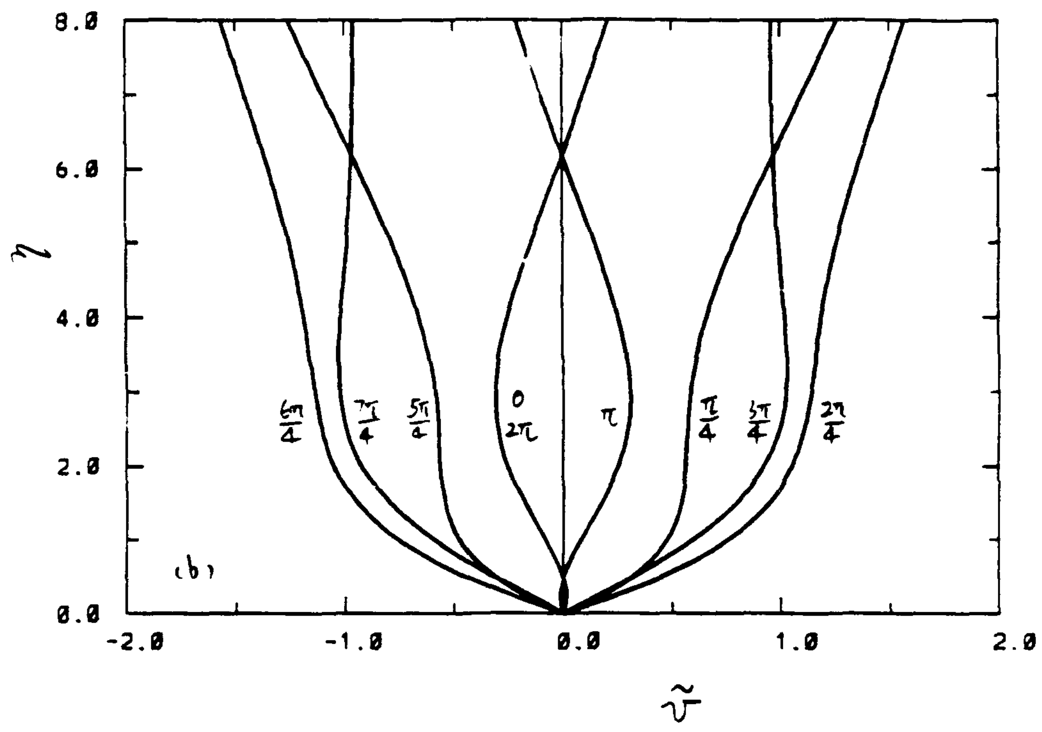
8.0
6.0
4.0
2.0
0.0
-2.0
-1.0
0.0
1.0
2.0
$\eta$
$\tilde{\nu}$
(b)
$\frac{6\pi}{4}$
$\frac{7\pi}{4}$
$\frac{5\pi}{4}$
0
$2\pi$
$\pi$
$\frac{\pi}{4}$
$\frac{3\pi}{4}$
$\frac{2\pi}{4}$

Fig. 11b

# Appendix B

# Standing Acoustic Waves in a Low Mach Number Shear Flow

To Appear in *AIAA Journal*, July 1992.

# Standing Acoustic Waves in a Low Mach Number Shear Flow

Meng Wang* and David R. Kassoy†

Center for Combustion Research
Department of Mechanical Engineering
University of Colorado
Boulder, CO 80309-0427

**Abstract**

Acoustic-shear flow interactions are studied in a rectangular cavity bounded by impermeable duct walls parallel to the flow direction and special perpendicular acoustic reflectors that permit the passage of a fully-developed, low Mach number shear flow. Fourier series-based asymptotic solutions are constructed to provide an explicit description of the evolution of an initially imposed axial standing wave disturbance. The bulk convective motion of the shear flow is shown to be responsible for periodic axial waveform deformations. Additionally, transverse and oblique standing acoustic waves as well as single frequency bulk oscillations arise from the refraction of the imposed axial acoustic disturbance by the mean flow velocity gradient. Combinations of these disturbances give rise to irregular acoustic pressure signals in the duct. Certain refraction induced transverse and oblique acoustic modes are amplified under resonant conditions. It is shown that, in the parameter ranges of solid rocket engines, the refraction and bulk convection effects are small in general.

* Research Associate.

† Professor.

# 1 Introduction

This work describes the spontaneous evolution of a spatially distributed small initial disturbance imposed on a low Mach number shear flow in a duct. An initial-boundary value formulation is used to predict the complete spectrum of standing wave modes (or equivalently, combinations of traveling waves) generated by the interaction between the initial disturbance and the shear flow in a finite rectangular region. The primary objectives of this study are to demonstrate that; (1) refraction of an axial wave arising from the relaxation of the initial disturbance is the source of a myriad of higher order (smaller) transverse and oblique acoustic waves; and (2) resonant conditions promote the amplification of a small subset of refraction induced transverse and oblique wave modes.

Traditional studies of acoustic-shear flow interaction [1, 2, 3] examine the *quasi-steady* properties of a sound wave, of the form $p = F(y)e^{i(\kappa x - t)}$, propagating in fully-developed shear flows above a flat surface or in a planar duct. Linearization techniques are used to derive the fundamental equation governing the cross-stream eigenfunction $F$ and the propagation constant $\kappa$. Asymptotic solutions [1, 3] and numerical solutions [2, 3] predict significant distortion of specific propagating wave modes as a result of acoustic refraction. When the wave is purely axial (the fundamental mode), the refraction effect is reflected in the variation of $F(y)$ across the shear flow field.

In contrast to the quasi-steady linear approach used in Refs. [1, 2, 3], Baum and Levine [4] used numerical methods to solve an initial-boundary value problem based on the Reynolds-averaged Navier-Stokes equations and the $k$–$\epsilon$ turbulence model. Their work is aimed at understanding mechanisms for energy exchange between the acoustic and mean flow fields in solid propellant rocket engines. In the model problem discussed in Ref. [4], an initially steady shear flow field in a rigid walled axisymmetric cylinder is disturbed continuously at an inlet or outlet plane to generate unidirectional traveling acoustic waves. The waves move only a few acoustic wavelengths before computations are terminated, so that the quasi-steady solution in Refs. [1, 2, 3] is not attained on the short time scale involved.

More recently, Wang and Kassoy [5] used an initial-boundary value approach to consider the two-dimensional planar duct counterpart of the refraction problem studied in Ref. [4]. A systematic perturbation procedure based on the small mean flow Mach number $M$ is used to demonstrate that nonlinear effects are $O(M)$ smaller than the refractive contribution to the total acoustic pressure. The Fourier series-based solution in Ref. [5] describes short-time acoustic transients arising from axial wave interaction with the shear flow, as well as their evolution into long-time quasi-steady forms. In the nonresonant case the solution includes not only the usual axial propagating mode, but also a finite number of oblique propagating modes, and an infinite number of non-propagating bulk modes that decay rapidly away from the plane acoustic source. When resonance is present, a pair of amplified, trapped transverse waves also appear. These distinct modes have not been extracted from the numerical computations in Ref. [4].

It is of interest to extend the aforementioned traveling wave models of acoustic-shear flow interaction to axially confined geometries in which multiple wave reflections occur. This is done in the present work by considering standing waves trapped between two wave reflectors separated by a finite axial distance in the duct examined in Ref. [5]. The idealized model is used as a paradigm to demonstrate the surprisingly complex response of an initially steady shear flow to an imposed axial velocity disturbance in the confined region, and to infer the acoustic convection and refraction magnitudes in solid rocket engine chambers. The inclusion of axial wave reflection effects in this study provides improved relevance to rocket engine acoustics, in comparison with the previous traveling wave studies.

Fourier series-based analytical solutions give explicit modal response that may not be easily extracted from numerical data. The initial disturbance generates a leading order acoustic field which is purely axial. It interacts with the shear flow to generate $O(M)$ acoustic disturbances consisting of purely axial standing waves, transverse standing waves, oblique standing waves, and bulk fluid oscillations (Helmholtz modes). The linear combination of these disturbances gives surprisingly irregular $O(M)$ pressure signals at a given location that could be mistakenly identified as a chaotic or turbulent response. The ratio of initial disturbance wavelength to duct width and the relationship between the disturbance and resonant frequencies are found to be important factors affecting the refraction magnitude, which is in general small except under resonant conditions. When resonance is present, amplifying modes exist, which can be represented as pairs of transverse and/or oblique traveling waves with growing amplitudes. The results of the present analysis are employed to show that, in the parameter ranges of typical solid rocket engine gasdynamics, refraction effects can produce only $O(10\%)$ variations in acoustic pressure.

# 2 Mathematical Formulation

The conceptual model of the present acoustic-shear flow interaction study is schematically illustrated in Fig. 1. A fully-developed shear flow sweeps through a parallel duct region of length $L'$, confined by rigid, impermeable side walls at $y' = \pm d'$. The thermodynamic state of the steady flow field is defined by $(p'_0, \rho'_0, T'_0)$, and the equilibrium speed of sound $c'_0 = \sqrt{\gamma R T'_0}$, where $R$ is the gas constant and $\gamma$ the ratio of the specific heats.

An axially distributed, $y'$-independent initial disturbance to the steady flow field evolves into transient acoustic oscillations on the acoustic time scale $t'_1 = L'/c'_0$, which is much shorter than the mean flow passage time because the maximum mean flow Mach number, $M = U'_{max}/c'_0$, is assumed to be small. Axial velocity components on the left and right boundaries of the flow configuration are assumed to be strictly equal to the shear flow velocity $U'(y')$. In other words, $x' = 0$ and $x' = L'$ represent fixed nodal surfaces for the axial acoustic velocity. This configuration is highly idealized, but provides an opportunity to develop an analytical investigation of trapped acoustic signals in a shear flow, when multiple wave reflections occur on the axial boundaries.

The dimensionless equations for the compressible, viscous, and heat-conducting fluid motion in the duct are similar to those in Ref. [5],

$$p = \rho T, \tag{1}$$

$$\rho_t + M\left[(\rho u)_x + (\rho v)_y\right] = 0, \tag{2}$$

$$\rho\left[u_t + M(uu_x + vu_y)\right] = -\frac{1}{\gamma M}p_x + \frac{M}{hR_e}\left(u_{yy} + \frac{4}{3}h^2 u_{xx} + \frac{1}{3}h^2 v_{xy}\right), \tag{3}$$

$$\rho\left[v_t + M(uv_x + vv_y)\right] = -\frac{1}{\gamma M h^2}p_y + \frac{M}{hR_e}\left(h^2 v_{xx} + \frac{4}{3}v_{yy} + \frac{1}{3}u_{xy}\right), \tag{4}$$

$$\begin{aligned}\rho\left[T_t + M(uT_x + vT_y)\right] = {} & -M(\gamma - 1)p(u_x + v_y) \\ & + \frac{M}{hR_e}\frac{\gamma}{P_r}\left(T_{yy} + h^2 T_{xx}\right) + \frac{M^3}{hR_e}\Phi,\end{aligned} \tag{5}$$

where the thermophysical properties have been assumed constant for convenience. Subscripts $t$, $x$, and $y$ denote partial derivatives. $R_e = U'_{max}d'/\nu'$ is the mean flow Reynolds number, $h = d'/L'$ the aspect ratio of the duct, $P_r$ the Prandtl number, and $\Phi$ the nondimensional dissipation function. Other nondimensional variables are defined in terms of dimensional quantities by

$$\begin{aligned}&(p, \rho, T) = \frac{(p', \rho', T')}{(p'_0, \rho'_0, T'_0)}, \qquad u = \frac{u'}{U'_{max}}, \qquad v = \frac{v'}{hU'_{max}}, \\ &x = \frac{x'}{L'}, \qquad y = \frac{y'}{d'}, \qquad t = \frac{t'}{t'_1}.\end{aligned} \tag{6}$$

The subsequent analysis is performed in the parameter ranges relevant to flow conditions in solid rocket engine chambers (excluding the exit nozzle), where the values of $M$ and $R_e$ are of $O(10^{-1})$ and $O(10^6)$, respectively [6]. Accordingly, it is reasonable to define the perturbation limit as $1/R_e \to 0$; $M \to 0$; and $1/R_e \ll M$. In addition, one assumes that the aspect ratio $h \leq O(1)$.

Given the steady, fully-developed shear flow velocities $u = U(y)$ and $v = 0$, one observes from (1)-(5) that the basic pressure distribution is independent of the $y$ direction, and that $dp/dx = O(M^2/hR_e)$, negligible compared to the $O(M^2)$ acoustic pressure to be considered. The high Reynolds number limit implies that viscous and thermal diffusion exerts little influence on the fluid motion, except in the thin acoustic boundary layers adjacent to solid surfaces, typically of thickness less than 1% of the duct width [5]. In this respect, the isentropic relations,

$$p = \rho^\gamma + O\left(\frac{M}{hR_e}\right), \qquad T = \rho^{\gamma-1} + O\left(\frac{M}{hR_e}\right), \tag{7}$$

together with the transport-free version of (2)-(4) (the Euler equations) adequately describe the fundamental physical phenomena in the core flow region.

The traveling wave study in Ref. [5] is based on acoustic velocity disturbances of $O(M)$ relative to the shear flow velocity $U(y)$. The corresponding acoustic thermodynamic disturbances must be $O(M^2)$, a magnitude frequently encountered in stable solid rocket motors, where an absolute pressure oscillation of 1 to 2% is often observed. When acoustic perturbations of the type

$$u = U(y) + M\hat{u}, \qquad v = M\hat{v}, \tag{8}$$

$$p = 1 + M^2\gamma\hat{p}, \qquad \rho = 1 + M^2\hat{\rho}, \qquad T = 1 + M^2\hat{T}, \tag{9}$$

are used in the transport-free version of (2)-(4), the following equations are obtained for the acoustic variables:

$$\hat{\rho}_t + \hat{u}_x + \hat{v}_y + MU(y)\hat{\rho}_x + M^2\left[(\hat{\rho}\hat{u})_x + (\hat{\rho}\hat{v})_y\right] = 0, \tag{10}$$

$$\hat{u}_t + M\left[U(y)\hat{u}_x + \hat{v}U'(y)\right] + M^2(\hat{u}\hat{u}_x + \hat{v}\hat{u}_y) = -\frac{\hat{p}_x}{1 + M^2\hat{\rho}}, \tag{11}$$

$$\hat{v}_t + MU(y)\hat{v}_x + M^2(\hat{u}\hat{v}_x + \hat{v}\hat{v}_y) = -\frac{\hat{p}_y}{h^2\left[1 + M^2\hat{\rho}\right]}. \tag{12}$$

Eqns. (10)–(12) show that the mean flow $U(y)$ affects only the $O(M)$ acoustic phenomena in the duct. The quadratic convective terms, representing the nonlinear effect in the wave system, are even smaller, of $O(M^2)$.

The wave field evolves from an initial axially distributed velocity disturbance:

$$t = 0, \qquad \hat{u} = A\sin(k\pi x), \qquad \hat{v} = \hat{p} = 0. \tag{13}$$

Since the left and right boundaries are fixed nodal surfaces for $\hat{u}$,

$$x = 0, 1; \qquad \hat{u} = 0. \tag{14}$$

The normal velocity component vanishes on the impermeable duct sidewalls. For mean flow $U(y)$ symmetric with respect to the center-plane ($y = 0$), the problem is symmetric and can be solved in the region $0 \le y \le 1$ only. The appropriate $y$ boundary conditions are

$$y = 0, 1; \qquad \hat{v} = 0. \tag{15}$$

# 3 Solution Development

The solution to the lowest order approximation to the equations in (10)–(15) can be written as

$$p_1 = -A\sin(k\pi t)\cos(k\pi x), \tag{16}$$

$$u_1 = A\cos(k\pi t)\sin(k\pi x), \tag{17}$$

$$v_1 = 0, \tag{18}$$

where $p_1$, $u_1$ and $v_1$ are defined by the asymptotic expansions

$$\hat{\Psi} = \Psi_1 + M\Psi_2 + O(M^2), \qquad \Psi = (u, v, p, \rho, T). \tag{19}$$

It follows from the isentropic relations (7), (9) and (19) that

$$p_1 = \rho_1, \qquad p_2 = \rho_2. \tag{20}$$

The leading order solution in (16)–(18) describes an axial mode with a harmonically time-varying amplitude, independent of the mean flow. In order to obtain information about how the shear flow affects the acoustic modes through convection and refraction effects, the next order solutions must be constructed.

The $O(M)$ acoustic equations derived from (10)–(12) and (19) take the form

$$p_{2t} + u_{2x} + v_{2y} = -U(y)p_{1x}, \tag{21}$$

$$u_{2t} + p_{2x} = -U(y)u_{1x} - v_1 U'(y), \tag{22}$$

$$v_{2t} + \frac{1}{h^2}p_{2y} = -U(y)v_{1x}, \tag{23}$$

where density has been replaced by pressure according to (20). Eqns. (16)–(18) can be combined with (21)–(23) to find the nonhomogeneous wave equation for $p_2$,

$$p_{2tt} - \left(p_{2xx} + \frac{1}{h^2}p_{2yy}\right) = -2Ak^2\pi^2 U(y)\cos(k\pi t)\sin(k\pi x). \tag{24}$$

The forcing function on the right side is $y$-dependent and excites fully two-dimensional $O(M)$ acoustic motion. The initial conditions for $p_2$ are simply (cf. (13), (19) and (21))

$$p_2(t=0) = p_{2t}(t=0) = 0. \tag{25}$$

The appropriate boundary conditions are derived by applying the results in (16)–(23) to (14)–(15), which gives

$$\begin{aligned} p_{2x}(x=0) &= -Ak\pi U(y)\cos(k\pi t), \\ p_{2x}(x=1) &= -(-1)^k Ak\pi U(y)\cos(k\pi t), \end{aligned} \tag{26}$$

and

$$p_{2y}(y=0) = p_{2y}(y=1) = 0. \tag{27}$$

Eqns. (24)-(27) constitute a well-defined elementary two-dimensional hyperbolic system with a distributed source and axial boundary excitations. One notices that boundary conditions (26) are not compatible with (25) at $t = 0$. As a result, a pair of propagating discontinuities in $p_{2x}$, or weak discontinuities as described by Landau and Lifshitz [7], are introduced at $x = 0$ and 1 at $t = 0$.

The solution to (24)-(27) can be written as

$$\begin{aligned}\frac{p_2}{A} &= -\cos(k\pi t)\sin(k\pi x)\sum_{n=0}^{\infty}\frac{\varepsilon_n}{2}\tilde{U}_n\cos(n\pi y) \\ &+ \sum_{m=0(m\neq k)}^{\infty}\sum_{n=0}^{\infty}\varepsilon_m\varepsilon_n\tilde{U}_n\Gamma_{mn}(k,t)\cos(m\pi x)\cos(n\pi y),\end{aligned} \tag{28}$$

where $\varepsilon_m$ and $\varepsilon_n$ are the Neumann's number whose value equals 1 if the subscript is zero and 2 if it is a positive integer. The coefficients $\tilde{U}_n$ and $\Gamma_{mn}$ are defined by

$$\tilde{U}_n = 2\int_0^1 U(y)\cos(n\pi y)dy, \tag{29}$$

$$\Gamma_{mn} = \frac{\left[1-(-1)^{m+k}\right]k\,(m^2+k^2)}{2\pi\,(m^2+\bar{n}^2-k^2)\,(m^2-k^2)}\left[\frac{2k^2-\bar{n}^2}{m^2+k^2}\cos(k\pi t)-\cos\left(\sqrt{m^2+\bar{n}^2}\,\pi t\right)\right], \tag{30}$$

where $\bar{n} = n/h$. If $m^2+\bar{n}^2 = k^2$, $\Gamma_{mn}$ should be evaluated by taking the limit $m^2+\bar{n}^2-k^2 \to 0$ in (30), which yields $O(t)$ amplification in $p_2$. It can be verified that (28) satisfies equation (24) as well as all the initial and boundary conditions.

A more concise form of the solution is derived by combining the two terms in (28), which yields

$$\frac{p_2}{A} = \sum_{m=0(m\neq k)}^{\infty}\sum_{n=0}^{\infty}\varepsilon_m\varepsilon_n\tilde{U}_n\Theta_{mn}(k,t)\cos(m\pi x)\cos(n\pi y), \tag{31}$$

where

$$\Theta_{mn} = \begin{cases}\frac{\left[1-(-1)^{m+k}\right]k(m^2+k^2)}{2\pi(m^2+\bar{n}^2-k^2)(m^2-k^2)}\left[\cos(k\pi t)-\cos\left(\sqrt{m^2+\bar{n}^2}\,\pi t\right)\right], & m^2+\bar{n}^2\neq k^2 \\ \frac{\left[1-(-1)^{m+k}\right](m^2+k^2)}{4(m^2-k^2)}\,t\sin(k\pi t), & m^2+\bar{n}^2 = k^2.\end{cases} \tag{32}$$

In the derivation of (31), $\sin(k\pi x)$ in (28) is expressed in terms of its Fourier cosine series whose derivative converges to zero instead of its true values at $x = 0$ and 1. As a result the boundary conditions (26) are not satisfied by (31). However, (31) gives correct $x$-derivatives elsewhere including the immediate neighborhood of $x = 0$ and 1. The values of $p_2$ are not affected at all because the series given by (31) is uniformly convergent throughout the entire domain. Thus one can justifiably use (31) to evaluate $p_2$ everywhere, and its first derivatives everywhere except at $x = 0$, 1 and at the locations of weak discontinuities where these derivatives are not defined.

The Fourier coefficients of the double series in (31) are proportional to $\tilde{U}_n$ which represents the shear flow effects, and vary with $k$ and $t$. One observes from (32) that for each nonresonant Fourier mode, the coefficient contains two harmonic functions of time with different frequencies. The first function, $\cos(k\pi t)$, has a frequency equal to that of the distributed forcing function in (24), or that of the imposed leading order acoustic pressure. It describes the time dependence of the Helmholtz mode of bulk oscillation with $x$ and $y$-dependent amplitudes.

The second cosine function in (32) is associated with wave phenomena. For each pair of $m$ and $\bar{n}$, the product

$$P_{mn} = \cos\left(\sqrt{m^2 + \bar{n}^2}\,\pi t\right)\cos(m\pi x)\cos(n\pi y) \tag{33}$$

represents a two-dimensional oblique mode, which can be decomposed into four plane traveling waves:

$$\begin{aligned} P_{mn} \;=\; & \frac{1}{4}\Big\{\cos\left[\sqrt{m^2+\bar{n}^2}\,\pi\left(t - z_{mn}^{++}\right)\right] + \cos\left[\sqrt{m^2+\bar{n}^2}\,\pi\left(t - z_{mn}^{+-}\right)\right] \\ & + \cos\left[\sqrt{m^2+\bar{n}^2}\,\pi\left(t - z_{mn}^{-+}\right)\right] + \cos\left[\sqrt{m^2+\bar{n}^2}\,\pi\left(t - z_{mn}^{--}\right)\right]\Big\}, \end{aligned} \tag{34}$$

where

$$z_{mn}^{++} = \frac{mx + ny}{\sqrt{m^2 + \bar{n}^2}}, \qquad z_{mn}^{+-} = \frac{mx - ny}{\sqrt{m^2 + \bar{n}^2}},$$

$$z_{mn}^{-+} = \frac{-mx + ny}{\sqrt{m^2 + \bar{n}^2}}, \qquad z_{mn}^{--} = \frac{-mx - ny}{\sqrt{m^2 + \bar{n}^2}}. \tag{35}$$

are the paths taken by the traveling waves reflecting from duct walls and the axial acoustic reflectors. The wave paths are oblique in general. However, when either $m = 0$ or $n = 0$, the traveling waves are either transverse or axial, respectively, and the number of traveling waves reduces to two. Since (31) contains an infinite number of Fourier modes, one concludes that $p_2$ consists of infinite numbers of axial, transverse and oblique standing waves, in addition to the bulk oscillation mentioned earlier. This is in sharp contrast to the results of the traveling wave study [5] where only a limited number of wave modes can propagate along a long duct. The multiple reflections of acoustic signals on the inserted acoustic reflectors create a more complex acoustic-shear flow interaction response.

Although the asymptotic solution given by (16), (19) and (31)-(32) is derived primarily for processes occurring on the acoustic time scale of the duct, it is seen to be uniformly valid on the mean flow passage time scale $t \sim O(M^{-1})$ as well, except for the resonant cases. Resonance occurs when the frequency of a transverse or oblique standing acoustic wave equals to that of the forced vibration. It causes $O(t)$ amplitude growth (cf. (32)) and invalidates the asymptotic expansion (19) as $t \sim O(M^{-1})$. Comparing to the $O(t^{1/2})$ resonant growth found for refraction induced traveling waves [5], it is concluded that a trapped wave system produces faster growth rate for the resonant mode, owing to the effect of multiple axial reflections. In general, the asymptotic solution remains valid until $t \sim O(M^{-2})$, the time required for the small nonlinear effects to accumulate, which leads to significant deformation of the leading order waveform and possible formation of a weak shock in the confined geometry [8].

A complete solution should include the thin acoustic bounadry layers adjacent to the duct walls. An approach identical to that used in Ref. [5] can be applied to reveal the structure of the transport-dominated layers. A preliminary analysis shows a basically uniform acoustic pressure distribution across the layer, whose thickness is proportional to the ratio of the fluid kinematic viscosity to the mode number ($k$) of the basic core pressure disturbance. A multitude of velocity standing modes induced by the core acoustic flow are strongly damped by viscous and thermal diffusion to satisfy no-slip and appropriate thermal boundary conditions [5, 9]. Since no fundamentally new discoveries are expected from a detailed analysis, it is not pursued here.

# 4 Example Calculations and Discussion

## 4.1 Acoustic convection and refraction

The effect of a sheared mean flow on acoustic processes can be more clearly elucidated by rewriting (31) as $p_2 = p_{2C} + p_{2R}$ where

$$p_{2C} = A\tilde{U}_0 \sum_{m=0(m\neq k)}^{\infty} \varepsilon_m \Theta_{m0}(k,t) \cos(m\pi x), \qquad (36)$$

$$p_{2R} = 2A \sum_{m=0(m\neq k)}^{\infty} \sum_{n=1}^{\infty} \varepsilon_n \tilde{U}_n \Theta_{mn}(k,t) \cos(m\pi x)\cos(n\pi y). \qquad (37)$$

The first component of $p_2$, $p_{2C}$, contains all the $n = 0$ Fourier modes. It is directly proportional to the shear flow velocity averaged across the duct ($\tilde{U}_0/2$) (cf. (29)), and is the correction to the basic acoustic pressure (16) that would arise in a pure slug flow. This effect, henceforth referred to as the bulk convection effect, is accountable for the axial standing wave disturbances and the $y$-independent part of the bulk oscillations in $p_2$. The magnitude of bulk convection increases with the average shear flow velocity and the mode number ($k$) of the basic acoustic disturbance, as can be shown from (32). When $Mp_{2C}$ is superimposed on the basic acoustic pressure $p_1$, the total acoustic pressure remains one-dimensional, although its waveform is slightly distorted in the axial direction by a time-dependent periodic function.

The quantity $p_{2R}$ in (37) arises from convection of the basic axial acoustic disturbance at the local differential velocity $U(y) - \tilde{U}_0/2$. Thus, $p_{2R}$ is associated with refraction of the axially distributed solution $p_1$ in (16) by the shear flow. It is seen to be intricately related to the specific shear flow velocity profile through the Fourier coefficients $\tilde{U}_n$. Both transverse and oblique standing acoustic waves are present, and amplitude amplification of certain modes is possible as a result of resonance phenomena. The $p_{2R}$ solution also includes bulk oscillations with $y$-dependent amplitudes as mentioned in Section 3.

The general features of the acoustic field described by (16) and (31)–(32) can be revealed graphically by evaluating these expressions numerically. In the subsequent calculations, each Fourier summation is carried out up to the 50th term, with a truncation error of less than $10^{-3}$ based on comparisons of the results with those from summations of 100 or more terms. Three types of shear flows $U(y)$, as well as different combinations of mode number $k$ and duct aspect ratio $h$, are employed to generate representative results. The amplitude of the initial disturbance $A$ is kept at unity since both $p_1$ and $p_2$ exhibit the same simple proportionality to it. Results are presented in terms of $p_{2C}$ and $p_{2R}$, mentioned above, for easier physical interpretation.

Figs 2a–2c display the time-variations of the three acoustic pressure components on the duct wall ($y = 1$), at axial locations $x = 0$, 1/4, and 1/2, respectively. The wave field is generated by the relaxation of the initial velocity disturbance $\hat{u} = \sin(\pi x)$ ($k = 1$) in a fully developed laminar flow field described by $U = 1 - y^2$. The duct section considered has equal length and width, so that $h = 1/2$. In each figure, the solid line denotes the basic acoustic pressure $p_1$ as calculated from (16). The amplitude of its oscillation is seen to decrease from maximum at the antinode $x = 0$ (cf. Fig. 2a) to zero at the nodal plane $x = 1/2$ (cf. Fig. 2c). The long and short dashed lines represent the bulk convective correction $p_{2C}$ and the refractive correction $p_{2R}$, calculated from (36) and (37) respectively. The former is a $y$-independent, periodic function of time whose amplitude and structure vary with logitudinal position $x$, as observed from the figures. The time response of $p_{2R}$ depends on both spatial coordinates and exhibits non-periodic, irregular oscillatory behavior, as a result of the superposition of signals with noncommensurate frequencies arising from transverse and oblique standing modes as well as the bulk modes. The slope discontinuities on both $p_{2C}$ and $p_{2R}$ curves denote the passage of the weak discontinuities created by the initial jump in $p_{2x}$ (cf. (26)). The curves in Figs. 2a–2c are plotted up to $t = 10$, at which the mean flow completes one passage through the duct section if $M = 0.1$, and an axial acoustic signal is reflected 10 times on the left and right boundaries. Longer-time calculations produce similar irregular patterns for $p_{2R}$ while $p_1$ and $p_{2C}$ continue their periodic variations. It is particularly interesting to notice in Fig. 2c that, although the basic acoustic pressure $p_1$ vanishes, the total acoustic pressure $\hat{p} = p_1 + M(p_{2C} + p_{2R})$ is nonzero because a mean flow field with shear is present.

The two-dimensional structure of the acoustic pressure due to refraction ($p_{2R}$) is illustrated in Figs. 3a and 3b, which depict $p_{2R}$ distributions in the duct for an acoustic-shear flow system characterized by $k = 3$, $h = 1/6$, and $U = 1 - y^2$, at $t = 5/8$ and 7, respectively. The two snapshots are more than 6 acoustic time units apart, and thus do not reflect the waveform evolution process, which occurs on a much shorter time scale. The lines of sharp slope changes associated with the propagating weak discontinuities are obvious on the $p_{2R}$ surfaces. The absolute magnitude of the refraction effect is small because $p_{2R}$ must be multiplied by $M$.

## 4.2 Effect of mean flow type

Figs. 4a and 4b illustrate the time history of $p_1$, $p_{2C}$ and $p_{2R}$ at $x = 0$, $y = 1$ under the same conditions as in Fig. 2a, except for different shear flow velocity types. In

Fig. 4a, $U = 1 - y$, corresponding to a fully-developed Couette flow in the half duct considered. The profile $U = (1 - y)^{1/7}$ is used to find the results shown in Fig. 4b. It is easily observed from Figs. 2a, 4a and 4b that the shear flow described by the one-seventh power law generates the largest bulk convection effect $p_{2C}$ because it has the largest average velocity. Analogously the parabolic flow creates a larger bulk convection effect than the linear flow. The refraction effects for the linear and parabolic flow types are of comparable magnitude. The one-seventh power law flow generates the smallest acoustic refraction because the velocity gradient is relatively small in most of the core flow region. The large velocity gradient is concentrated within a thin layer near the wall which is too narrow to promote acoustic refraction on a global scale in the core.

The refraction induced acoustic pressure fluctuations at specified locations are plotted alone in Figs. 5a and 5b for the parabolic and one seventh power mean flow types, under conditions $k = 1$ and $h = 1/2$. The solid and dashed lines, representing $p_{2R}$ at an axial position $x = 1/2$ on the center-plane ($y = 0$) and duct wall ($y = 1$) respectively, resemble each other but are completely out of phase, implying the relative importance of refraction in the duct. It is strikingly noteworthy that superpositions of various linear wave structures resulting from shear flow interactions with a simple axial distanbance can produce fairly irregular pressure signals, which might be mistakenly attributed to nonlinear phenomena had the data been collected from numerical or experimental investigations. The shear velocity described by the one-seventh power law is again shown to generate smaller $p_{2R}$ than the other two cases.

## 4.3 Effect of mode number and duct aspect ratio

The earlier traveling wave study [5] suggests that the magnitude of acoustic refraction phenomena is controlled by, among other parameters, the ratio of the wavelength to the duct width. For a duct of fixed width, higher frequency waves induce larger refraction effect. In the present analysis, due to the finite axial length of the flow geometry, the relationship between $p_{2R}$ and the parameters $k$ and $h$ is more complex (cf. (37) and (32)) Nonetheless, numerical evaluations show that when $k$ is away from resonant frequencies of the duct the same trend is apparent.

The nonresonant $p_{2R}$ curves in Figs 6a and 6b are plotted at $x = 0$, $y = 0$ and 1 using the same shear flow velocity $U = 1 - y^2$. The $k$ and $h$ values are selected such that while $k$ increases from 1 in Fig. 6a to 3 in Fig. 6b, the aspect ratio $h$ decreases in proportion so that the wavelength to duct-width ratio remains constant. As expected, the refraction induced pressure fluctuations in the two figures are comparable in magnitude, and the frequency of fluctuation increases with $k$. The $p_{2R}$ signals are all fairly irregular. The location $x = 0$ is chosen in Figs. 6a and 6b because it corresponds to the anti-node for $p_1$, where the $p_{2R}$ curves are of typical magnitude for both cases. At other $x$-positions $p_{2R}$ fluctuates in a similar manner with different rates and amplitudes (see, for example, Fig. 5a).

Fig. 7 shows a near resonant case that results in a long period beat pattern. Here $k = 4$, $h = 1/4$, so that for $m = 1$ and $n = 1$, $m^2 + \bar{n}^2 = 17$ while $k^2 = 16$. The $p_{2R}$ curves are plotted at $x = 1/8$, $y = 0$ and 1, for $U = 1 - y^2$. Beats of even longer periods and larger maximum amplitudes can occur at suitable parameter combinations. If the numerical evaluation of the solution had been limited to times less than half the beat period, the result could have been erroneously interpreted as an amplified mode.

Fully resonant solution behavior is shown in Figs. 8a and 8b, where $p_{2R}$ on the duct wall is depicted at $x = 1/10$ and $x = 1/2$, respectively, for $U = 1 - y^2$. In Fig. 8a $k = 5$, $h = 1/5$, so that the transverse mode ($m = 0$, $n = 1$) is amplified. Fig. 8b corresponds to the condition $k = 5$ and $h = 1/\sqrt{21}$, which promotes the amplification of an oblique mode ($m = 2$, $n = 1$). One may observe beat patterns superimposed on the long-time growth arising from the interference by near-resonant modes.

The considerable enhancement of the refractive acoustic pressure by resonance requires a new asymptotic solution on the flow time scale $t \sim O(M^{-1})$ to accomondate refraction phenomena in the leading order acoustics. Likewise, when certain modes oscillate at near-resonant frequencies of the system, or when the mode number $k$ becomes large and the aspect ratio $h$ small, so that $Mp_2 \sim O(p_1)$, a new theory needs to be developed.

## 4.4 Inferences about solid rocket engine acoustics

Solid rocket combustion chamber dimensions are usually associated with radius to length ratios less than or equal to $O(1)$. Experimental observations suggest that the first few acoustic modes, especially the $k = 1$ mode, are most frequently encountered in rocket chambers. Based on the above analysis, the convection and refraction induced acoustic pressure correction terms are at most $O(M)$ relative to the leading order acoustic pressure, or $O(M^3)$ relative to the overall pressure. Although resonance in $p_{2R}$ significantly magnifies the acoustic refraction, it occurs rarely for low $k$ modes. In fact the resonant condition $m^2 + (n/h)^2 = k^2$ indicates that there can be no resonant modes if $kh < 1$, which is likely to be the case given the sizes of $k$ and $h$ mentioned above. Thus, a mean flow with $M = 0.1$ causes at most $O(10^{-1})$ changes in acoustic pressure, or $O(10^{-3})$ changes in total pressure. The nonlinear effects, represented by quadratic terms in the convective operators and responsible for acoustic streaming, are $O(10^{-1})$ smaller. They are of no importance on the time scale considered here and accumulate only on the longer time scale $t \sim O(10^2)$.

The resonant phenomenon discussed above appears in second order acoustic quantities only, and is excited by interactions with a sheared mean flow. It should be distinguished from the more powerful resonance of leading order acoustic pressure in a rocket engine configurations, often associated with excitations arising from chemical heat release, which is beyond the scope of this paper.

# 5 Summary

In this paper a mathematical model is established to study the interaction between a low Mach number parallel shear flow and an axially distributed acoustic disturbance trapped in a section of a planar duct. The solution development is based on asymptotic expansions defined for the small mean flow Mach number limit ($M \rightarrow 0$). The Fourier series-based analytical solution in terms of standing modes gives explicit modal response of the acoustic-shear flow interactions. The major conclusions are:

- Bulk (slug flow) convection induces purely axial standing acoustic waves and $y$-independent bulk oscillations at the frequency of the imposed initial disturbance. The magnitude of the bulk convection effect increases with the average shear flow velocity and the mode number ($k$) of the leading order acoustic pressure.

- Refraction generates purely transverse and oblique standing waves as well as bulk oscillations with both $x$- and $y$-dependent amplitudes. The magnitude of refraction increases with the shear flow velocity gradient, the duct-width to length ratio ($h$), and the mode number of the leading order acoustic pressure ($k$). The refraction size also increases if the frequencies of the induced acoustic modes become close to the resonant frequency.

- Combination of the above effects gives irregular pressure signals at given positions in the duct. They are of $O(M)$ relative to the imposed leading order acoustic pressure.

- Axial wave reflections cause faster resonant growth of acoustic refraction. Resonance does not occur for $hk < 1$.
- Refraction effects are very small in both traveling and standing wave model studies, in the parameter ranges of solid rocket engines.

The primary point is that quite elementary disturbances can evolve into surprisingly complex wave structures as a result of refraction effects, although these effects are small in the parameter ranges of solid rocket engines. This simplified analysis gives insight into the acoustic modal interactions with the shear flow, which have not been extracted from computational data in past studies. In fact there appears to be a specific need to develop data analysis tools that are capable of using grid point flow data to determine the propagating wave patterns present in an acoustically excited shear flow.

## Acknowledgements

This work was supported by Air Force Office of Scientific Research through a grant AFOSR 89-0023.

# References

[1] Pridmore-Brown, D.C., "Sound Propagation in a Fluid Flowing Through an Attenuating Duct," *Journal of Fluid Mechanics*, Vol. 4, 1958, pp. 393–406.

[2] Mungur, P. and Gladwell, G.M.L., "Acoustic Wave Propagation in a Sheared Fluid," *Journal of Sound and Vibretion*, Vol. 9, No. 1, 1969, pp. 28–48.

[3] Hersh, A.S. and Catton, I., "Effect of Shear Flow on Sound Propagation in Rectangular Ducts," *The Journal of the Acoustical Society of America*, Vol. 50, No. 3, 1971, pp. 992–1003.

[4] Baum, J.D. and Levine, J.N., "Numerical Investigation of Acoustic Refraction," *AIAA Journal*, Vol. 25, No. 12, 1987, pp. 1577–1586.

[5] Wang, M. and Kassoy, D.R., "Transient Acoustic Processes in a Low Mach Number Shear Flow," Submitted to Journal of Fluid Mechanics, 1990.

[6] Price, E.W., "Experimental Observations of Combustion Instability," *Progress in Astronautics and Aeronautics*, Vol. 90, 1984, pp. 733–790.

[7] Landau, L.D. and Lifshitz, E.M., *Fluid Mechanics*, Pergamon, London, 1959, pp. 344–346.

[8] Wang, M. and Kassoy, D.R., "Evolution of Weakly Nonlinear Waves in a Cylinder with a Movable Piston", *Journal of Fluid Mechanics*, Vol. 221, 1990, pp. 27–52.

[9] Lighthill, M.J., "Acoustic Streaming," *Journal of Sound and Vibration*, Vol. 61, No. 3, 1978, pp. 391–418.

# List of Figures

7. Near-resonant variations of refractive acoustic pressure $p_{2R}$ with time at locations $x = 1/8$, $y = 0$ and 1, as the initial acoustic disturbance $\hat{u}(t = 0) = \sin(4\pi x)$ relaxes in the shear flow field $U = 1 - y^2$. The duct aspect ratio $h = 1/4$.

8. Resonant amplifications of refractive acoustic pressure $p_{2R}$ on the duct wall ($y = 1$), at specified axial locations, as the initial acoustic disturbance $\hat{u}(t = 0) = \sin(k\pi x)$ relaxes in the shear flow field $U = 1 - y^2$. (a) $k = 5$, $h = 1/5$, $x = 1/10$; (b) $k = 5$, $h = 1/\sqrt{21}$, $x = 1/2$.

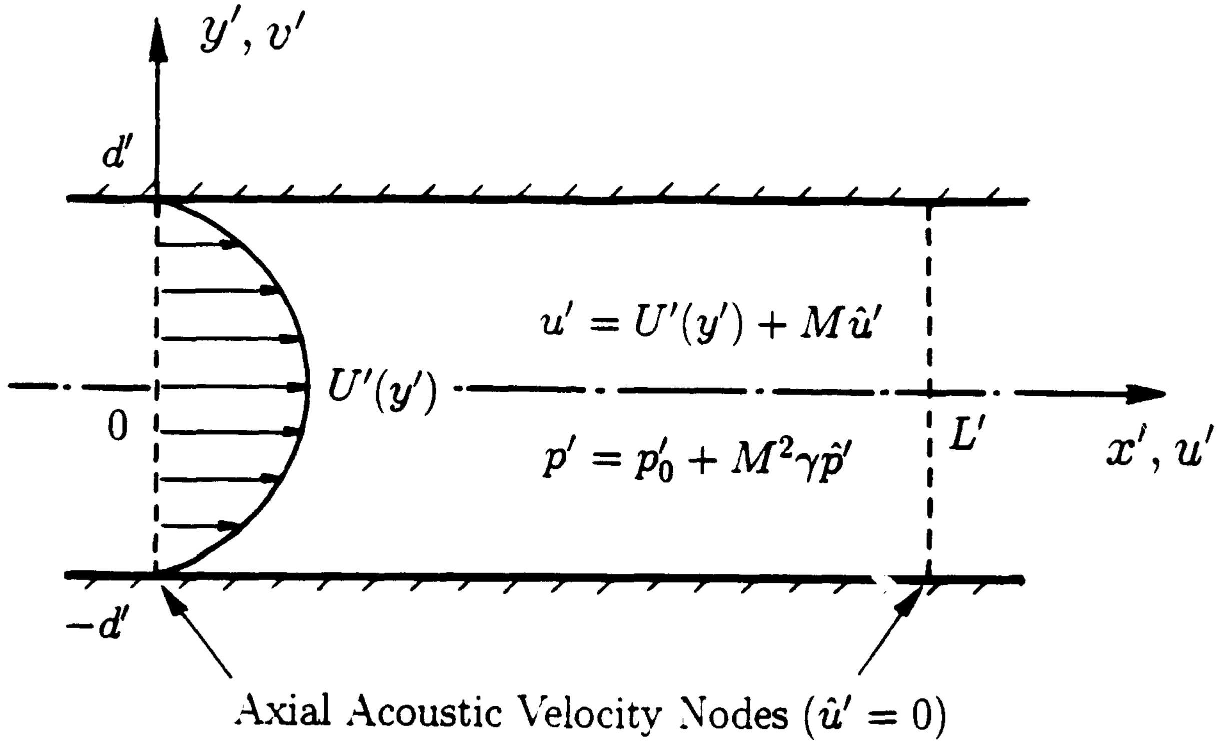

$y', v'$
$d'$
$u' = U'(y') + M\hat{u}'$
$U'(y')$
0
$p' = p'_0 + M^2\gamma\hat{p}'$
$L'$
$x', u'$
$-d'$
Axial Acoustic Velocity Nodes ($\hat{u}' = 0$)


Fig. 1

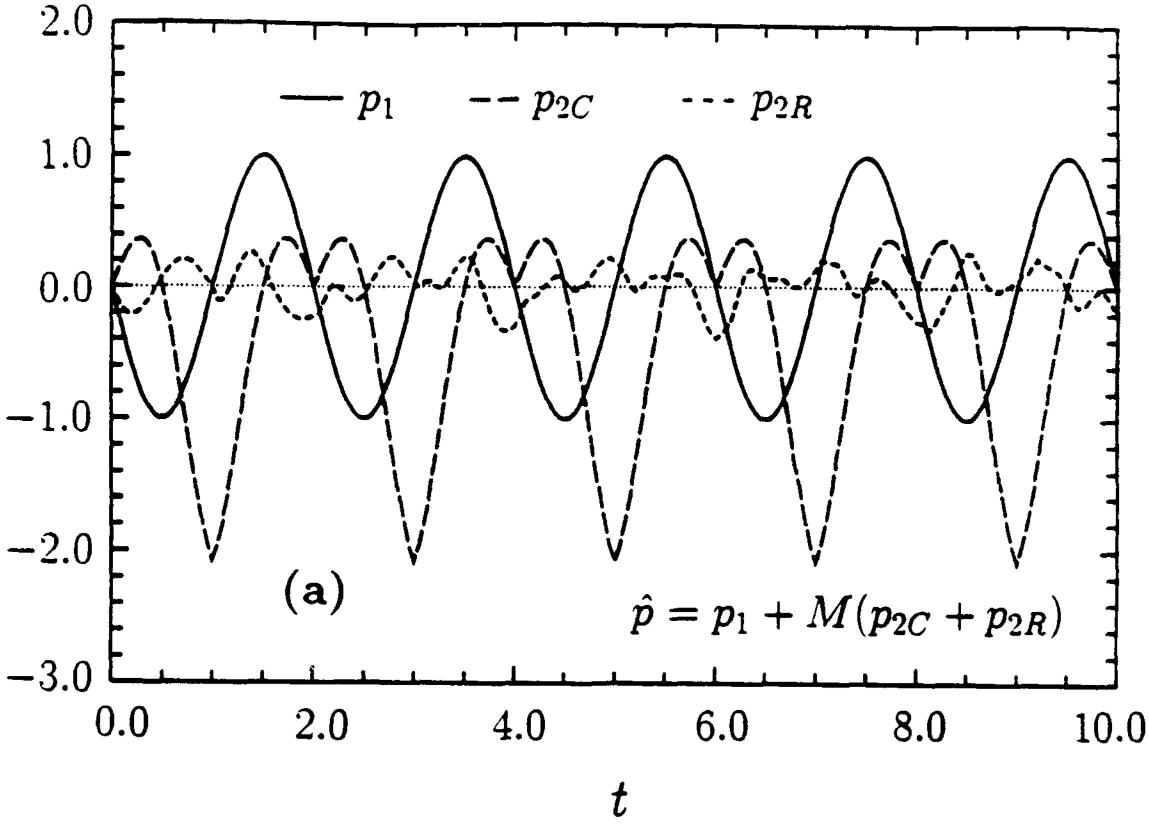


Fig 2a

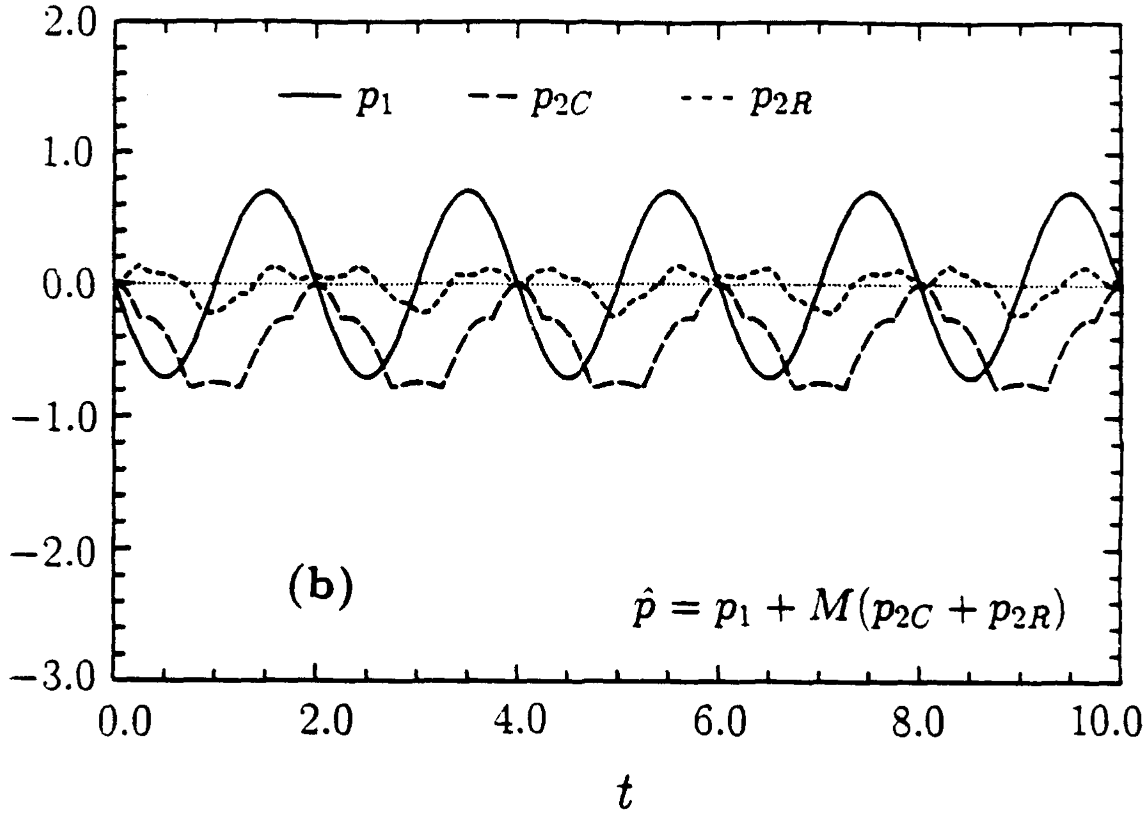


Fig 2b

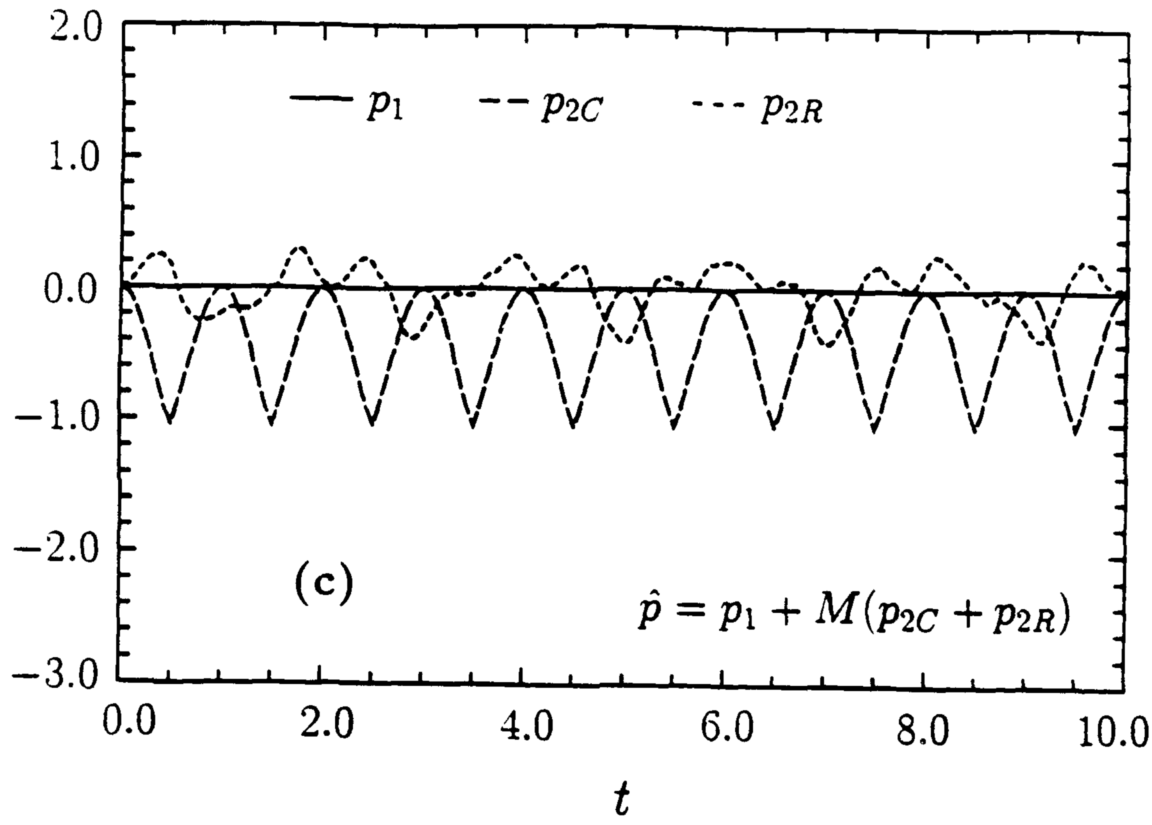


Fig 2c

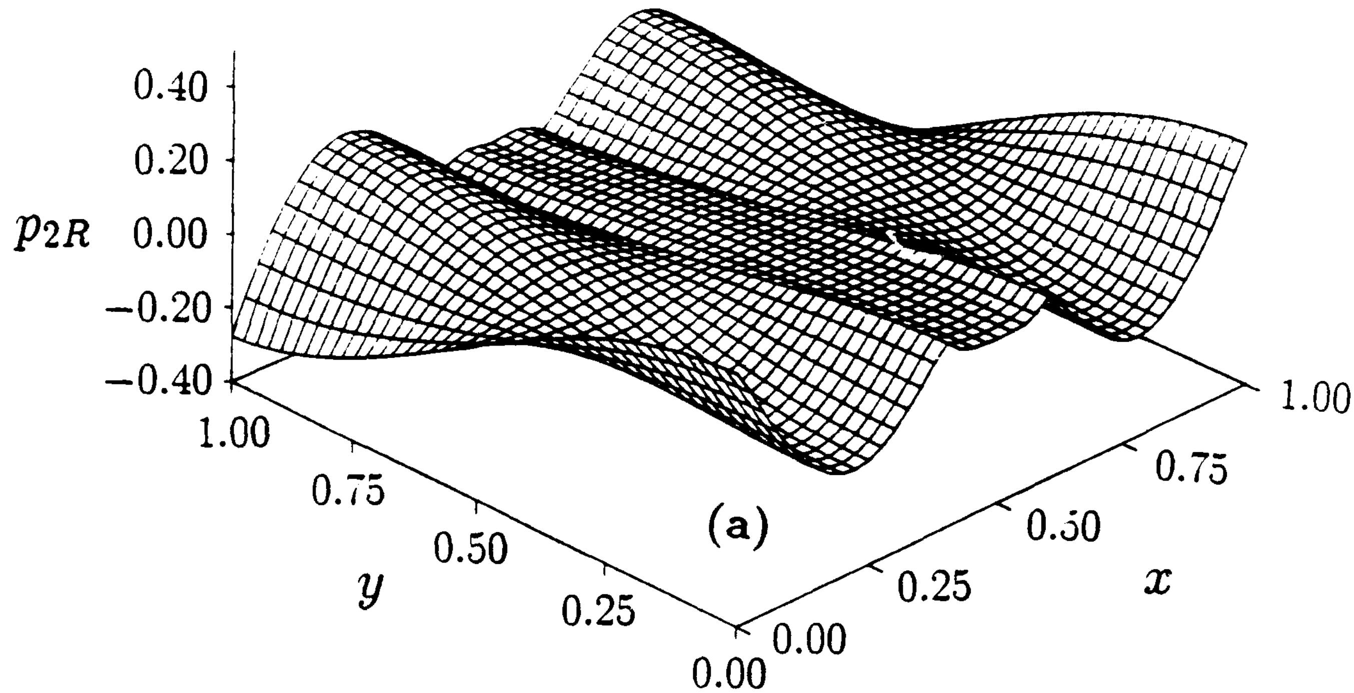
0.40
0.20
$p_{2R}$
0.00
−0.20
−0.40
1.00
0.75
0.50
$y$
0.25
0.00
0.00
0.25
0.50
$x$
0.75
1.00
(a)

Fig 3a

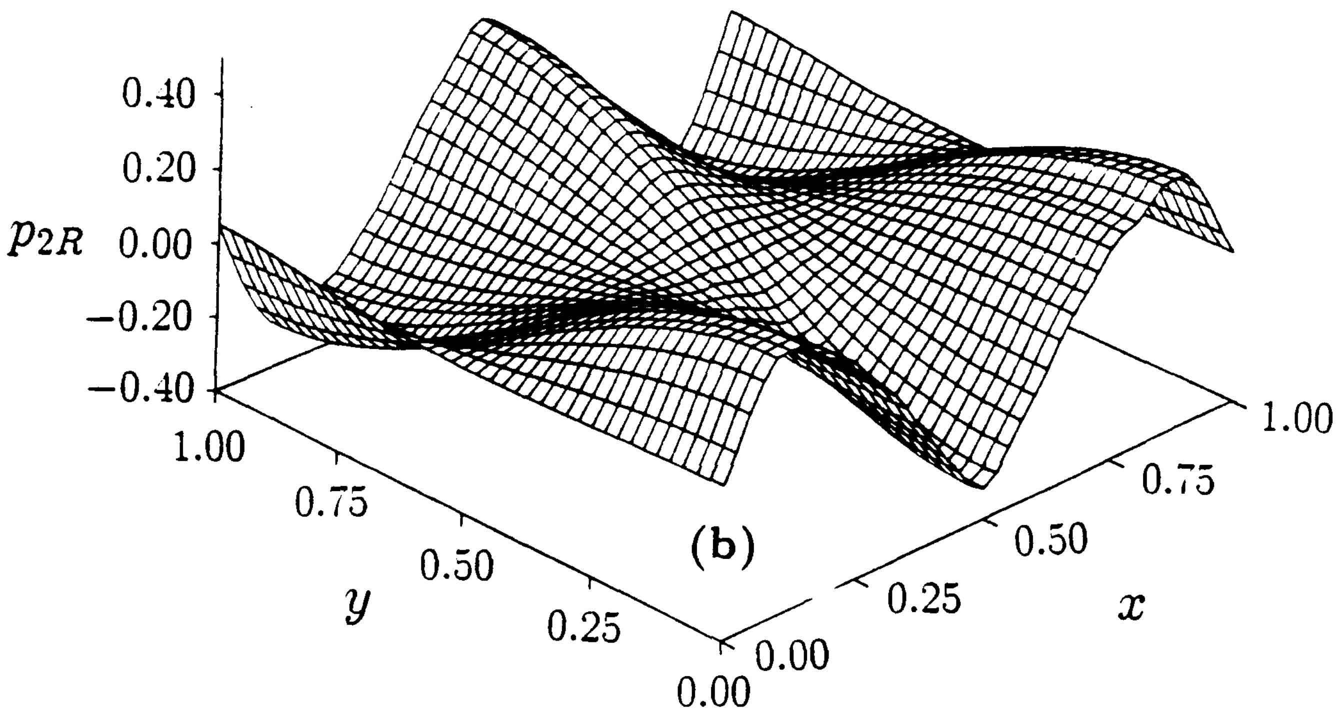
0.40
0.20
$p_{2R}$
0.00
−0.20
−0.40
1.00
0.75
0.50
0.25
0.00
$y$
(b)
0.00
0.25
0.50
0.75
1.00
$x$

Fig 3b

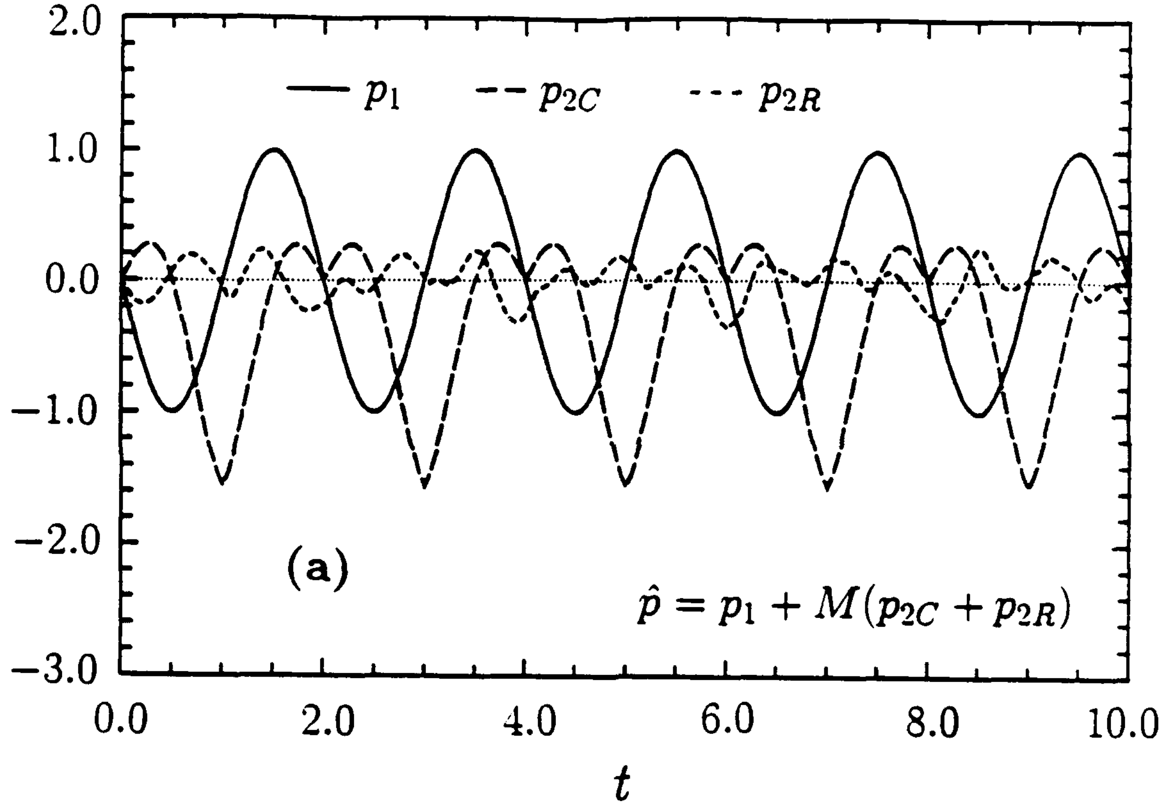


Fig 4a

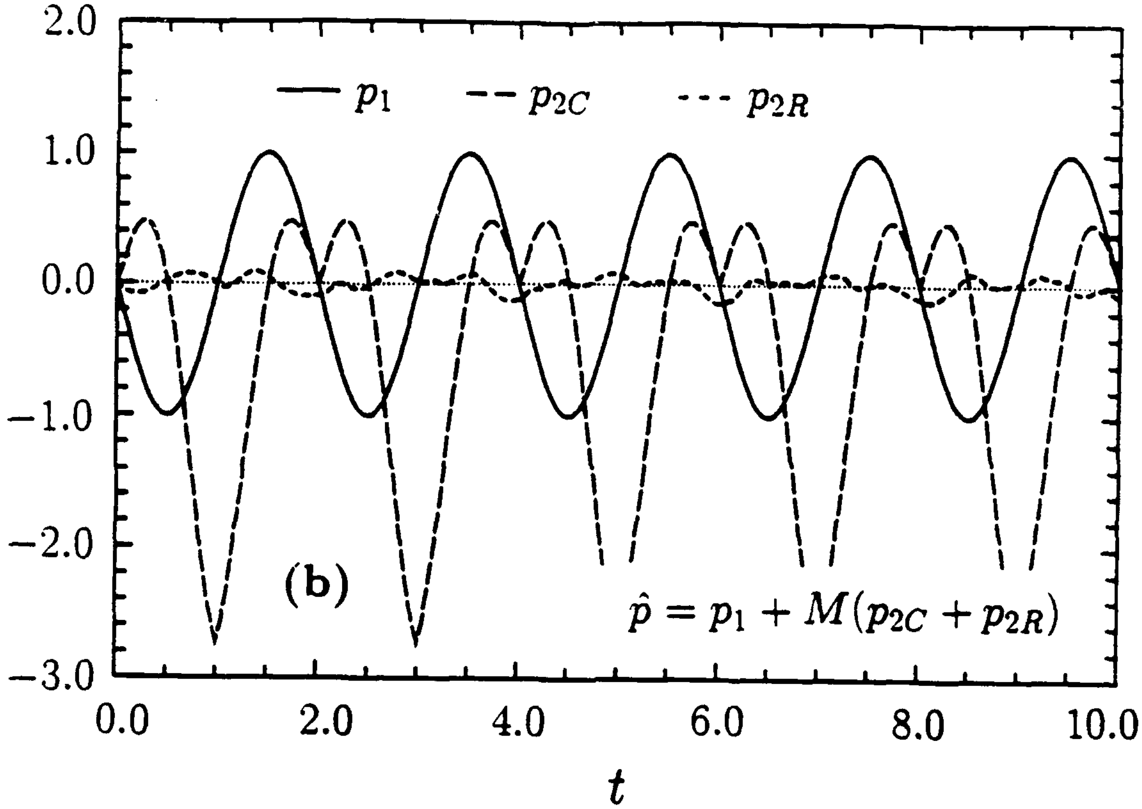


Fig 4b

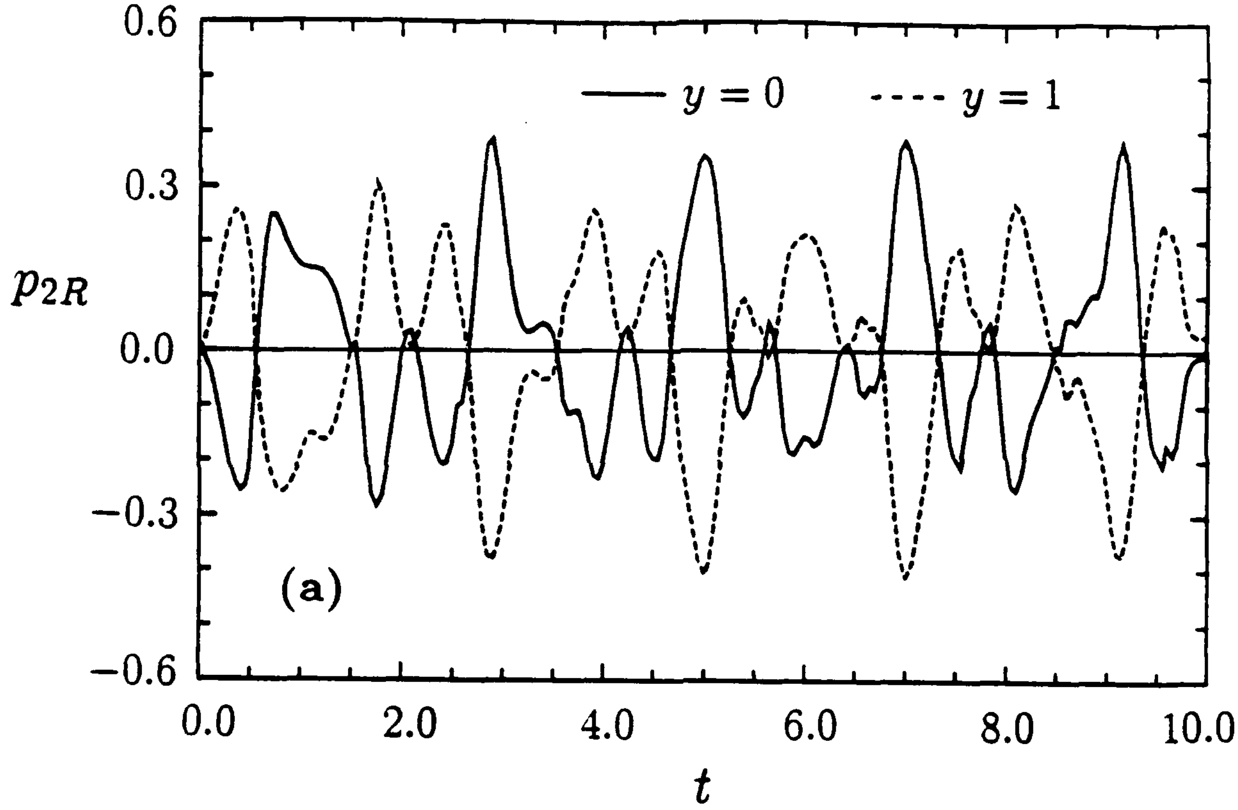


Fig 5a

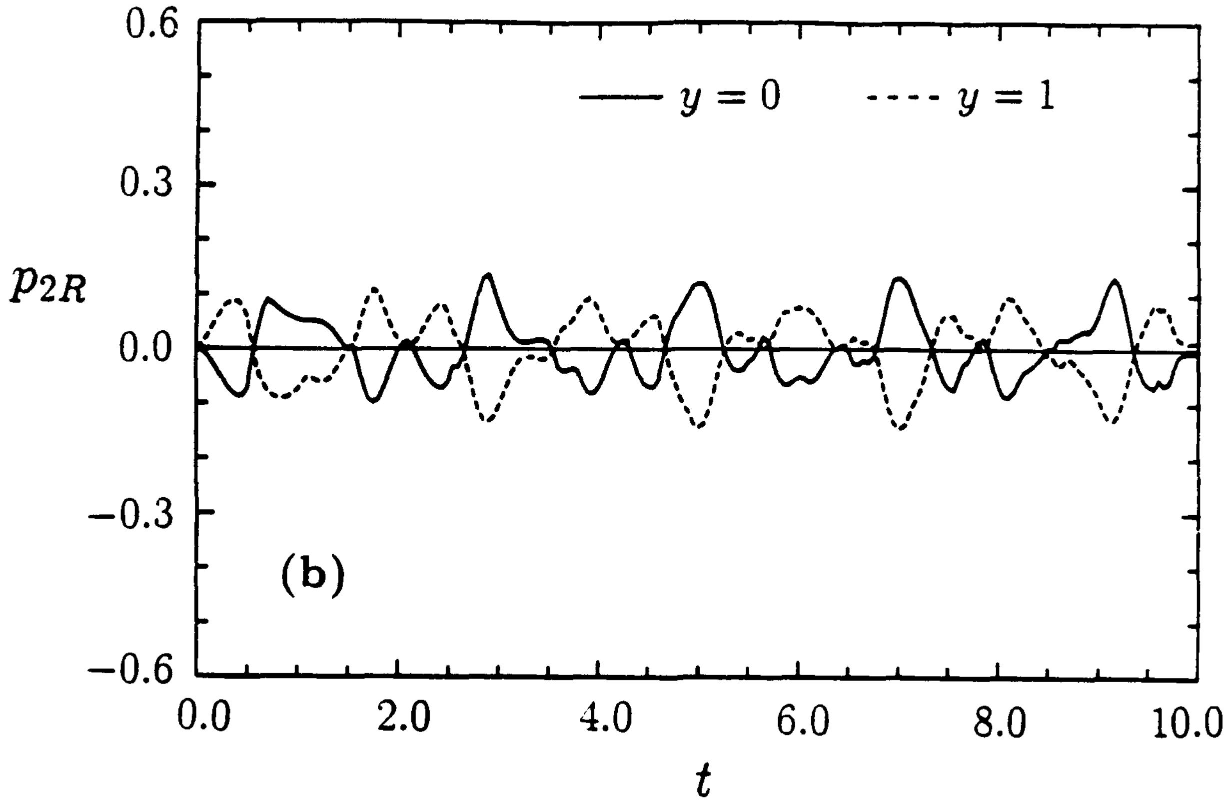


Fig 5b

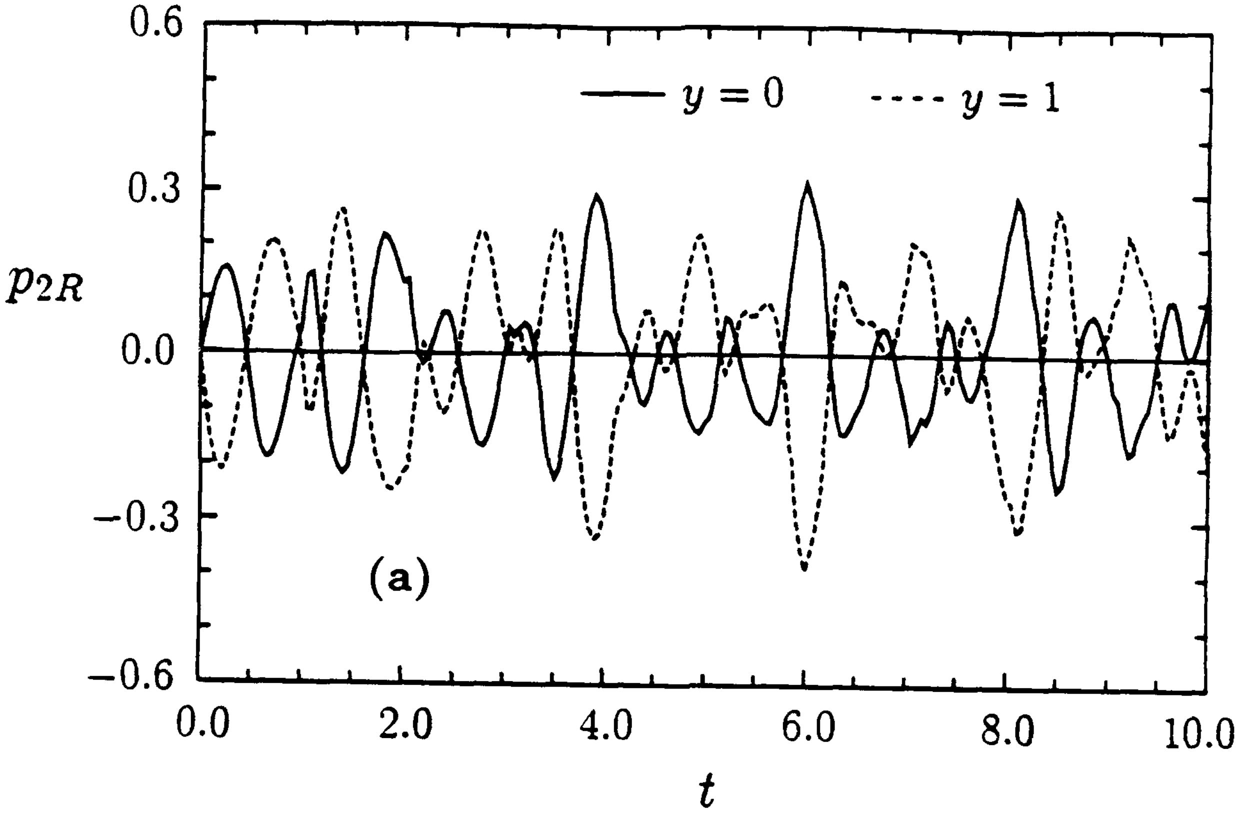


Fig 6a

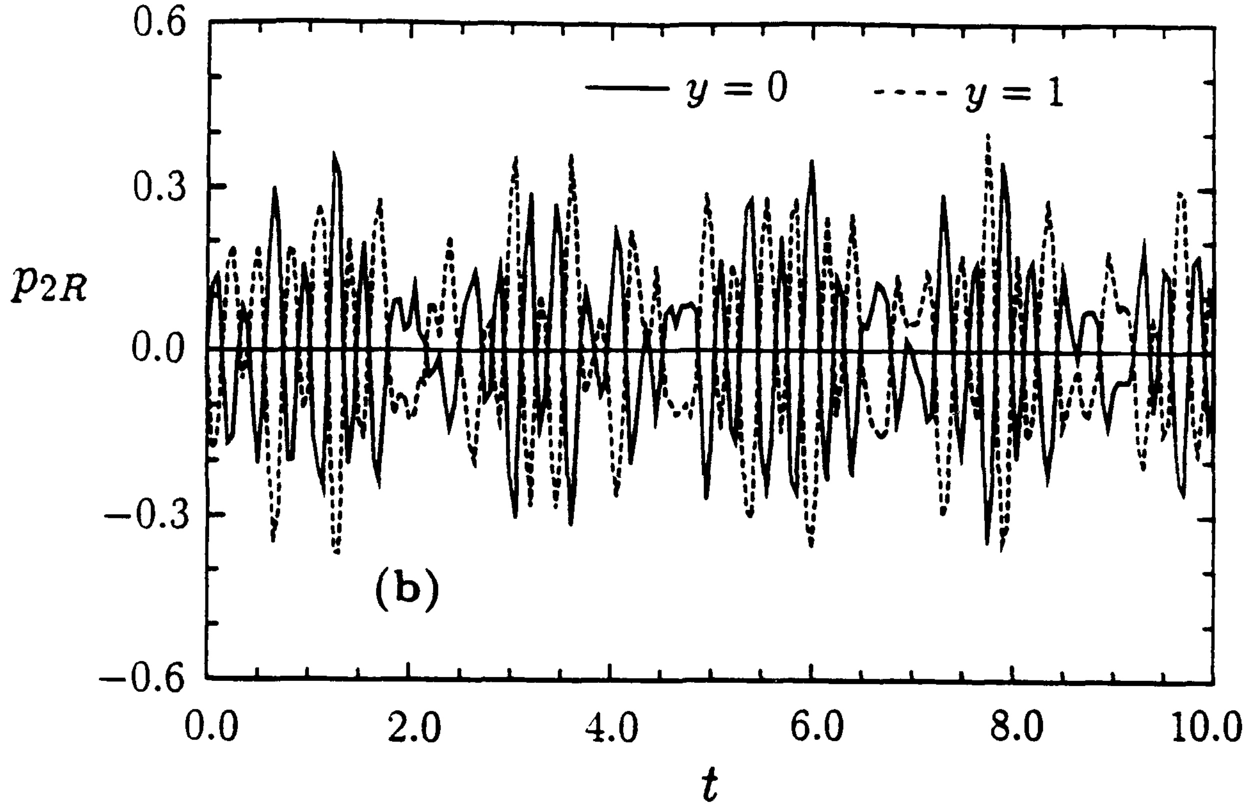


Fig 6b

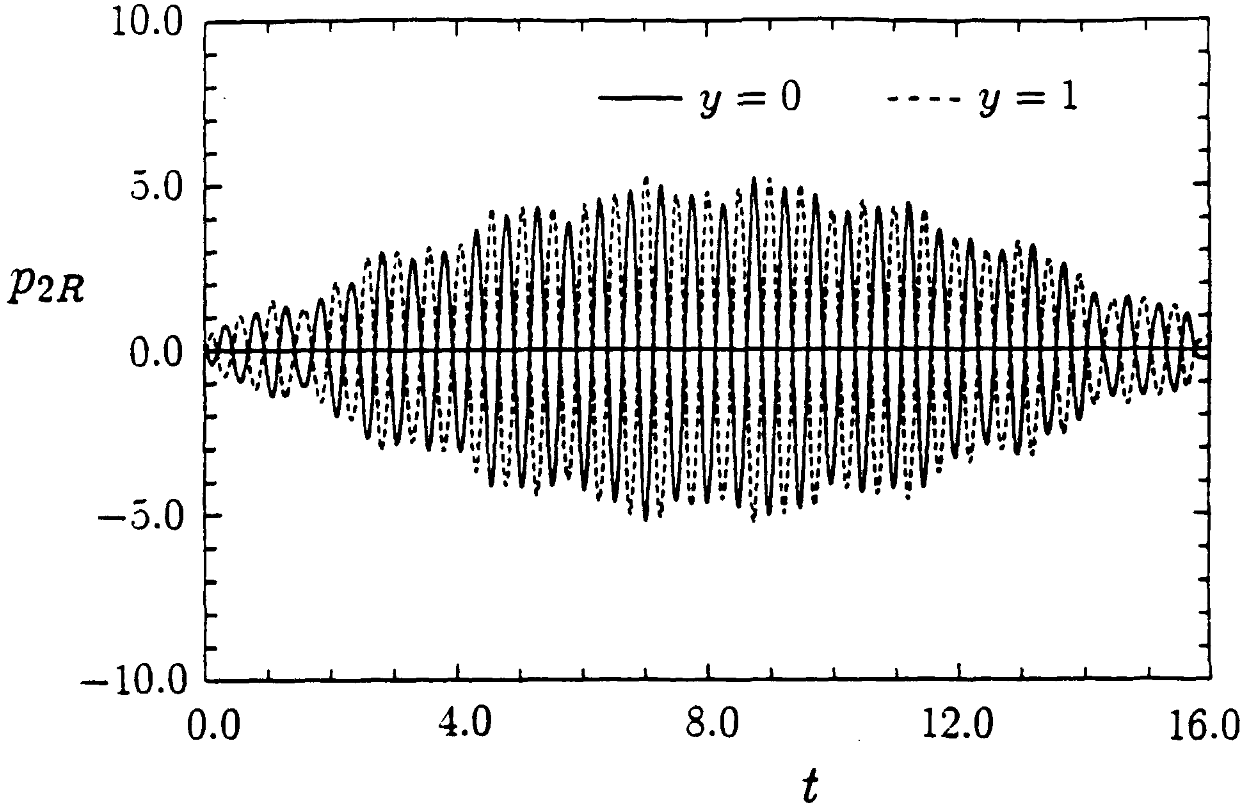


Fig. 7

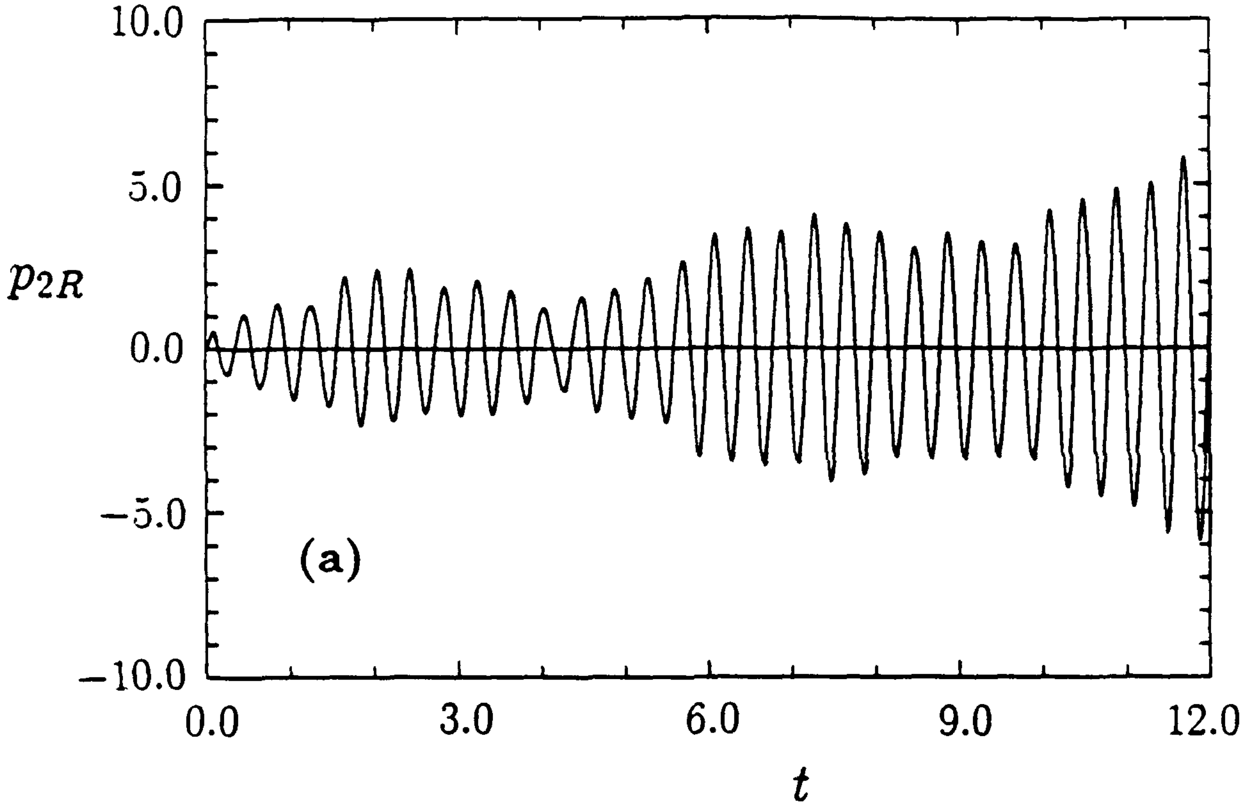


Fig 8a

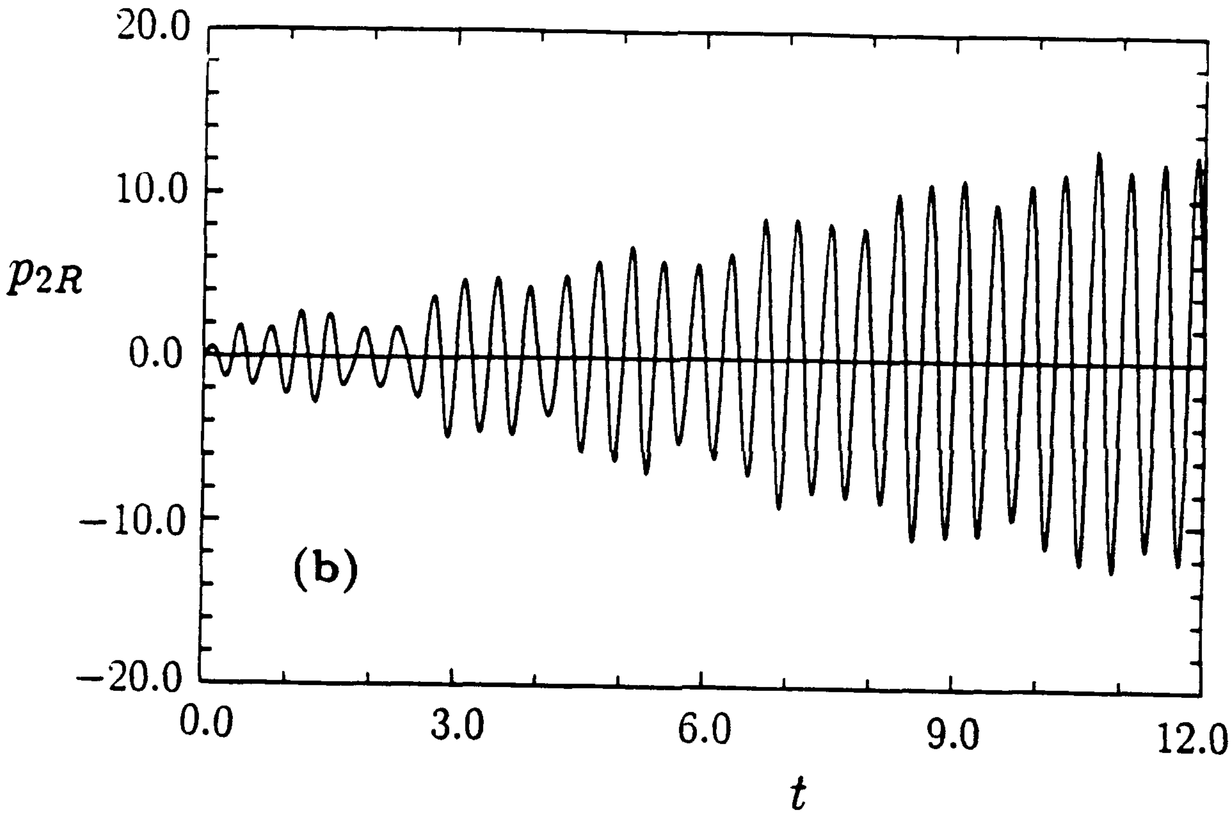


Fig 8b